DESIGN AND VERIFICATION OF AN AUTOMATED COMPENSATOR PROCESS

by

Kyle Malkoske

A practicum presented to the Faculty of Graduate Studies of the University of Manitoba

in partial fulfillment of the requirements for the degree of

MASTER OF SCIENCE

Department of Physics

University of Manitoba

Winnipeg, Manitoba, Canada

THE UNIVERSITY OF MANITOBA

FACULTY OF GRADUATE STUDIES

*****

COPYRIGHT PERMISSION PAGE

DESIGN AND VERIFICATION OF AN AUTOMATED COMPENSATOR PROCESS

BY

Kyle Malkoske

A Thesis/Practicum submitted to the Faculty of Graduate Studies of The University of Manitoba in partial fulfillment of the requirements of the degree of

Master of Science

ABSTRACT

Compensators have long been used to provide a uniform dose distribution at a specified plane in a patient. In this report, the design and implementation of an automated compensator process is discussed with emphasis on the fabrication procedure and quality assurance (QA) aspects. The method has been implemented on the FOCUS CMS 3D treatment planning system (TPS), which designs compensators to account for both external surface variations and internal tissue inhomogeneities. The compensators are milled by an automated milling machine in a special fixture that imitates the block tray to which the compensators will be affixed during the treatment. This allows for precise placement of the compensator in the treatment field. An extensive QA protocol is presented which independently verifies the accuracy of the FOCUS design as well as the fabrication of the compensator. The design is verified by means of a reconstruction of transverse slices in the patient which can be compared directly to the actual patient contour determined by the computed tomography (CT) simulation. The original CT contours could be regenerated with an accuracy of approximately ±5% of the maximum patient thickness. The fabrication is checked by taking a film radiograph of the compensator in treatment position. Using step wedges comprised of the same alloy used in the compensators, the map of pixel intensities in the digitized film image was converted to compensator thicknesses that can be compared directly to the original design. The fabrication QA procedure was determined to have an accuracy of 0.37mm (1 s.d.), corresponding to a difference in x-ray transmission of 1.9% at 6MV. The process has been experimentally verified for five phantom geometries of increasing complexity.

Acknowledgements

I would like to acknowledge the service of certain individuals, without which this work would not have been possible. First, to my supervisor, Dr. Jeff Bews, for not only your guidance and resourcefulness in the project, but also for being a mentor in the development of my career. Thanks also to Bob Miller, for your technical expertise and endless patience during the development of the compensator fabrication process. Thanks to Randall Roels and Victor Goertzen for their support in the development of the interface program. To my fellow graduate students, most notably James Beck and Heather Andres, thank you for many hours of thought provoking discussions and motivation. I would also like to express my gratitude to the practicum defense committee, Dr. Jeff Bews, Dr. Boyd McCurdy, Dr. Keith Furutani, Dr. Jim Birchall, and Dr. Amit Chowdhury, for their review and constructive criticism of the work. Finally, and most importantly, thanks to my wife Tanya, for your continuous support during my graduate studies.

Table of Contents

1 Introduction

This practicum report details the design and verification of an automated compensator process. Compensators are physical devices placed in the path of radiation therapy treatment beams in order to modulate and customize the incident radiation to a specific patient geometry. Their design and fabrication has evolved from a very manual, time consuming process [El 59] to one that is performed in an automated fashion under computer control.

The objective of this work was to develop methods for implementing an automated compensator process. Through in-phantom measurements under a variety of geometries, the accuracy with which a commercially available 3D treatment planning system designs compensators was investigated. Its ability to compensate for both surface contours and internal inhomogeneities was examined. A method was developed for interfacing the planning system compensator designs to an automated milling machine where the compensators were fabricated. Methods were also developed to perform quality assurance on both the compensator design and fabrication prior their application in a patient's treatment. These methods were both fast and comprehensive.

The document is separated in four major chapters. Chapter 1 gives the reader some background into the motivation for using compensators in radiotherapy treatment, and provides a description of the treatment planning system with which this process was implemented. In Chapter 2 the methods involved in the implementation of the automated compensator fabrication and quality assurance aspects are discussed. Chapter 3 details the results of in-phantom verification measurements and QA for several compensator designs. Based on the QA results, some general guidelines for accepting a clinical

compensator are formalized. Finally, Chapter 4 offers some general conclusions and final comments.

1.1 Radiotherapy treatment

In radiation therapy, we strive to deliver a therapeutic dose to a specified planning target volume (PTV) while sparing the critical normal structures that surround it. *Dose* is defined as to the amount of energy imparted to a medium per unit mass (with SI unit the *Gray* (Gy) which is equal to 1 joule/kg). The PTV normally contains regions of primary tumor, suspected microscopic disease and any lymph node involvement, plus margins to allow for organ motion and patient setup error. A dose is prescribed to the PTV with the aim of achieving a particular level of cell killing. Because of the complicated 3D geometry of the patient, delivering this dose to the PTV while maintaining acceptable dose levels in surrounding structures can be difficult in practice. As photon attenuation is approximately exponential with distance traveled in a medium, an *x*-ray beam will deposit a maximum dose just below the entrance surface of the patient and less at depth. Thus, the dose distribution required to treat deep-seated tumors cannot be achieved using a single beam. Multiple radiation beams entering the patient at different angles must be used in these situations.

Photons are the most common form of radiation used in external beam radiation therapy worldwide. Therapeutic energy photons are produced by a linear accelerator (linac) or the decay of ^{60}Co to ^{60}Ni. In the former of these methods, a high energy electron beam is directed onto a high atomic number target (usually gold or tungsten). The electrons are deflected from their paths as they pass by the vicinity of a target

nucleus and radiate energy in the form of photons by a process called *bremsstrahlung* [Kh 94]. Also, some of the incident electrons will ionize target atoms, leaving a vacancy in one of the atoms orbital electron shells. This vacancy is promptly filled by an electron from a higher energy shell, with the excess energy from the transition being released as a characteristic x-ray ("characteristic" since the energy of the x-ray is equal to the energy difference between the transition states). In the latter method, radioactive ^{60}Co is produced by bombardment of ^{59}Co with neutrons. The ^{60}Co then β-decays in two branches to metastable states of ^{60}Ni, which decay to the ground state with the emission of two monoenergetic gamma rays of energies 1.17 and 1.33MeV, which are utilized for treatment. In both linacs and ^{60}Co treatment machines, the photon beams are shaped and made suitable for treatment by a series of collimators and filters in the head of the machine.

1.2 Photon interactions in matter

The action of photons in matter is indirect. They undergo various interactions that liberate electrons in the material, and it is these electrons that ultimately deposit dose. For megavoltage clinical photon beams these interactions are primarily via Compton scattering. Here, the photon interacts with a loosely bound atomic electron ejecting it from the atom at some angle, which depends on the initial energy and angle of the incident photon. The photon consequently loses energy and is scattered off at some angle while conserving energy and momentum. As the energy of the incident photon increases the scattering of the photon and Compton electron becomes more and more forward directed.

1.3 Motivation for compensator use

Applying a uniform dose to the PTV while sparing the surrounding normal tissues is the goal of conformal radiation therapy. The problem of delivering this uniform dose is compounded by the fact that the patient's external surface may be spatially varying within the surface area that the beam covers. Furthermore, the patient is composed of tissues of various densities, which influence the manner in which photons interact. The problem would be greatly simplified if each beam "saw" an effectively homogeneous patient with a flat surface, for in that case the isodose lines are roughly perpendicular to the central axis (CAX) of the beam.

1.3.1 Effect of a curved surface on the dose distribution

A flattening filter is placed in the path of a linear accelerator photon beam so as to make the isodose lines roughly perpendicular to the central axis of the beam, when incident on a flat water surface (Figure 1-1 A). The surface of a patient, however, is rarely so ideal. When the same beam is incident on an irregular surface, the isodose lines tilt with the surface contour (Figure 1-1 B). However, the dose distribution is not simply shifted synchronously with the surface. Instead the dose at a particular depth from the surface will decrease as the source-to-surface distance (SSD) increases. This is primarily due to the inverse square law reduction in fluence with distance from the source.

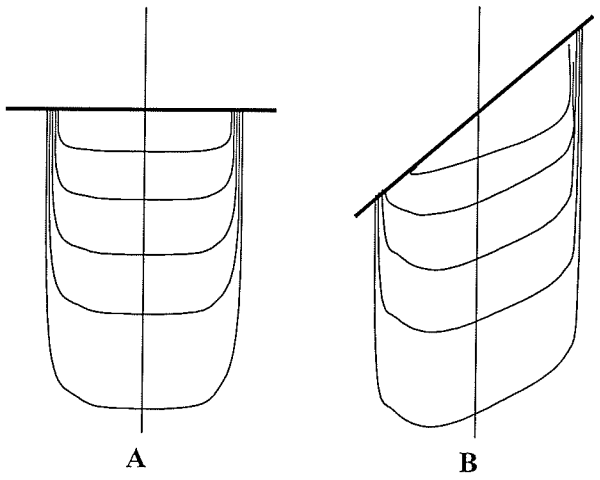

Figure 1-1: Isodose distributions for a flat surface (A) and a tilted surface (B). Due to the presence of the flattening filter, a field incident on a flat water phantom produces isodose lines roughly perpendicular to the beam central axis. For the tilted surface, the dose increases near the bottom of the decline (on the left of the CAX) due to the reduced depth of overlying tissue.

1.3.2 Effect of internal inhomogeneities

The type of interactions photons undergo in traversing a material varies as a function of energy and material type. For a 6MV photon beam, the Compton effect dominates, and this has benefits from the radiation therapy perspective. The Compton interaction cross section per unit mass, σ/ρ, is not strongly dependent on atomic number, which simplifies calculations in heterogeneous media. In fact σ/ρ is proportional to the number of electrons per gram, which is roughly constant for most body materials (Table 1-1). Because of this, 3D treatment planning is performed on the basis of electron density (number of electrons per cm^3) in the patient, which is determined from a computed tomography (CT) simulation.

Table 1-1: Densities and electron densities of various body tissues (Taken from ICRU 46 [IC 46])

Material	Density (g/cm^3)	Electrons per gram ($\times 10^{23}$)	Electron density ($\times 10^{23}$ e^-/cm^3)
Soft tissue	1.000	3.310	3.310
Muscle (ICRP)	1.050	3.314	3.480
Adipose tissue	0.950	3.347	3.180
Blood	1.060	3.311	3.510
Heart	1.050	3.314	3.480
Kidneys	1.050	3.314	3.480
Liver	1.060	3.311	3.510
Lung	0.260	3.315	0.862
Cortical Bone	1.920	3.099	5.950

From Table 1-1 it is evident that the inhomogeneities which we have to be primarily concerned with at 6MV are lung and bone. Most other body tissues are essentially water equivalent.

1.3.3 Dealing with surface contours and inhomogeneities

Several methods have been proposed to account for patient specific geometry. The most common ones used clinically are presented below.

1.3.3.1 Bolus

The simplest means of removing a patient surface contour is with the use of a bolus. Here a tissue equivalent material (usually wax) is cast on the patients surface such that the bolus' surface is flat (Figure 1-2). Although this method is successful in removing the effect of the patient contour, it has the disadvantage of destroying the skin sparing effect at megavoltage photon energies (arising from the buildup of secondary electrons in the patient). Furthermore, bolus would normally be used only to account for external surface variation, neglecting the effects of inhomogeneity in the patient.

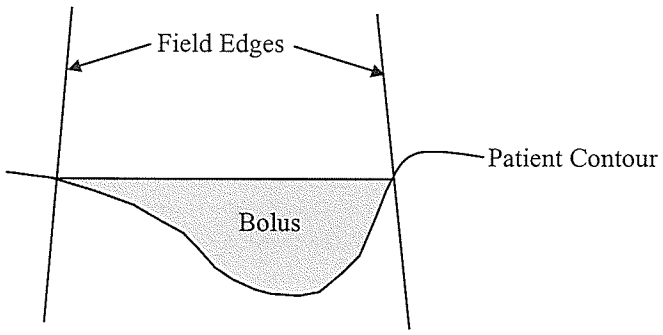

Figure 1-2: An external contour can be negated with the aid of a wax bolus. It is essentially poured in to fill the volume of missing tissue.

1.3.3.2 Compensating filters

Ellis *et al*, reported on the first use of compensators in 1959 [El 59]. As their name implies, these devices were designed to compensate for the actual geometry of the patient, similar to bolus. The main difference between a compensator and bolus is that the compensator is retracted from the patient surface a distance large enough so that most the electrons generated in the compensator do not reach the patient (about 15cm from the skin is usually sufficient) (Figure 1-3). This results in a restoring of the skin sparing effect. The classic Ellis filter comprised series of blocks that were placed on a 2D grid in the path of the beam. The height of each block was dependent upon the amount of missing tissue along the diverging fan line passing through it. If the compensator was composed of a "tissue equivalent" material (wax), then the thickness of compensator along a given fan line was made equal to the corresponding thickness of missing tissue along that fan line. However, since the thickness of missing tissue in the treatment field can be quite large at some anatomical sites, there is an advantage to using higher density materials like lead or brass, so that the compensator thicknesses can be reduced, according to the linear attenuation coefficient of the material.

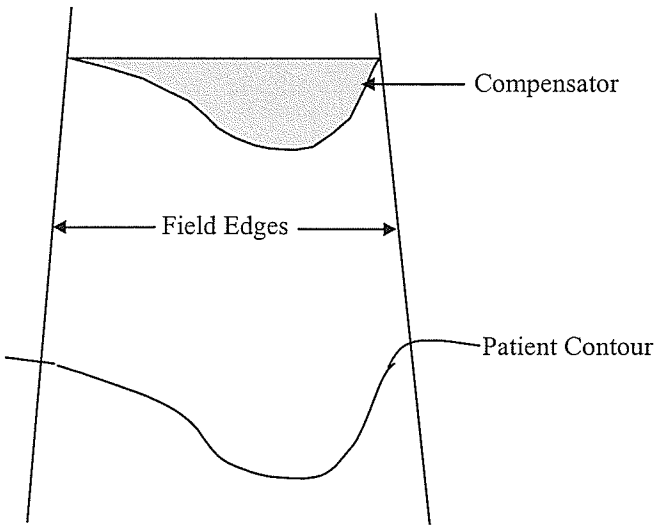

Figure 1-3: A compensator performs the same function as bolus, except the device is retracted from the patient surface so as to preserve the skin sparing effect.

It is well known that the linear attenuation coefficient of a beam modifying filter used in a linac beam varies as a function of field size, thickness of the filter material and depth of measurement in the patient [Bo 82]. The field size variation is due to changes in the amount of photon scatter originating in the filter and patient. As the field size is increased, additional scattered photons from the edges of the field are directed towards the central axis, giving the appearance of less attenuation of the beam at that point. The resulting decrease in the linear attenuation coefficient as a function of field size has been verified experimentally [Ju 94].

The dependence of the attenuation coefficient on thickness of compensator material is primarily due to beam hardening. The term "beam hardening" refers to the preferential removal of low energy photons in the polyenergetic spectrum of a linac beam. This stems from the increase in the photon interaction cross section, σ, as the energy decreases, since photons become more and more likely to interact via the

photoelectric effect ($\sigma_{PE} \propto Z^{3-4}$). Consequently, the mean energy of the photon beam on the exit side of the compensator tends to increase with filter thickness, resulting in a decrease in the linear attenuation coefficient. Similarly, beam hardening occurs in the patient, causing the mean energy of the beam to increase slightly with depth.

The first compensators were designed simply to account for missing tissue. With the advent of 3D computed tomography (CT) simulation and computerized treatment planning systems (TPS), which can calculate dose while accounting for tissue inhomogeneity, filters may now be designed to compensate for irregular surface contours and patient internal structure. Due to computerization, complex compensators are designed very efficiently in the treatment planning process.

Ellis type filters have largely been replaced with compensators generated by milling machines. The advantage here is that the compensator resolution can be greatly improved. Unfortunately, this can lead to large manufacturing times, which has somewhat discouraged the use of compensators. Presently, the use of automated milling machines has significantly improved this aspect, as technicians are no longer required to be present during the milling process. In this report, the clinical development of such a process will be discussed at length.

1.3.3.3 MLC intensity modulation

In the past decade, intensity modulation (IM) by means of a multi leaf collimator (MLC) has become realizable. Here, a spatially variant field intensity (similar to that on the exit side of a physical compensator) is delivered by a series of fields shaped by an MLC. The leaves either move in a series of discrete steps ("step and shoot" MLC-IM) or

continuously while the beam is on (dynamic MLC-IM). One immediately obvious advantage of this technique is that physical devices need not be fabricated for each patient. However, this technique does have several disadvantages. Firstly the resolution of the IM is significantly reduced as compared to a physical compensator since the leaves are generally 1cm thick at isocenter (although this has been improved to 5mm on some recent machines). Also since the treatment is delivered as a series of field segments, treatment times are increased by about a factor of three [Ch 00]. Radiation leakage through the leaves also poses a problem, as does the loss of charged particle equilibrium and its resulting effect on the dose calculation when the field segments reach very small field sizes [Fi 01]. Furthermore, MLC-IM treatments are very difficult to verify and perform quality assurance (QA) on.

The debate as to which method of IM (physical compensators or MLC) is most suitable rages on today. While it is clear that the MLC technique has a significant advantage by removing the excess demand required by the production of physical beam modifiers, there still remain several issues with MLC-IM that need to be addressed before their widespread clinical use is established. Compensators, on the other hand, have been in clinical use for a long time, with their properties well documented in the literature. As the compensator process continues to be refined, they will undoubtedly maintain a significant role in the clinic for years to come.

1.4 Conventional Compensator design and fabrication approach

Several techniques for constructing compensators have been presented in the literature. A few of the traditional design and fabrication approaches are presented below.

1.4.1 Styrofoam cutters

Styrofoam cutters are traditionally used to cut out blocking material shapes. However, adaptations have been made to these devices, permitting their use in compensator design and fabrication.

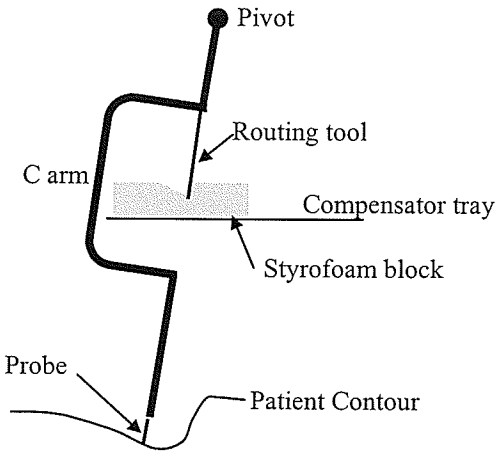

Figure 1-4: Stryofoam cutter arrangement used to fabricate compensators.

A probe which samples points on the patient's surface is attached to the opposite end of a pivoting C arm (Figure 1-4). The patient is setup below the device in treatment position, such that the position of the pivot corresponds to the position of the source. The C arm wraps around a tray containing the uncut block of Styrofoam, which is positioned at its location in the treatment field (with respect to the source). A spring is located in the shaft between the C arm and the pivot so that movement in three dimensions by the probe

is mimicked by motion of a Styrofoam routing tool, which cuts the patient contour out of the Styrofoam as the probe is drawn across the patient surface (or immobilization cast). The tool can either be a drill or a heating element. Using this technique the patient contour, corrected for beam divergence, is reproduced in the Styrofoam block. The hollowed out mould is subsequently filled with tissue-equivalent paraffin wax [Be 71].

One advantage of this technique is that the compensator fabrication is fast, as after the mould has been cut, the melted wax is simply poured into it. Also, high resolution in the compensator can be obtained. On the other hand, as the resolution increases the time required to design the compensator also increases significantly. Furthermore, compensators designed by this technique can obviously only account for external surface contours.

1.4.2 Diverging rod apparatus

Khan [Kh 68], described a physical device which could be used to design geometrically retracted missing tissue compensators. It consisted of a group of thin rods which simulate rays diverging from the source. As the device is lowered onto the patient, the rods, which are free to move, reproduce the patient contour at the compensator to skin distance before being locked in place. A paper barrier is attached to the top of the rods so that melted wax can be poured onto the retracted patient contour mould. Although this method succeeds in making the compensator design and fabrication process very simple, it provides very poor compensator resolution, and is awkward to manage due to its size and weight. It is also strictly a missing tissue compensation system.

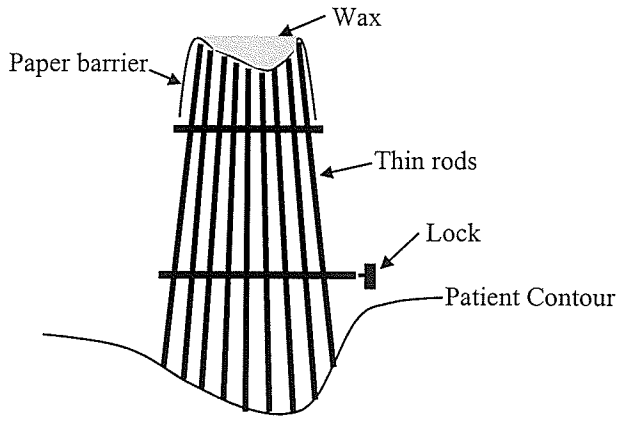

Figure 1-5: Diverging rod apparatus used for constructing missing tissue compensators.

1.4.3 Conventional (manual) CCMB system

1.4.3.1 Design

The conventional compensator design process at CancerCare Manitoba (CCMB) utilizes a pantograph system to measure the patient's surface contour. For the equivalent square field size, the tissue phantom ratios (TPR) at the high point depth, d_{HP}, (corresponding to the shortest SSD) and the field pseudo center depth, d_{pseudo}, (at roughly the geometric center of the field) are determined from tables for the given beam energy (6MV). Then, the transmission, T, that the compensator needs to provide along a ray passing through the field pseudo center to compensate for the missing tissue along that ray is given by,

$$T = \frac{TPR(r_{eq}, d_{HP})}{TPR(r_{eq}, d_{pseudo})} \quad (1\text{-}1)$$

The difference in tissue thickness at the high point and pseudo center of the field is then used to generate an attenuation factor, F, whose inverse describes the amount of beam attenuation per centimeter of tissue deficit,

$$F = \frac{d_{HP} - d_{pseudo}}{T} \quad \textbf{(1-2)}$$

The compensator thickness is milled in a series of 0.38mm steps, and correspondingly there exists tables of compensator transmission factors for each step. The planning procedure is to first calculate a tissue deficit from the high point thickness for a given step size, by multiplying the compensator step transmission factor by F. Then the pantograph distance is set to this tissue deficit and points within the field on the patient's cast at this level are digitized, and manually these points are then connected by a line. The procedure is repeated for subsequent steps until the tissue thickness drops to about 2cm. A contour plot of the patient's surface is thus generated, where each contour line corresponds to a given step in the compensator. The transverse coordinates of the contour plot are then de-magnified to the compensator tray distance, according to a beam divergence factor.

Provided the patient has had a plastic immobilization cast made, the method has the advantage that the patient need not be present during the design process. Its disadvantages, however, include being human resource intensive (approximately half a day per compensator), and the fact that only the external patient surface can be accounted for.

1.4.3.2 Fabrication

The compensators are milled manually out of an alloy consisting primarily of Pb (>98% by mass), following the contour plot discussed in the previous section. Skilled technicians are able to mill the compensator with high accuracy in the transverse directions. However, the compensator thickness accuracy is limited by the 0.38mm step size on the contour lines. This corresponds to approximately a 2.2% step in terms of compensator x-ray transmission (expressed as a percentage of full transmission). A typical clinical head and neck compensator takes roughly an hour to fabricate.

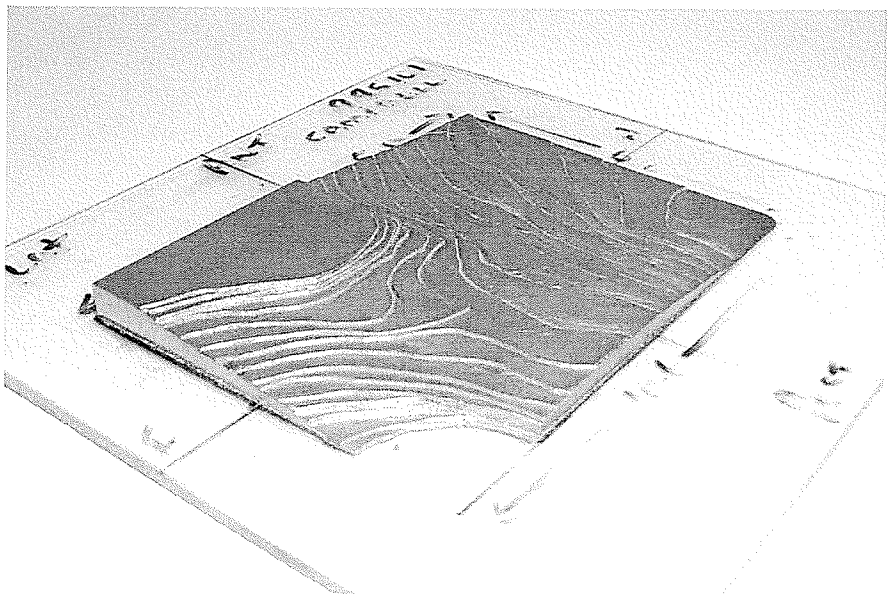

Figure 1-6: Photograph of a head and neck compensator fabricated by the conventional CCMB method.

1.5 Newer Approaches

From the above discussion it is clear that there is a need for an accurate, fast, and automated system of designing, fabricating and performing routine QA on compensators in the clinic. The solution to these problems leads us into the focus of this work.

1.5.1 Design

Most institutions today perform computer based planning using 3D treatment planning systems (TPS). These computers use CT data to generate a 3D reconstruction of the patient on which treatment planning can be performed. The CT data contains the patient electron density information and hence internal inhomogeneities can be accounted for in the dose calculation. Compensators can be designed by these planning systems, which account for both patient contour and internal inhomogeneities. The first obvious advantage of this is that the design is fast since it is done solely by the computer. Moreover, the TPS compensator designs contain increased accuracy as they are based on a dose calculation in the patient rather than simply a thickness of missing tissue. Therefore, the effects of scatter and beam penumbra, for instance, can be accounted for in the design.

On the other hand, since CT simulations are required for all the patients undergoing compensator treatments if the design is to be done by the TPS, an increase in the patient load on the CT simulator may be required. However, since 3D conformal radiation therapy (which requires patient CT data) is rapidly becoming the standard of care, the increase in patient load on the CT simulator is something that is inevitable in a progressing clinic.

1.5.2 Fabrication

Dedicated milling machines whose sole function is to mill compensators designed specifically by treatment planning systems are now commercially available. The milling is done in an automated fashion under computer control, based on a compensator file

exported by the TPS. In our fabrication technique, the compensator file exported by FOCUS is converted to code suitable to be read by a computer numerically controlled (CNC) milling machine. The advantage of the CNC is that a machinist is not required to operate the mill while the compensator is being fabricated. Furthermore, with a standard library of referenced tools on the CNC, and a reproducible setup procedure, the precision with which the compensators can be fabricated is high.

At CCMB, the compensators are milled from plates consisting primarily of lead (>98% by mass), but also containing a small fraction of antimony. The density of this alloy is roughly 10 times that of water. Therefore, the compensator thicknesses are approximately one tenth of the missing tissue thicknesses that they replace. Since the compensator alloy consists primarily of lead, it will be referred to as 'Pb' for the remainder of this report.

1.6 Treatments suited for compensator use

1.6.1 Head & neck cancer

Compensators are routinely used at CCMB for treatment of cancers in the head and neck region. These are typically squamous cell carcinomas, usually brought on by tobacco and alcohol abuse [Kh 98]. The tumor masses normally develop in the mouth, tongue, larynx, pyriform and paranasal sinuses, and parotid [Kh 98]. As an example, treatment of the pyriform sinus usually involves two lateral fields to treat from the pharynx to the base of the neck matched to an anterior field to treat tracheostomy, supraclavicular and superior mediastinal lymph nodes (Figure 1-7). Compensators are

used in the 6MV lateral photon fields to remove the effect of the surface contour and provide a uniform dose to the patient midline.

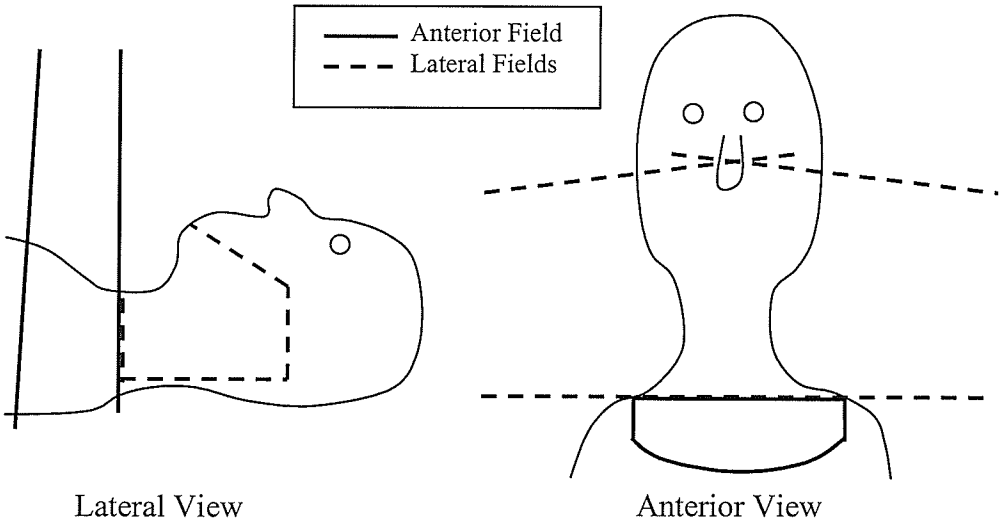

Figure 1-7: Positioning of the fields in a typical treatment of carcinoma of the pyriform sinus. Compensators are applied in the lateral fields [Kh 98].

1.6.2 Mantle field

The so-called *mantle field* is a large anterior field on the chest shaped like an inverted Ψ. Lungs and vocal cords are spared using high density blocking material. This field is often used as a part of a Hodgkin's disease treatment (along with paraaortic and pelvic fields). The variation in the patient's surface across such a large field requires compensation to maintain a relatively uniform dose distribution at the patient midline.

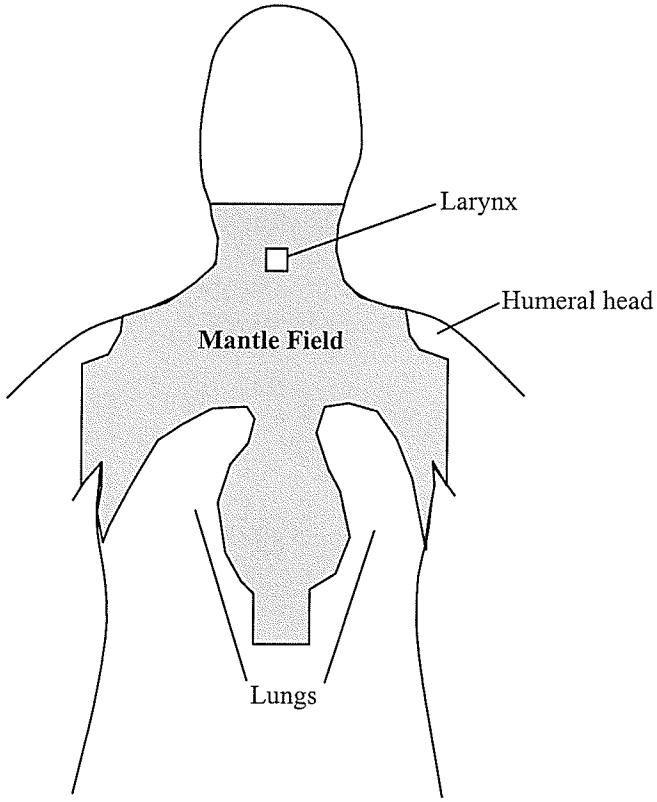

Figure 1-8: Human torso contour showing the position of the mantle field (shaded region). The lungs, humeral heads and larynx (vocal cords) are typically blocked using lead or cerrobend [Pa 70].

1.6.3 Breast cancer

Breast cancer treatments traditionally include a pair of tangential parallel opposed 6MV photon fields (Figure 1-9). Wedges have been conventionally used to compensate for missing tissue, due to their simplicities. However, wedges cannot compensate in all transverse planes due to the varying surface contour. Furthermore, the beams normally include portions of the lung, whose electron density is roughly ¼ that of water, and which will receive a larger dose than neighboring tissues. Applying compensators to account for internal inhomogeneities accounts for this change in photon transport in the lung. It has been shown that dose uniformity in the PTV can be increased by 20% using custom made compensators rather than wedges [Ch 99].

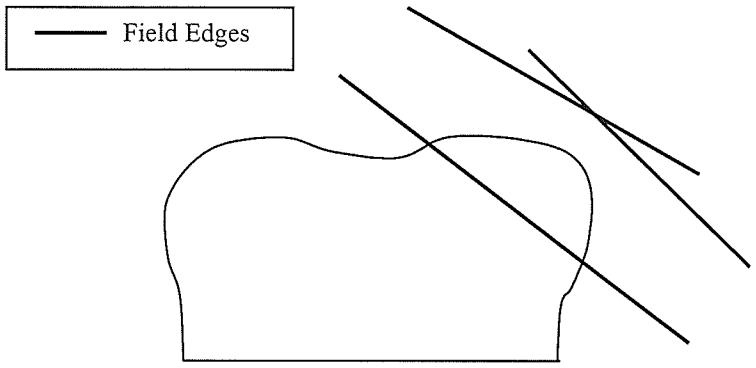

Figure 1-9: Transverse slice contour at the level of the breast showing the placement of the parallel opposed tangential fields.

1.7 FOCUS CMS 3D treatment planning system

The compensator process described in this report has been implemented on the FOCUS CMS v2.6.1 TPS. A brief introduction to the FOCUS calculation algorithm and details of its compensator design process are discussed below.

1.7.1 Clarkson algorithm

The FOCUS Clarkson algorithm is a correction-based method, which essentially takes the dose measured in a homogeneous water phantom and applies various correction factors to account for the actual patient shape and density. The primary dose is altered due to the presence of inhomogeneities in the patient and transmission through beam shaping and modulating devices such as blocks, wedges and compensating filters. The calculation of scatter dose, however, is only dependent on the field shape, and thus changes in scatter dose as a result of variations in patient density, surface contour and the presence of beam modulators are not explicitly modeled. If multiple beams are used in a

treatment, the dose from each beam is calculated separately and the results summed together at each calculation point.

1.7.2 FOCUS design of compensators

FOCUS provides optional compensation in one dimension (lucite compensators) or two dimensions (Ellis or milled compensators) (Figure 1-10). The following discussion will be limited to 2-D milled compensators as they were the focus of this work.

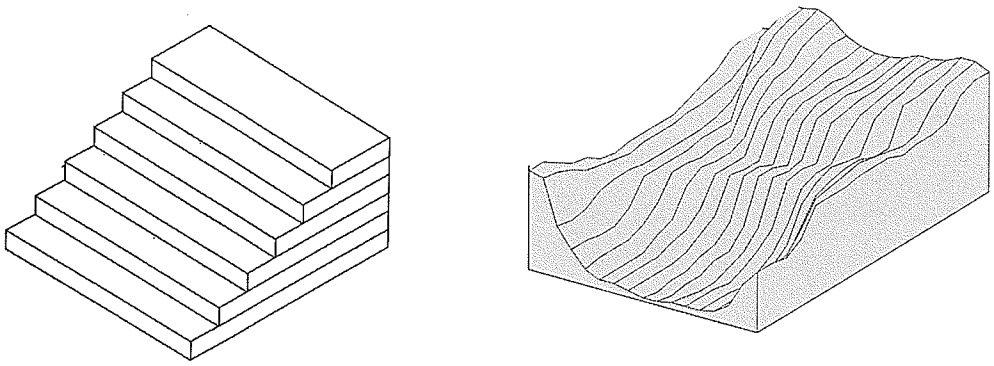

1D lucite compensator 2D milled compensator

Figure 1-10: FOCUS CMS can provide simple 1D compensation consisting of stacked lucite plates or 2D compensation consisting of a 2D array of filter thicknesses. For the 2D case, the compensator can be constructed of square blocks [Ha 61] or via an automated milling machine (as shown).

1.7.2.1 Definitions

The FOCUS nomenclature is defined below with reference to Figure 1-11.

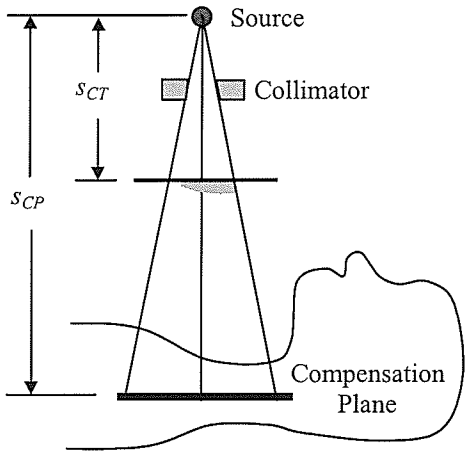

Figure 1-11: Compensator geometry to illustrate the FOCUS nomenclature.

- *Compensation Plane*

A plane perpendicular to the central axis of the beam throughout which a uniform dose distribution is desired. The compensation plane can be tilted with respect to the central axis by using virtual or dynamic wedging during the treatment delivery.

- *Source to compensation plane distance* (s_{CP})

The distance between the source and the compensation plane along the central axis of the beam.

- *Source to compensator tray distance* (s_{CT})

The distance from the source to the tray upon which the compensator is mounted along the central axis. At CancerCare Manitoba, compensators are mounted on a separate tray, which is affixed to the patient side of the block tray. Therefore, s_{CT} is the

distance from the source to the bottom of the compensator tray when it is in treatment position.

- *Effective linear attenuation coefficient* (μ_f^{eff})

The effective linear attenuation coefficient of the compensating filter material is used to scale the thickness of the filter relative to the thickness of missing tissue for which it was designed to compensate. The "*eff*" superscript signifies that the attenuation coefficient used in the calculation is a weighted, energy averaged value for the particular polyenergetic beam being used. The "*f*" subscript simply identifies that the effective attenuation coefficient is that of the filter material. The measurement of this parameter is described in Section 2.1. Not only is μ_f^{eff} a function of x-ray energy, it is also dependent on field size and depth of measurement [El 87], due to scattering and beam hardening in the flattening filter, compensator and patient. FOCUS provides the user with the option to customize μ_f^{eff} for each patient. However, as its dependence on the above variables is relatively small, we have followed the FOCUS recommendation of using a single value of μ_f^{eff} measured for a 10 × 10cm field at a depth of 5cm [CMS].

- *High point*

The point on the patient with the shortest SSD within a specified area (normally the open field defining limits) projected to the central axis. This is the point corresponding to the maximum transmission through the compensator.

- *Transmission Array* ($T(i,j)$)

A two dimensional array describing the transmission of the primary beam through the compensator. This array is later converted into an array of compensator thicknesses.

1.7.2.2 Dose calculation matrix

FOCUS calculates the dose on a diverging depthline/fanline matrix (Figure 1-12). The separation of the fan lines is a constant specified by the user. The separation of the depthlines is based on a constant radiological distance, ρd, if the heterogeneity correction is applied in the calculation, and otherwise is constant if a homogeneous calculation is applied. The dose is calculated on the intersection points of the depthline/fanline grid, where the density at each intersection point is assigned the average density along the ray between that depth line and the next one nearest the source [CMS]. The treatment

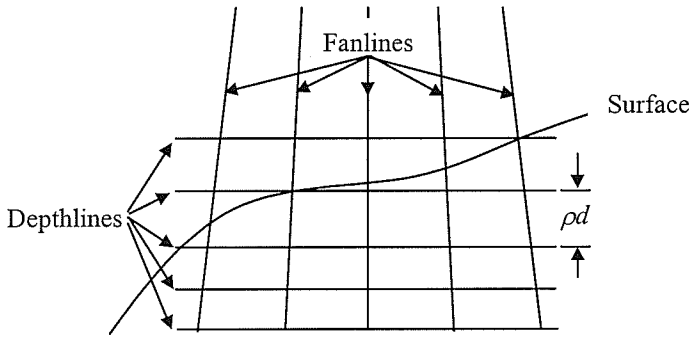

Figure 1-12: Fanline/depthline matrix used in the FOCUS Clarkson calculation algorithm. The dose is calculated at the intersection of the fanlines and depthlines.

planner is required to specify a rectangular calculation grid, to which FOCUS interpolates the dose from the calculations on the depthline/fanline grid.

1.7.2.3 Patient high point determination

As previously defined, the high point is the location in the compensator where the maximum x-ray transmission occurs. The search area in the beam's eye view is restricted to either the open field (defined by the collimators), the blocked field, or a user-defined area. Normally, the open or blocked field would be the most likely search area to be applied. However, some special situations may require a user-defined area, such as lateral head and neck compensators in which the field includes portions of the shoulders, in order to avoid very large compensator thicknesses. For the open and blocked field searches, the search area is confined to regions where the primary dose is greater than 90% of the central axis dose, and points in the compensator design outside this region are simply truncated (Figure 1-13). This restriction usually limits the high point from being found in approximately the last 1cm of the field edge, corresponding to approximately 0.5cm in the compensator. When a user-defined region is specified, the search extends throughout its entire area.

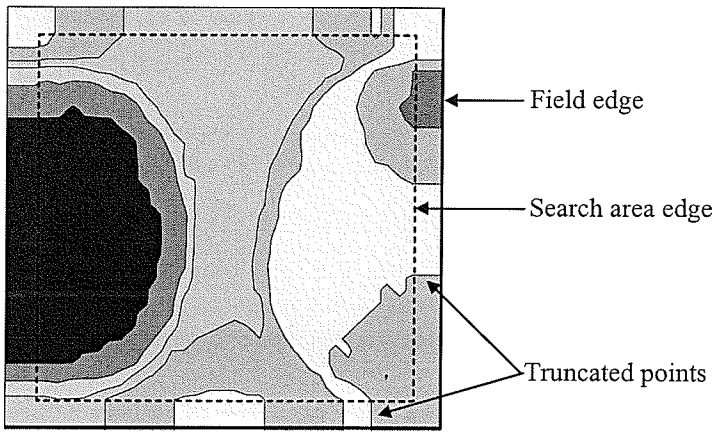

Figure 1-13: Contour plot of a compensator showing the geometrically retracted location of the field edge, and the edge of the search in the open or blocked field option. Compensator points outside of the search area edge are simply truncated.

1.7.2.4 Generation of the transmission array

The FOCUS Clarkson algorithm compensates for surface contours and internal inhomogeneities by modifying the incident beam intensity such that the dose distribution at the compensation plane is the same as that resulting from an identical beam incident on a homogeneous phantom with the SSD equal to the SSD of the patient high point [CMS]. The intensity modulation is achieved by passing the open beam through a transmission function, defined in a plane normal to the central axis of the beam. The high point searching area can be customized by the user so as to ignore excessively high structures in the open field that are outside the area of the target volume (such as the edge of a shoulder in the lateral beams of a head and neck treatment, as previously discussed).

FOCUS bases its transmission array on the ratio of "flat" to uncompensated dose at the compensation plane in the actual patient [CMS]. Here "flat" dose corresponds to the dose in a homogeneous, flat phantom described above. The function of the transmission array is shown in Figure 1-14.

At the compensation plane distance, an irregular grid of points, (i,j), perpendicular to the central axis is established by tracing the diverging fanlines from the Cartesian grid set up by FOCUS on the compensator to the compensation plane. For each point, the transmission required to produce the flat dose distribution is given by

$$T(i,j) = \frac{D_{flat}(i,j)}{D_{uncomp}(i,j)} \quad (1\text{-}3)$$

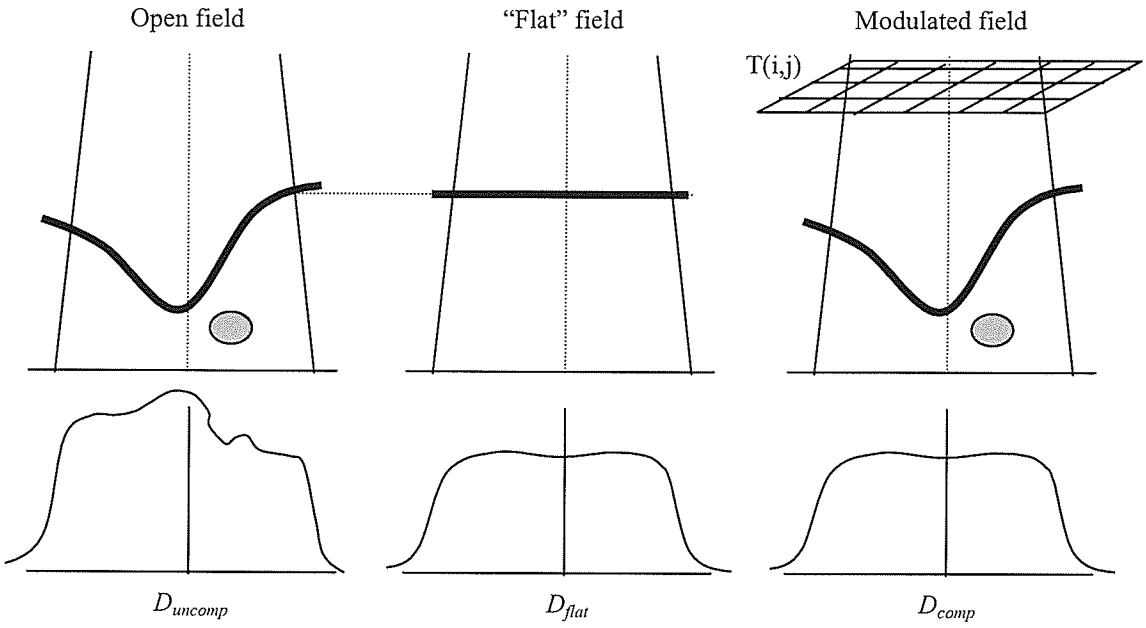

Figure 1-14: Action of the transmission array on the open field. The transmission array is generated such that the open field dose, D_{uncomp}, is transformed into the dose deposited by the same beam incident on a homogeneous flat phantom at the high point SSD, D_{flat}.

If any part of the compensation plane lies in the build-up region, its uncompensated dose will be assigned the value of the dose at d_{max}. The transverse coordinates of the transmission values calculated in equation (1-3) are then scaled along the diverging fan lines back to the compensator tray distance, s_{CT}. This method of design is very fast as it requires only two calculations per point at the compensation plane. The resulting unnormalized transmission array in equation (1-3) is then normalized to the transmission at the high point, with any value greater than 1.0 being truncated to 1.0. Finally, since the modulation in this case is performed by a compensating filter, the normalized transmission array is converted into an array of compensator thicknesses, $t(i_{CT},j_{CT})$, through

$$(1\text{-}4) \quad t(i_{CT}, j_{CT}) = -\frac{\ln(T_{norm}(i_{CT}, j_{CT}))}{\mu_f^{eff}}$$

where (i_{CT},j_{CT}) is the position of the point (i,j) retracted to the compensator tray distance.

1.7.2.5 Dose calculation in the compensated field

FOCUS calculates the dose in the compensated field by including an additional correction factor, $CMPFAC(x,\theta)$, dependent on the transverse radial distance, x, and angle with respect to the x-axis, θ. $CMPFAC(x,\theta)$ is the fraction of primary fluence transmitted through the compensating filter along each fanline. Note that in the FOCUS version 2.6.3 Clarkson algorithm, the effect of the compensator in the path of the beam is simply an exponential reduction in the primary fluence based on the effective attenuation coefficient of the filter material. Scatter radiation originating in the compensator and reaching the patient is not explicitly modelled. The latest versions of FOCUS (starting with v. 2.7.0) incorpate more sophisticated modelling of beam hardening and scattering in the compensator in their newer algorithms [CMS 01].

1.8 Compensator quality assurance (QA)

Compensators are individually designed for each beam on any compensated treatment. Since the design and fabrication are completely independent procedures (and most often performed by different personnel) the potential for errors in the compensator process can become a significant issue. The traditional checks performed on clinical compensators typically involve a few thickness measurements at a small number of

points and a visual comparison with the original design. Thus, only a small portion of the compensator is checked quantitatively. Rarely is the accuracy of the design itself examined. At some centres, the general practice is to design a compensator for a "test" phantom and measure the dose in the phantom at the compensation plane [Ch 93]. However, this method tests both the design and fabrication at the same time leaving the user unsure as to which of the two may be responsible for any discrepancies. Furthermore these tests are performed during commissioning of the compensator system and then only periodically afterwards.

Several authors have discussed methods of performing more comprehensive QA on the fabrication of the compensator. Taking a transmission image of the compensator with film [Ch 93] and more recently an electronic portal imaging device (EPID) have both been applied. Low et al [Lo 96] described a method of verifying compensator thicknesses by comparing the fluence measured by an EPID with a theorectical fluence map generated by separating the fluence into primary and scattered components and convolving each with a spatially invariant geometric kernel. Pasma et al [Pa 99] applied a similar technique with a simpler fleunce model based on measured transmissions through the absorber material. The latter group could determine a brass compensator thickness to an accuracy of 0.5mm (1 s.d.). Unfortunately, these techniques often require complex theoretical modeling, making it a lengthy procedure to implement them clinically. We have adopted a more simplified and direct technique of verifying the fabrication. The compensator is imaged in treatment position with a calibrated step wedge composed of the same material. The images can be acquired via either a radiographic film or an EPID, although only results using film are presented in this

report. In the resultant digitized images the pixel intensity at the known thicknesses of compensator material in the step wedge are used to generate a calibration curve for converting pixel intensity to compensator thickness. The calibration is then subsequently applied to each pixel in the image to produce a map of thickness in the compensator.

The above techniques possess no means of independently checking the design of clinical compensators on an individual basis prior to their use in treatment, where for a complex patient geometry the design algorithm may have failed. In the present work, we have adapted a procedure for reconstructing the patient contour from the 2D array of compensator thicknesses exported by our treatment planning system. For those compensators designed for missing tissue only, we then directly compare the reconstructed transverse slices with the original CT slices from the simulation. This provides a completely independent check of each compensator design.

2 Materials and Methods

In this chapter, the methods involved in implementing and testing the compensator process are discussed at length. Technical aspects of the fabrication process are presented along with the additional resources which are required beyond the 3D treatment planning system. The series of experiments used to test the compensator process, along with the dosimetry tools required is also detailed. Finally, the philosophy of a complete compensator QA program is argued, along with a description of the QA procedure which has been developed to complete the compensator process.

2.1 Measurement of μ_f^{eff}

As mentioned in Chapter 1 (Section 1.7.2.1), the linear attenuation coefficient of a compensator material will vary with depth in the patient, compensator thickness and field size. However, FOCUS does not account for these effects in its compensator design algorithm, instead adopting a constant value for the linear attenuation coefficient, independent of depth, filter thickness and field size. Because of this approximation, the attenuation is said to be described by an "effective" linear attenuation coefficient, μ_f^{eff}. Figure 2-1 shows the linear attenuation coefficient of Pb measured as a function of depth at our institution [An 01]. The measurements were done at 6MV for a 10 × 10cm field at an SSD of 100cm.

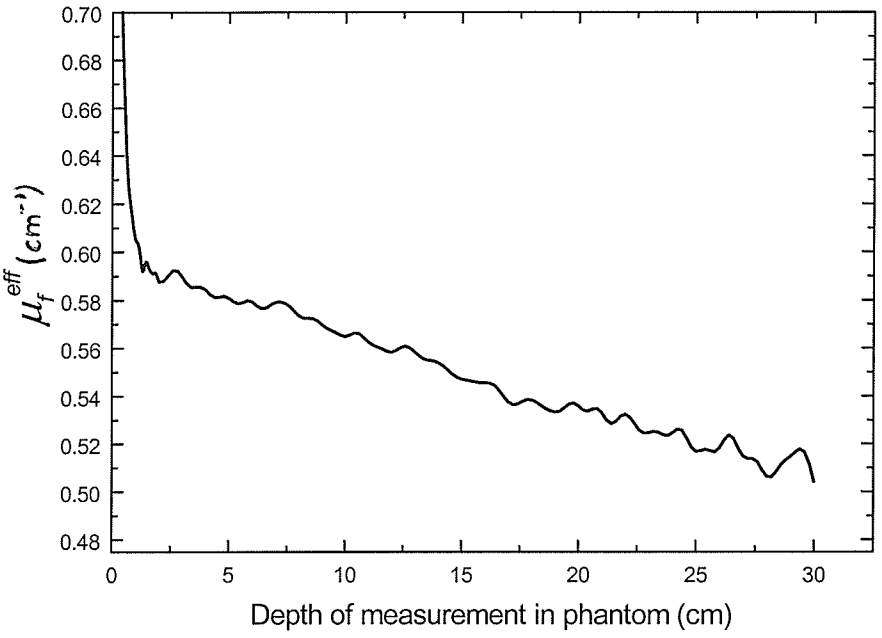

Figure 2-1: Central axis measurements of the effective linear attenuation coefficient of Pb as a function of measurement point depth in a water phantom. The decrease with depth is due to beam hardening in the phantom.

The attenuation coefficient was measured using a 3.6mm thick Pb plate placed on the compensator tray in the head of the treatment unit, and applying

$$\mu_f^{eff}(d) = \frac{-\ln\left(D_t(d)/D_O(d)\right)}{t} \qquad (2\text{-}1)$$

where D_t and D_O are the doses measured with and without the Pb plate, respectively. It is not uncommon for the depth of the compensation plane to vary by 10cm over a treatment field, over which Figure 2-1 shows that a large variation in μ_f^{eff} will occur.

Following the FOCUS recommendations, μ_f^{eff} was measured at an SSD of 100cm, a depth of 5cm and a surface field size of 10 × 10cm, using a thimble-type ionization chamber in a flat solid water phantom. The ionization charge was measured during 100MU exposures, using 3 Pb plates of thickness 1.9, 2.6 and 4.9mm, which adequately covers the range of thicknesses encountered in a typical compensator. The charge as a function of Pb plate thickness was least squares fit to a single exponential of the form

$$y = A\exp(-\mu_f^{eff} t) \quad (2\text{-}2)$$

using the Levenberg-Marquardt algorithm in Microcal ORIGIN™ data processing software [ORIG]. The charge measurements as a function of Pb plate thickness along with the fit is plotted on a natural log scale in Figure 2-2. The data is described well by a single exponential, however, the fact that all the points do not lie on the least squares fit line shows that μ_f^{eff} is variable, due to changes in scatter and beam hardening in the compensator. The resulting value for the effective linear attenuation coefficient was $\mu_f^{eff} = 0.59 \pm 0.02\text{cm}^{-1}$, where the uncertainty quoted represents the standard error of μ_f^{eff}. This value was used by FOCUS for the compensator design, and is also used to verify the design and fabrication as a part of the QA outlined in Section 2.5.

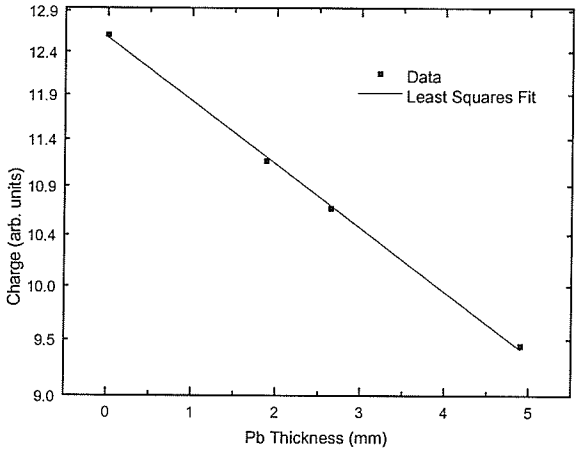

$$SSD = 100\text{cm}$$
$$r = 10 \times 10\text{cm}$$
$$d = 5\text{cm}$$

$$\mu_f^{eff} = 0.59 \pm 0.02\text{cm}^{-1}$$

Figure 2-2: The measurement of the effective linear attenuation coefficient was performed with a variety of compensator thicknesses in order to average the effects of beam hardening and scatter in the compensator. The dose measured at 5cm depth as a function of Pb thickness was fit to a single exponential decay with a decay constant of $0.59 \pm 0.02\text{cm}^{-1}$. Note that the error bars in both thickness and dose are completely encompassed by the size of the data points.

To illustrate the slight dependence on field size, the measurements were repeated for 5 × 5 and 20 × 20cm fields (Figure 2-3). Although the decrease in μ_f^{eff} appeared evident, it could not be fully confirmed, as the differences were all within the error bars on each measured value of μ_f^{eff}.

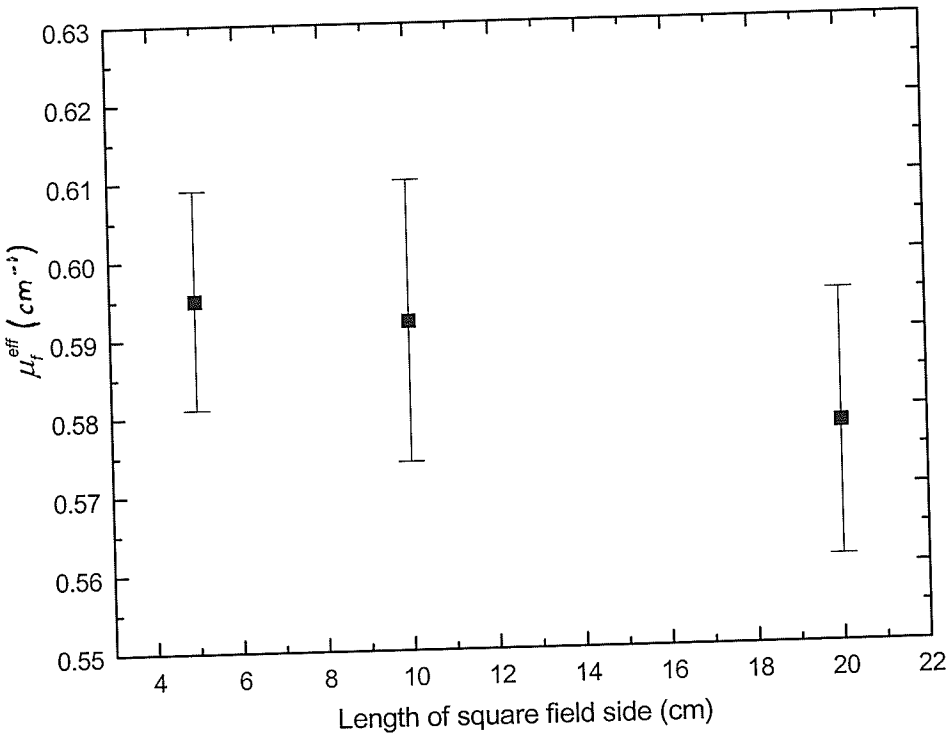

Figure 2-3: Measurements of the effective linear attenuation coefficient of Pb as a function of field size, using the same experimental setup discussed above. The data appears to show the expected decrease with increase in field size, however the error bars on each point are too large to make any definite conclusions.

2.2 Compensator Fabrication

The compensator file exported by FOCUS contains a 2D array of compensator thicknesses in ASCII file format. The file structure is formatted to be read directly by a commercially available milling machine that is dedicated to compensator fabrication (Huestis, inc.). We have developed an interface program which converts the file to EIA RS-274/ISO 1056 format which can be read by a computer numerically controlled (CNC) milling machine. One obvious advantage of the CNC over a dedicated machine is that it can be used for other projects when not fabricating compensators.

2.2.1 Selection of compensator material

Several authors have reported on a variety materials used for fabricating compensators. Ansbacher et al [An 92] evaluated a commercial planning system's compensator package using filters constructed of paraffin wax, tissue-equivalent wax, Cerrobend and a gysum/steel granulate mixture. They found that the differences in uniformity at the compensation plane for all of the different filter materials was around 1% or less. Van Santvoort et al [VS 95] described a number of conditions to be fulfilled for the production of compensators. They suggested the use of a medium density material. This avoids the elevated transmission sensitivity of a high density compensator, where small errors in thickness may result in large errors in compensator transmission as a result of the large attenuation coefficient of the material. Furthermore, it avoids the bulkiness of a low density compensator, which is difficult to accommodate in the accelerator head. They also stressed the need for a compensating material to be reusable in order to save in the overall long term cost of the program. In this regard, they indicated the use of a stainless steel granulate, which is poured into a milled styrofoam mould. However, attaining a consistent mould pour is difficult in practice. Brass and aluminum have also been used as medium density compensator materials [El 59]. Their rigidity is highly desirable from the milling perspective, and their attenuation coefficients at 6MV (approximately $0.36cm^{-1}$ for brass and $0.12cm^{-1}$ for aluminum) keep their sizes manageable compared to tissue equivalent compensators, but relatively large compared to Pb compensators. However, they both have a very high melting point (927°C for brass and 659°C for aluminum [OSU]), which makes their ability to be recycled highly

impractical. Thus, the use of one of these materials can become quite costly for a radiation therapy program over time.

As previously mentioned, at our institution we use Pb compensators doped with a small fraction of antimony (<2% by mass) are used. This small fraction of antimony may alter the attenuation coefficient by only approximately 0.01% [NIST]. The purpose of the antimony is simply to harden the Pb, rendering it easier to machine. The compensator plates were assumed to be homogeneous, with a constant ratio of lead to antimony. The validity of this approximation was tested by measuring transmission factors for seven different compensator plates milled to the same thickness (5.7mm). The measurements were performed along the central axis of a 10 × 10cm field at an SAD of 100cm and a depth of 1.5cm (d_{max}), using an ionization chamber in a solid water phantom. The standard deviation of the resulting transmission factors was only 0.4%.

The choice of Pb is favourable as the resulting small compensator thicknesses make them easy to mount on the patient side of the block tray. Furthermore, since Pb has a low melting point (216°C), at the end of a patient treatment the Pb compensators are melted down and recycled into new compensators. The elevated transmission sensitivity that is inherent in using such a high density compensator material must be combated by an accurate fabrication procedure. It will be shown that the accuracy of the milling procedure is about 0.2mm, which corresponds to only a 1.2% change in x-ray transmission.

2.2.2 Setup on the mill

Critical to the proper utilization of a compensator in a patient's treatment is the accurate alignment of the compensator in the treatment field. This step is often done by manually aligning cross-hairs scribed on the compensator tray after fabrication with the central axis cross-hairs scribed on the block tray. Although this technique is probably accurate to about 1-2mm, there is still a significant margin for error including gross mistakes such as mis-aligning axes on the compensator and block tray (for example, matching the x axis of the compensator to the y axis of the field). To avoid such errors we have designed a standard compensator tray, large enough to accommodate a compensator designed for up to a 32 × 32cm field at isocenter, which mounts into a special fixture on the CNC in only one possible orientation. This fixture mimics the block tray with a set of four tapped holes, which secures the compensator to the bottom of the tray. One of the holes is offset, such that the compensator tray can only be mounted on the fixture (and later on the block tray) in a single orientation. All of the cutters used in compensator fabrication are referenced to the center of this fixture, which coincides with the central axis of the treatment beam, and stored in a library in the CNC memory. The pre-milled Pb is oversized (larger than the treatment field at the compensator distance) and fixed to the compensator tray prior to milling. As a result, the milling procedure determines the position of the compensator in the treatment field and the manual task of fixing the Pb to the compensator tray has essentially no impact.

2.2.3 Interface program

The compensator interface program is a translator between FOCUS and the CNC. There are several different approaches that can be taken in milling the compensator and these details are found in the interface program. Our technique consists of two stages; a prepping stage and the compensator milling stage. In the prepping stage, a 1″ end mill cleans the Pb plate off to the largest thickness in the 2D array, in order to avoid excess cutting by the finer resolution tool used in the compensator milling stage. In the second stage a 1/8″ (3.2mm) end mill traverses a raster path over the area of the compensator, following the contour described by the 2D thickness array contained in the FOCUS file (Figure 2-4). The cutting is done in a series of passes, with the end mill

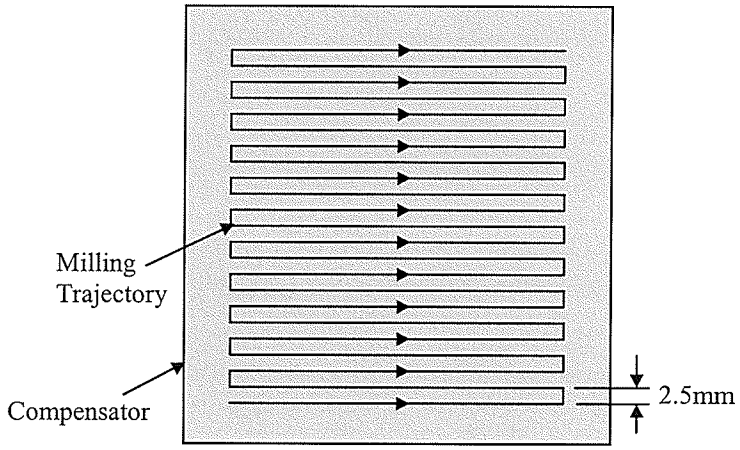

Figure 2-4: Top view of compensator on the mill, showing the raster path traversed by the cutter in the compensator milling stage.

stepping down in the z (thickness) direction by 1mm decrements down to the final thickness. As such, the end mill never cuts more than 1mm during any pass. This approach is adopted because of the malleability of the Pb. Attempting to clear too much

material in one pass causes the tool to clog and simply push the Pb, rather than cut it cleanly. Since the end mill has a finite diameter, its size must be taken into account during the cutting process. To include this effect, the program recognizes that the cutter should be cutting on its leading edge when moving up an incline and shifted to cut on its trailing edge when proceeding down a decline, with linear interpolation between the points (Figure 2-5). Failure to include this correction results in cutting the compensator to less than the desired thickness (shown by the dashed line in Figure 2-5). Simultaneously the cutter is cutting on center in the *y* direction. The entire milling procedure (including approximately 5 minutes for setup) takes about 15 minutes for a typical head and neck compensator.

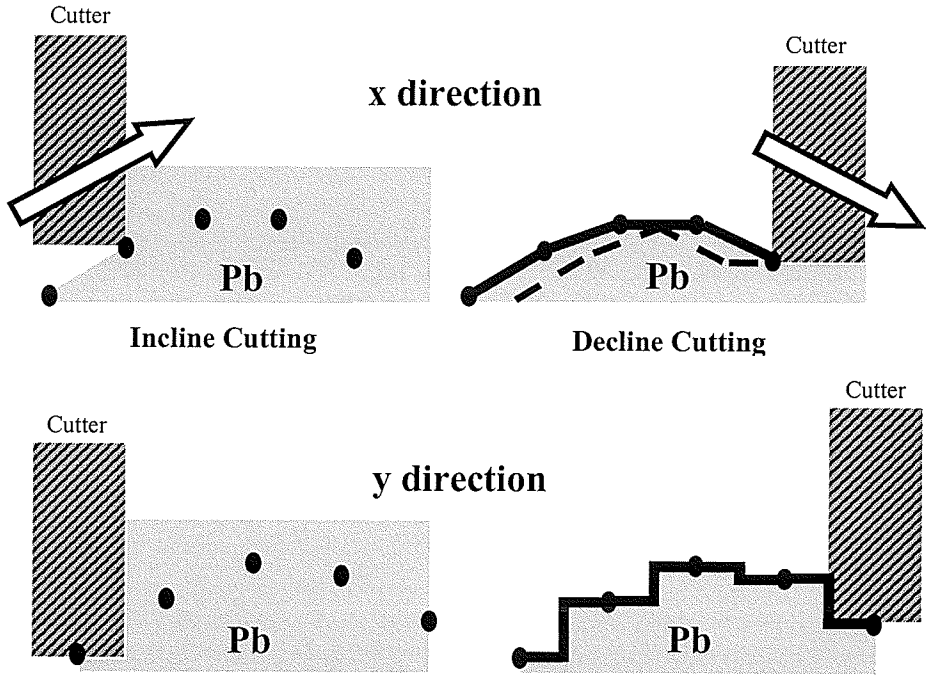

Figure 2-5: In the *x* direction, the interface program shifts the cutter during the milling procedure to cut on its leading edge when moving up an incline, and on its trailing edge when moving down a decline. The thick black line joining the compensator points defines the surface contour milled in this direction, which appears to be the most accurate representation of the compensator points, neglecting any higher order interpolation. If the tool were cutting on center, with no compensation for the end mill diameter, the contour defined by the dashed line would be cut instead. In the y direction, perpendicular to the direction of cutter motion, the bit is cutting on center, which carves out an Ellis type filter as shown.

The resolution of the points in the thickness array, contained in the FOCUS compensator file, was 2.5mm. Therefore, by milling with a 3.2mm end mill we over cut by 0.35mm on both sides of the cutter in each pass, which helps to maintain a clean finish on the compensator. We found this sufficient resolution to provide accurate compensation for a variety of geometries to be discussed below. The FOCUS compensator file contains thicknesses past the collimator limits, out to the maximum scope of the beam fan lines (typically a 40 × 40 field size at isocenter). However, thicknesses outside of the region where the primary dose is less than 90% of the primary central axis dose have been truncated as discussed in Section 1.7.2.3. In our milling procedure, the transverse compensator limits are defined by first rounding up the geometrically retracted field edge to the nearest compensator point in the FOCUS export file, and then adding a 7.5mm margin. Here, the retracted field size, r_{CT}, is calculated using,

$$r_{CT} = \left(\frac{s_{CT}}{s_{CP}} \right) r_{CP} \quad (2\text{-}3)$$

where r_{CP} is the field size at the compensation plane. For a typical compensation plane distance (100cm), this corresponds to the compensator being milled at least 1.3cm past the geometrical field boundary. Thus the compensator does not interfere with the standard practice of shifting field edges in the join up region of matched fields (since these shifts are usually at most 1cm). An additional margin of at least 7mm is also present around the milled portion of the compensator, which is maintained at the compensator high point thickness (from the prepping stage). This margin serves two

purposes. First it gives the technicians some leeway when placing the Pb plates on the compensator tray prior to milling, and secondly it provides additional shielding around the field.

2.2.4 Accuracy of the milling procedure

The accuracy of the milling procedure was determined by comparing the thicknesses in the FOCUS compensator file with independent measurements performed on the CNC. The CNC measurements were done with a spring loaded probe mounted in the tool chuck. The zero thickness was referenced by lowering the probe onto the compensator tray until the gauge on the probe displayed a reference reading, R_0. At this location, the z reference position on the CNC was set to zero. The thickness at a given location in the compensator was then determined by slowly lowering the probe onto the compensator until the gauge regained the reference reading, R_0 (Figure 2-6).

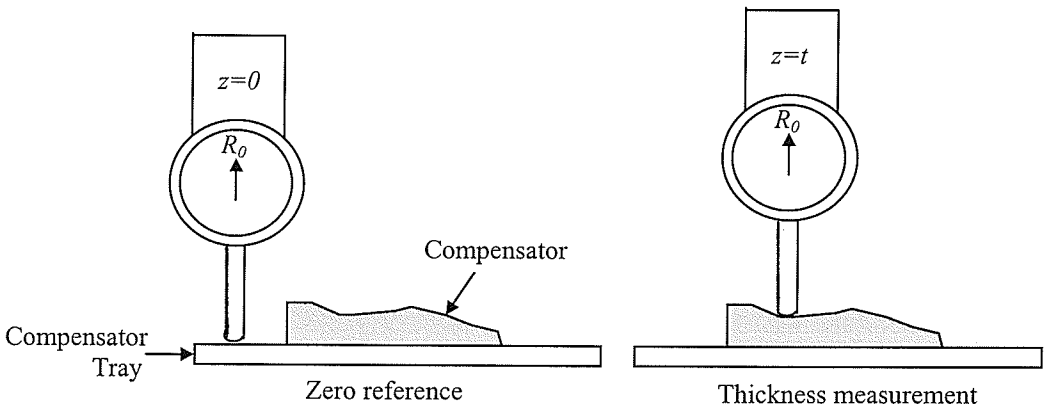

Figure 2-6: Setup for measuring the thickness of the compensator at a given point using the CNC.

The latter CNC z position then corresponded to the thickness of compensator, t, at that point. The uncertainty associated with each thickness measurement was 0.1mm, due to physically measured fluctuations in the thickness of the plastic compensator tray.

Thickness measurements were performed at 9 interest points on each of the 6 compensators used in the experiments described in Section 2.3. The points are shown in Figure 2-7, where w and l are the full width and length of the compensator, respectively, and the coordinate origin is located at the geometrical center of the compensator.

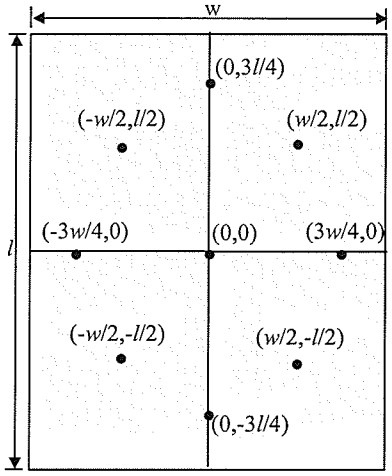

Figure 2-7: Locations of the 9 interest points on the compensator. The thickness measured using the CNC probe at these locations was compared to the corresponding thicknesses in the FOCUS compensator file, to examine the accuracy of the milling procedure.

2.3 Dosimetric verification of compensators

A series of experiments were designed to test the ability of FOCUS to accurately design compensators for a variety of phantom geometries. These experiments ranged from simple surface contours on homogeneous phantoms, to an anthropomorphic phantom. For each phantom geometry, a single dose profile within the compensation plane containing the largest degree of non-uniformity was measured and analyzed. The dose along this profile as predicted by FOCUS was found by specifying interest points at

the corresponding coordinates on the phantom data set. Interest points are points for which FOCUS will explicitly calculate and print the dose. These interest point doses were then compared to the measured doses at the same locations in phantom, measured by either film or an ionization chamber. Comparisons were made for both the open and compensated fields. All experiments were performed at a photon energy of 6MV using a Siemens MX2 linear accelerator.

2.3.1 Experiment 1: Ramp phantom

The first experiment was designed to test FOCUS's ability to construct a compensator to account for a simple surface contour. A 45° ramped phantom was generated by placing a 10 × 10cm field at an SSD of 100cm on the center of the surface of a horizontal water phantom with a gantry angle of 45° (Figure 2-8). The compensation plane was placed at a 10cm depth on the central axis.

The dose profile was measured along the x axis as shown in Figure 2-8, with a thimble-type ionization chamber driven on motorized stages (see section 2.4.1).

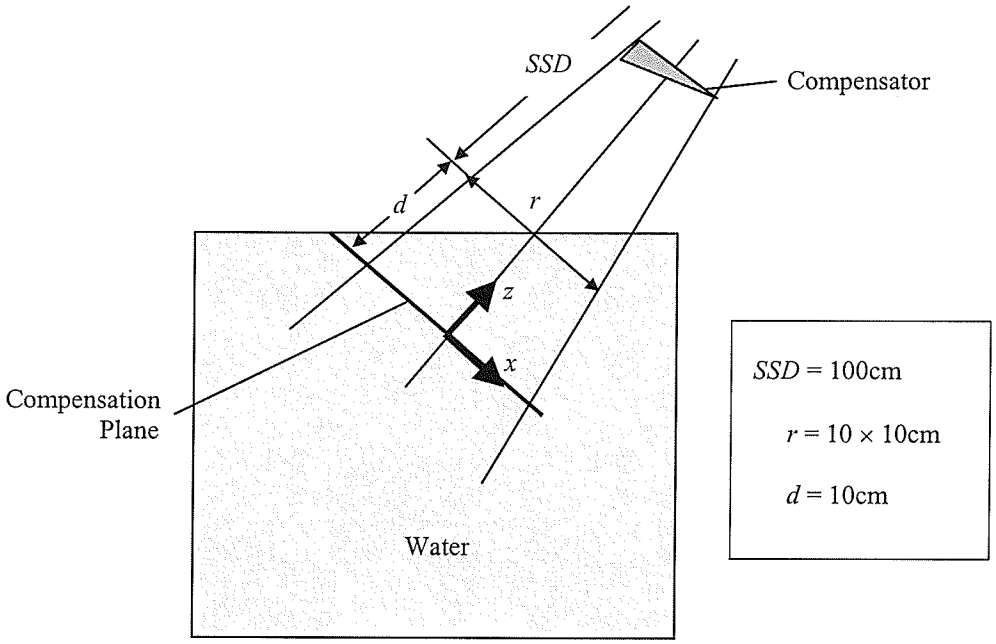

Figure 2-8: Experimental phantom geometry used in experiment 1.

This phantom was manually drawn in FOCUS by tracing a scaled blueprint of the water tank with a digitizing tablet. The tablet sampled points at a rate of 1 point per 5.0cm. A single transverse slice was drawn and subsequently copied at 1.0cm intervals to other transverse slices in order to complete the 3D geometry of the water tank. FOCUS then interpolates the data to transverse slices 2mm thick and 2mm apart. Dose calculation points that did not fall onto one of these interpolated axial slices, are assigned the dose at the corresponding transverse position on the nearest neighboring slice. Beam geometry was set up to mimic the phantom measurements and interest points were defined along the x axis. 200cGy was prescribed to the point where the central axis intersected the compensation plane.

2.3.2 Experiment 2: Cork inhomogeneity phantom

The water tank described in the ramp phantom study was used in a second experiment designed to test the ability of FOCUS to compensate for an internal inhomogeneity. A similar experiment was used by Basran et al [Ba 99] to test the Helax 3D planning system's heterogeneity compensation. An irregularly shaped piece of cork was suspended 4cm below the surface of the water and a compensator was designed to negate the effects of the cork at a depth of 13.0cm (Figure 2-9). The cork was 13.8cm wide with a maximum thickness of 4.9cm and a radius of curvature of 50cm on its curved surface. An adjustable frame was constructed, which attached to a wall of the water tank and firmly held the cork below the surface of the water. The frame never came within 5cm of the field edge as indicated by the light field. The depth and level of the cork was checked by measuring the distance from the cork to the surface of the water at several locations along its length. Adjustments were made until the maximum deviation between these measurements was less than 1mm. An SSD of 100cm, a field size at the surface of 15 × 15cm and a gantry angle of 0° were used for this experiment. Again, an ionization chamber was used to sample the isodose distribution and the profile along the x-axis at the compensation plane.

The phantom was drawn on FOCUS in a similar manner as the water phantom described in experiment 1. The electron density of the cork was determined by CT scanning it in a bucket of water with a Siemens SOMATOM Plus 4 CT scanner. The CT slices were passed through a calibrated conversion from CT number to electron density based on the CT numbers of materials of known electron density. The electron density of the cork was found to be $\rho_e = 0.24 \pm 0.04(\text{max.dev.})$ relative to water. In treatment

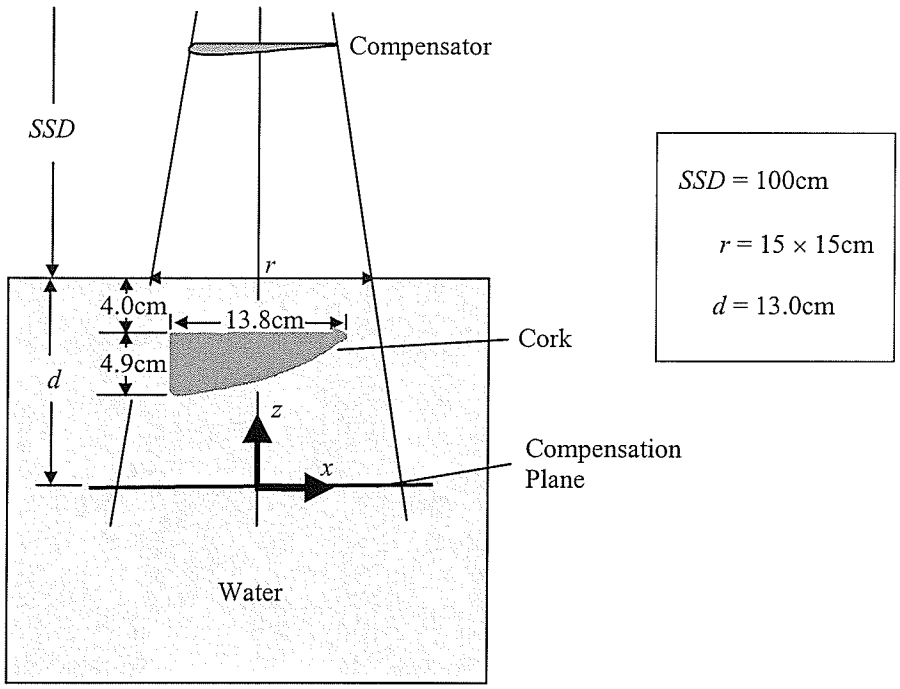

Figure 2-9: Experimental phantom geometry used in experiment 2.

planning this experiment, a bulk density of 0.24 relative to water was assigned to the cork inhomogeneity. As before, beam geometry was reproduced and interest points were placed along the compensation plane, and 200cGy was prescribed to the point where the central axis intersected the compensation plane.

2.3.3 Experiment 3: Anthropomorphic phantom

Experiments 1 and 2 were designed to independently observe FOCUS's ability to compensate for surface contours and internal inhomogeneities. In experiment 3, we examined the design of a compensator for a heterogeneous phantom with a surface contour. The phantom was constructed by filling a plastic female chest immobilization

cast with wax, and adding additional cork and plaster inserts to simulate lung and hard bone respectively. The inhomogeneities were elliptical cylinders with a thickness of 4.7cm, and semi-major and minor axes lengths of 16cm and 14cm, respectively (Figure 2-10).

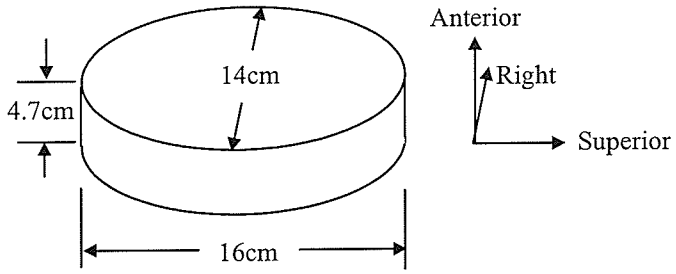

Figure 2-10: Illustration of the shape of the two inhomogeneities placed in the anthropomorphic phantom.

They were placed 3.2cm below the anterior surface of the phantom (along the central axis), posterior to the breasts, with their semi-major axes aligned in the superior inferior direction. The phantom was CT scanned and the images downloaded to FOCUS to yield the required 3D geometry and electron density information. Five millimeter slice thickness and spacing were used in the CT acquisition. Electron densities of the cork and plaster relative to water, as determined from the CT number to electron density conversion file in FOCUS, were 0.24 ± 0.04 (max. dev.) and 1.39 ± 0.04 (max. dev.), respectively.

The plane of compensation was chosen at a depth of 11.4cm along the central axis of the beam at a SAD of 100cm. The field size at the SAD was 15 × 15cm. The dose distribution at the compensation plane was measured by sandwiching a film between the phantom and a 5cm thick block of wax, the latter providing backscatter to the film.

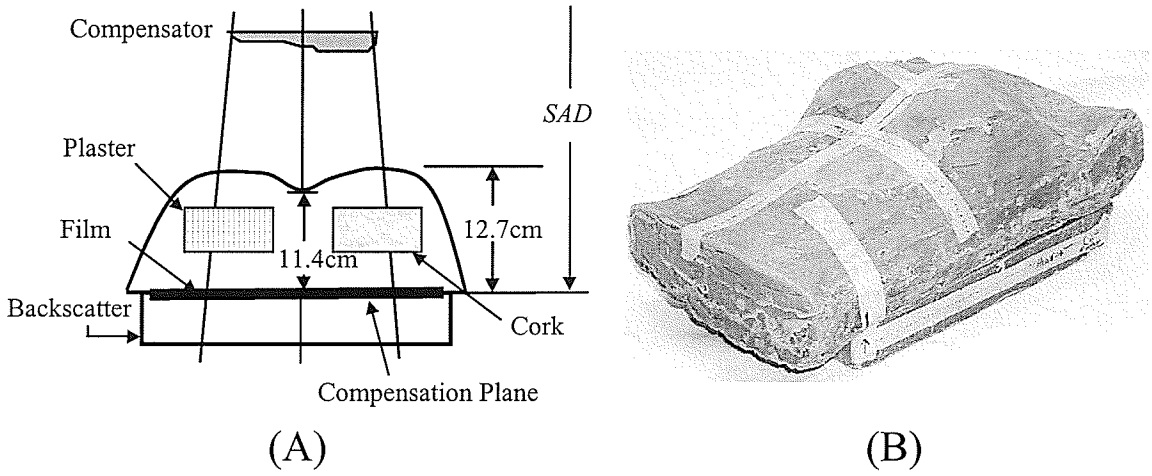

Figure 2-11: Geometry of the anthropormorphic phantom used in experiment 3. **(A)** Transverse section through the phantom. Two cylindrical inhomogeneities were placed at depth in the wax phantom and a compensator was designed provide a uniform dose at the SAD of 100cm. **(B)** Photograph of the phantom.

Figure 2-12 shows the location of the profile with respect to a coordinate system on the compensation plane, with its origin on the central axis of the beam. A dose of 100cGy was prescribed to isocenter in FOCUS.

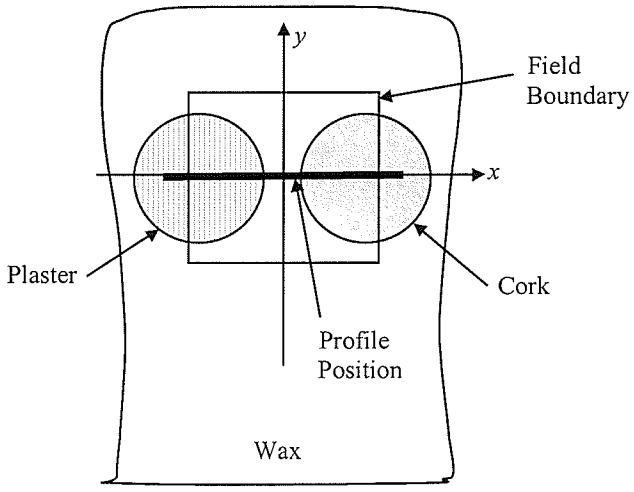

Figure 2-12: Anterior beam's eye view of the anthropomorphic phantom to illustrate the locations of the inhomogeneities with respect to the beam central axis. FOCUS calculations and measurements were compared at points spaced 2mm along the *x* axis, which exhibited the most non-uniform dose distribution in the open field.

2.3.4 Experiment 4: Clinical trial A; Head and neck phantom

The most common treatment site employing compensators at our institution is the head and neck region. This treatment typically involves two stages. The first consists of two lateral half-blocked parallel opposed beams which typically treat the primary tumor, and involved neck nodes. Missing tissue compensators are used to remove the effects of the highly variable surface contour in the neck and jaw regions.

The goal of this experiment was to test FOCUS's capacity to design missing tissue compensators in two-field head and neck treatments. A plastic head and neck patient immobilization cast was filled homogeneously with wax. The phantom was sliced sagitally along the midline and a film was sandwiched between the two halves (Figure 2-13). Parallel opposed asymmetric fields were positioned with their common isocenter at the plane of the film, where the compensation plane was defined.

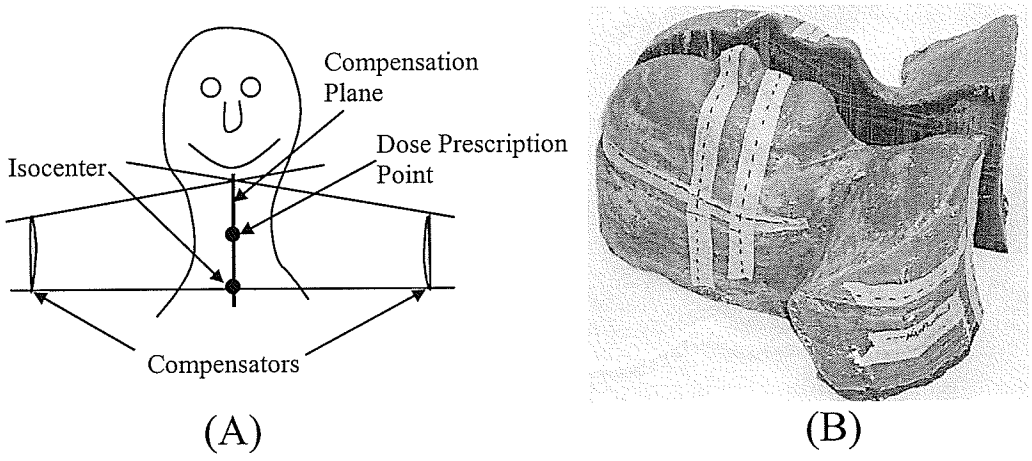

Figure 2-13: Experimental setup for experiment 4. (A.) Two beam lateral beam arrangement positions. (B.) Photograph of the phantom.

The treatment parameters are summarized below:

Beam 1 (right lat)	*Beam 2 (left lat)*
SAD = 100	*SAD* = 100
Gantry = 270°	Gantry = 90°
Asymmetric field size at SAD (cm)	Asymmetric field size at SAD (cm)
Posterior = 5.0 Anterior = 10.0	Posterior = 5.0 Anterior = 10.0
Foot = 0.0 Head = 15.0	Foot = 0.0 Head = 15.0

Prescription dose to geometric center of the compensation plane = 100cGy

Note that FOCUS designs the compensators independently for each beam. The location of the dose profile where FOCUS and the measured data were compared is shown in Figure 2-14.

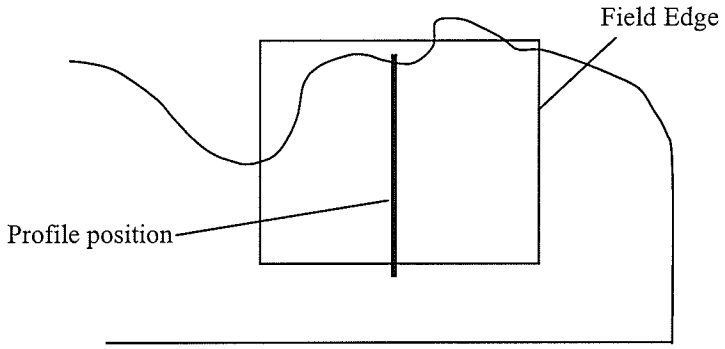

Figure 2-14: Saggital slice down the phantom midline, to illustrate the location of the dose profile where FOCUS and the measured data were quantitatively compared.

2.3.5 Experiment 5: Clinical trial B; Mantle phantom

Another clinical location for which compensator use is desirable is the superior portion of a mantle field due to the large variation in the patient's surface contour in this region. The same phantom used in experiment 4 was sliced in a coronal plane and a film

was sandwiched between the two halves for this experiment. A single anterior field at an SAD of 100cm was positioned on the phantom such that the beam isocenter was in the plane of the film (at a depth of 9.2cm along the central axis). The field size at the SAD was 15 × 16cm and a dose of 100cGy was prescribed to isocentre. A measured dose profile in the compensation plane along the *x* direction but offset from the central axis by 2cm was compared to that predicted by FOCUS (Figure 2-15).

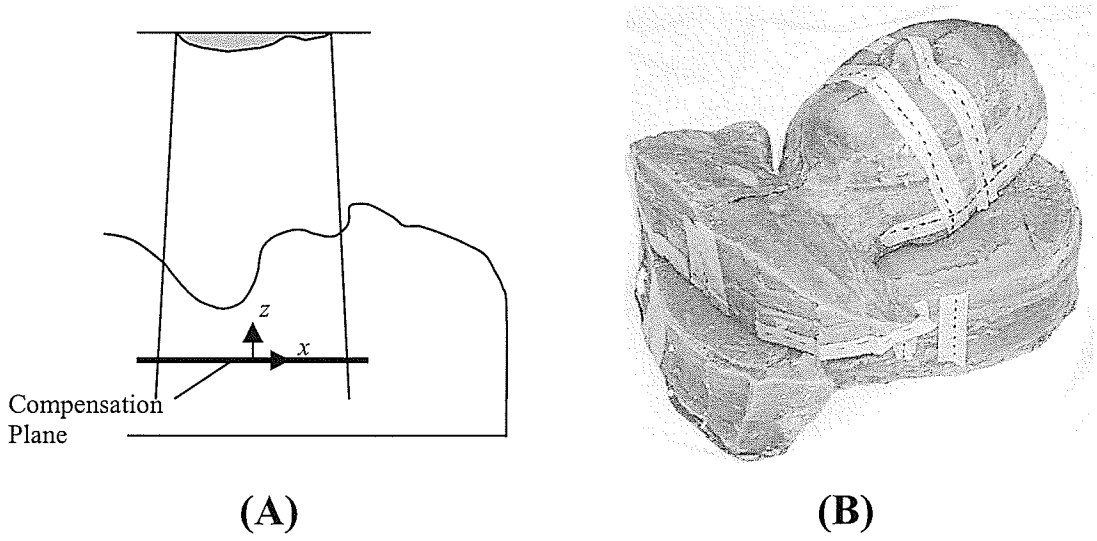

Figure 2-15: Experimental setup for experiment 5. (A) AP field. (B) Photograph of the phantom.

2.4 Dosimetry

In this section, the ionization chamber/electrometer dosimetry used in experiments 1 and 2, and the film dosimetry used in experiments 3-5 will be described.

2.4.1 Water tank/Ionization chamber

Experiments 1 and 2 utilized a beam scanning water tank (PTW Freiburg MP3-S, # 41002-0037). The tank has inner dimensions 50 × 59 × 50cm (Figure 2-16). It

contains a motorized staging system consisting of a chamber mounting platform driven on threaded stainless steel rods in three dimensions. Two thimble-type ionization chambers (PTW Freiburg, M-31002-0423) each with a sensitive volume of 0.125cm^3 were used in the experiments. The data chamber was mounted on the motorized platform which could be driven along the x, y, or z axes under computer control in 0.1mm increments.

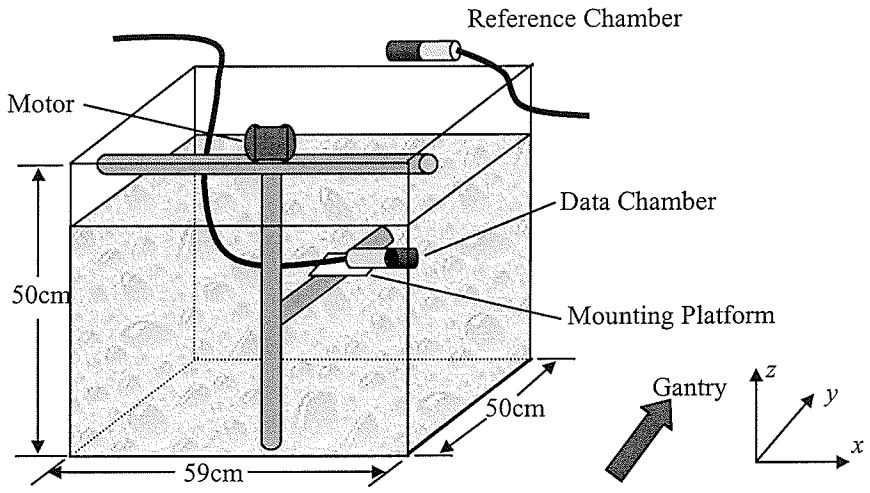

Figure 2-16: Geometry and orientation of the water tank used in experiments 1 and 2.

A second ionization chamber was placed in air, in the corner of the field, upstream of the phantom, to be used as a reference chamber for the relative dose measurements. Here, incoming measurements from the data chamber were divided by measurements taken simultaneously by the reference chamber in order to remove the effects of fluctuations in the accelerator output, and changes in the air density in the data chamber. Both ionization chambers were linked to an electrometer (PTW Freiburg, # 41004-0038) via coaxial cables, and operated at 400V. The external gain and polarity settings on the

electrometer were kept constant throughout the experiments. The electrometer, which also houses the electronics to drive the motorized stages, was interfaced to a computer running MEPHYSTO v.6.3 beam scanning software. The software allowed easy manipulation of the data chamber position in pre-defined patterns, such as depth dose curves, and profiles.

Accurate alignment of the data chamber in the radiation field is critical to the evaluation of the performance of the compensators in these experiments. After the tank was leveled, the SSD along the central axis was set using the optical distance indicator on the linac. The chamber was then centered in the *x-y* plane using the light field and in the *z* direction using the surface of the water. The chamber could be moved 0.3mm from the reference position along any of the axes before it was visually clear that it had been dislodged from center.

2.4.1.1 Measurements

Measurements of the dose profile at the compensation plane were performed for both the open and compensated fields. The relative dose profiles were measured using the vector scan option, which scans a profile in any user defined direction in 3-space. Here, a 0.5mm spacing between points was chosen.

2.4.1.2 Calibration

The dose profiles in experiments 1 and 2 were measured using the vector scan option in Mephysto. These measurements, however, are of the relative dose to the water phantom, as the chamber pauses at each position along the profile and collects charge

liberated through ionization events for constant time (0.3s). To subsequently convert the measured relative dose distribution to an absolute dose distribution, the following procedure was applied.

Our institution applies a modified TG 21 protocol for calibrating linear accelerators [TG 21]. The 6MV beam used in the experiments, was calibrated to deliver 1.000cGy per monitor unit (MU) on the central axis at a depth of 1.5cm, an SAD of 100cm, and a field size at depth of 10 × 10cm. During the series of measurements, this calibration geometry was setup and a point dose measurement was made at the calibration point. The total liberated charge, Q_{cal}, in the chamber for a 200MU exposure was collected, by setting the integration time on the electrometer to be larger than the total exposure time. This measurement was corrected for changes in air density in the chamber using,

$$(2\text{-}4) \quad Q'_{cal} = Q_{cal}\left(\frac{760.0}{P}\frac{(273.2+T)}{295.2}\right)$$

where P is the atmospheric pressure measured in mmHg, and T is the temperature of the water in °C. The corrected measurement of integrated charge, Q'_{cal}, was proportional to a dose of D_{cal} = 200cGy, and hence the conversion factor, C_{cal}, from charge to dose could be generated,

$$(2\text{-}5) \quad C_{cal} = \frac{Q'_{cal}}{D_{cal}} \qquad [\text{nC/cGy}]$$

Next, the chamber was positioned at the dose prescription point on the profile, x_P, in the phantom setup, and the prescription dose was delivered (using the monitor unit setting calculated by FOCUS), while the electrometer collected the total charge, $Q_{abs}(x_P)$, liberated in the chamber during the exposure. Multiplication of the temperature/pressure corrected charge, $Q'_{abs}(x_P)$, with C_{cal}, yielded the absolute dose to the phantom at the dose prescription point, $D_{abs}(x_P)$. Finally, the relative dose measurements, $D_{rel}(x)$, along the profile were converted to absolute dose using,

$$(2\text{-}6) \quad D_{abs}(x) = \frac{D_{rel}(x)}{D_{rel}(x_P)} D_{abs}(x_P)$$

where $D_{rel}(x_P)$ is the relative dose at the prescription point.

2.4.1.3 Uncertainties

The main sources of uncertainty in the chamber measurements arise from fluctuations in the beam output, the electrometer output, and variations in the setup of the entire system. Their cumulative effect was estimated independently for experiments 1 and 2 by setting up the tank and measuring the absolute dose profile at the compensation plane a total of 5 times. The uncertainty in the dose at a point along the profile was assigned the standard error of the mean measurement at that point.

2.4.2 Film dosimetry

Experiments 3-5 used radiographic film as a radiation dosimeter at the compensation plane. Film was desirable in these cases since it could be placed in the phantom with minimal displacement of wax, and sample an entire transverse section of the field in a single exposure.

The film used in the experiments was Kodak X-OMAT™ V Ready-Pack (Eastman Kodak, USA). Each film was 25.4 × 30.5cm, housed in a thin, light-tight paper jacket. The central axis of the beam was referenced by marking the x and y axes on the film with small pin holes. The exposed films were processed with a Konica SRX-101 film processor (Konica Corp., #10527351). This same film was used for routine compensator QA, to be discussed in section 2.5.2.

The profile at the compensation plane was digitized at 2mm intervals with a manual densitometer (Sargent –Welch Model PDD, Cat. No. 3865T, Ser. No. 3300). The unit uses a tungsten-halogen cycle lamp to measure the film optical density through a 1mm aperture [SA 78]. Optical density, *OD*, is defined as

$$OD = -\log_{10} T \quad (2\text{-}7)$$

where T is the transmittance, given by

$$T = \frac{\Phi}{\Phi_0} \quad (2\text{-}8)$$

where Φ_0 and Φ are the flux before and after the light has passed through the film, respectively. The contribution to *OD* made by the film base and fog, was measured on an unexposed but developed film (0.18) and was subtracted from each reading.

Prior to digitizing a film profile, the densitometer was calibrated using a step wedge of 21 known optical densities ranging from 0.05 to 4.05 in steps of approximately 0.2 (Sargent-Welch, Cat. No. 3826A, Ser. No. 506)

2.4.2.1 Calibration

It is well known that the response of film is generally not linear with dose. Therefore, a calibration curve must be generated to convert optical density to absolute dose. This was achieved by exposing 4 films to 4 known doses over a range of doses expected to be encountered in the experiments, and measuring their corresponding optical densities. Typically, if a dose of 100cGy for example, was prescribed to the central axis point on the compensation plane, then calibration films would be taken at doses of 70, 90, 110, and 130cGy. A known dose was delivered to the film by exposing it to a 6MV beam using the beam calibration geometry (as described in Section 2.4.1.2). Under those conditions, 1MU = 1cGy. The calibration data was fit to a second order polynomial of the form

$$D(\text{cGy}) = a_0 + a_1 OD + a_2 OD^2 \quad (2\text{-}9)$$

Since the film processor output was found to fluctuate on a daily basis (Figure 2-17), a separate film calibration was performed each time a set of phantom measurements was executed.

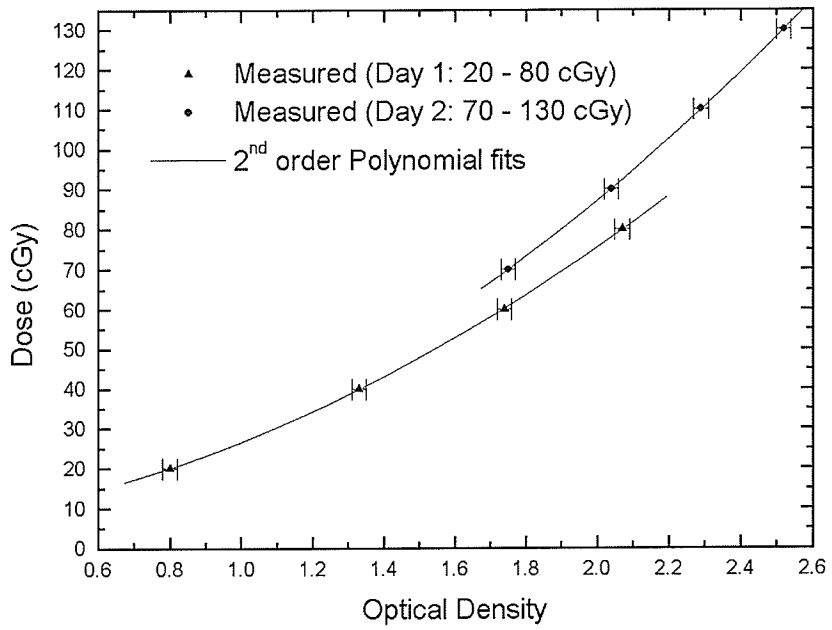

Figure 2-17: Typical film calibrations performed on different days in different ranges of optical density. The most linear response occurs at around $OD = 2.2$. Note the variation in the data between $OD = 1.7$ to 2.1, stressing the need for a calibration to be performed every day that data is acquired, due to fluctuations in the output of the film processor.

2.4.2.2 Uncertainties

The sources of uncertainty in the film dosimetry are the systematic error in the densitometer (quoted as $0.02OD$ by the manufacturer) and the sensitivity of the film, and the random error arising due to the film processing and variations in the experimental setup. Film processing appeared to be the dominant source of error giving rise to uncertainties in the dose measurements up to approximately 3%. This was estimated by exposing 3 films in a standard geometry, consisting of a 10 × 10cm field at an SAD of

100cm in a solid water phantom (Figure 2-18). The total error due to the processing and setup in the phantom measurements for experiments 3-5 was estimated by performing the experiment 5 times and calculating the standard error of the mean dose, point by point along the profile.

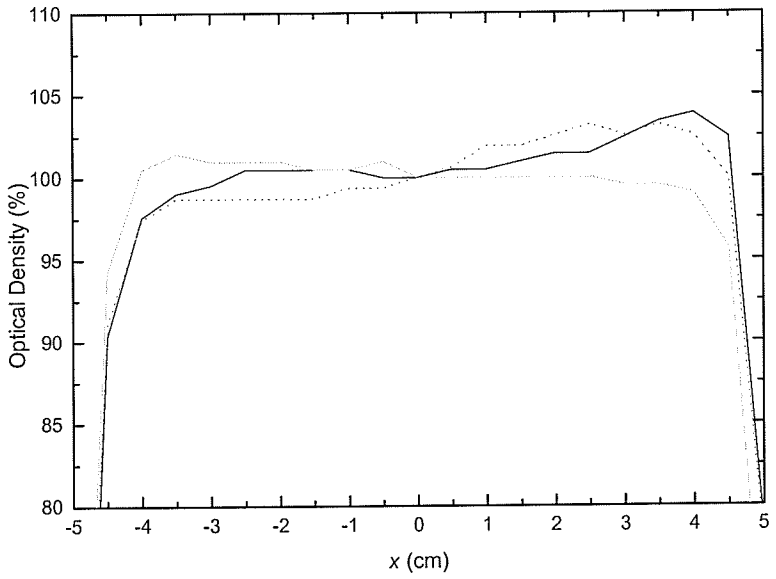

Figure 2-18: Profiles through a 10 × 10xcm field at d_{max} repeated 3 times to illustrate the variations in the film processor output. The points on the profile were measured with the manual densitometer. This random error can only be reduced by more experimental repetitions, and places a large restriction on the accuracy of film dosimetry.

2.4.3 Comparison with FOCUS CMS

The accuracy of the FOCUS dose calculation in the open and compensated fields was quantified with a point by point comparison along a profile in the compensation plane. Along this profile, the dose in the inner beam central high dose, low dose gradient (<30%/cm) region was analyzed. The AAPM Task Group 53 [TG 53] has recommended acceptability criteria for photon dose calculations of external beams in this region for a variety of situations. Those situations pertinent to the experiments performed in this

Table 2-1: TG 53 recommended acceptability criteria for irregular phantom geometries. Percentages are quoted as a percent of the central ray normalization dose.

Phantom Situation	Inner Beam (%)	Applicable to experiment #
Homogeneous, external surface contour	3	1,4,5
Inhomogeneous	5	2
3-D inhomogeneous	7	3

study are displayed in Table 2-1. To examine the agreement between FOCUS calculations and the measured data within the high dose-low dose gradient region, the root mean squared (RMS) deviation, σ_{RMS}, and maximum percent deviation, $\sigma_{\max}$, between the two was calculated. The percent deviation, σ_i, between FOCUS and the measured data at a profile location, x_i, is given by

$$(2\text{-}10)\quad \sigma_{x_i} = 100 \times \left(\frac{D_{FOCUS}(x_i) - D_{meas}(x_i)}{D_{meas}(x_i)} \right)$$

The corresponding RMS deviation across a profile consisting of N points was calculated using

$$(2\text{-}11)\quad \sigma_{RMS} = \sqrt{\frac{\sum_{i=1}^{N} \sigma_{x_i}^2}{N-1}}$$

2.5 Quality assurance

Routine quality assurance (QA) of each compensator prior to its use in a patient treatment is a two-part process. The accuracy of both the compensator design and

fabrication should be checked independently of each other, and independently of the treatment planning system (TPS) calculations.

A semi-automated compensator QA program has been developed, which performs both of these checks for every compensator before its application in a patient's treatment.

2.5.1 Compensator design QA

An independent check of the TPS compensator design prior to its use in patient treatment is a step that is often overlooked in clinical practice. Yet an error in the design by the TPS, or by the treatment planner operating the TPS is a very real possibility. After all, this is the main reason physicists perform manual calculations in everyday treatment plan checking. It is suggested here that the compensator design be included in this check. The question arises, how would we approach a methodology for verifying the design of the compensator? Performing a second, independent compensator design would be challenging in practice, due to the difficulty in extracting the patient and beam geometry from the TPS.

The approach we have adopted requires only the exported compensator thickness array and a few treatment beam parameters as chosen during the planning process and printed out in the treatment plan output sheets. It involves reconstructing the patient contour by determining the amount of tissue that produces the equivalent beam attenuation as the thickness of compensator material along each fanline through the filter. A contour at a given slice location is reconstructed by subtracting these thicknesses from the patient high point thickness. The reconstructed contour is then scaled and overlayed onto the original patient contour from the CT simulation for comparison. Essentially, the

compensator design process is reversed. It should be pointed out that although the method is useful for verifying missing tissue compensators, it poses no mechanism by which compensators designed to account for internal inhomogeneities can be quantitatively verified.

2.5.1.1 Patient contour reconstruction

Compensator thicknesses in the FOCUS export file are specified on a 2D rectangular grid. Tracing a point on the compensator to a corresponding point on the patient is complicated by the 3D nature of the geometry. Each (x,y,z) coordinate on the compensator is first traced back along the diverging fan line to the surface of the compensator tray (Figure 2-19). The radial transverse distance, r, from the central axis to the point where the ray intersects the tray is given by

$$r = \sqrt{(x - z\tan\theta_x)^2 + (y - z\tan\theta_y)^2} \quad \textbf{(2-12)}$$

where θ_x and θ_y are the angles of the diverging beam projected to the x-z and y-z planes, respectively (Figure 2-19), given by

$$\tan\theta_x = \frac{x}{s_{CT} + z} \quad \text{and} \quad \tan\theta_y = \frac{y}{s_{CT} + z} \quad \textbf{(2-13)}$$

The thickness along the ray through the compensator is

$$(2\text{-}14)\quad t_{comp} = z\sqrt{\tan^2\theta_x + \tan^2\theta_y + 1}$$

from which the transmission can be calculated using

$$(2\text{-}15)\quad T = \exp(-\mu_f^{eff} t_{comp})$$

.

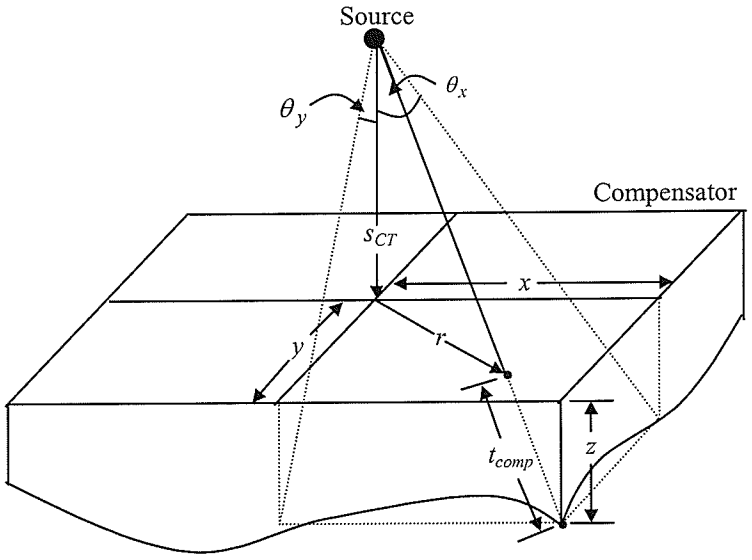

Figure 2-19: Each compensator point in the thickness array is traced back along a diverging ray to the source, in order to determine the actual thickness traversed by the ray through the compensator. Note source to compensator tray distance, s_{CT}, is much greater than shown.

The FOCUS compensators are designed to provide the same dose at the compensation plane that would arise from an identical beam incident on a flat, homogeneous phantom, with SSD equal to the minimum SSD within a specified area

(recall Figure 1-14). Mathematically speaking, the result of the compensator operating on the open (uncompensated) dose distribution, D_{uncomp}, produces the compensated dose distribution, D_{comp}. That is,

(2-16) $D_{comp} = T \times D_{uncomp}$

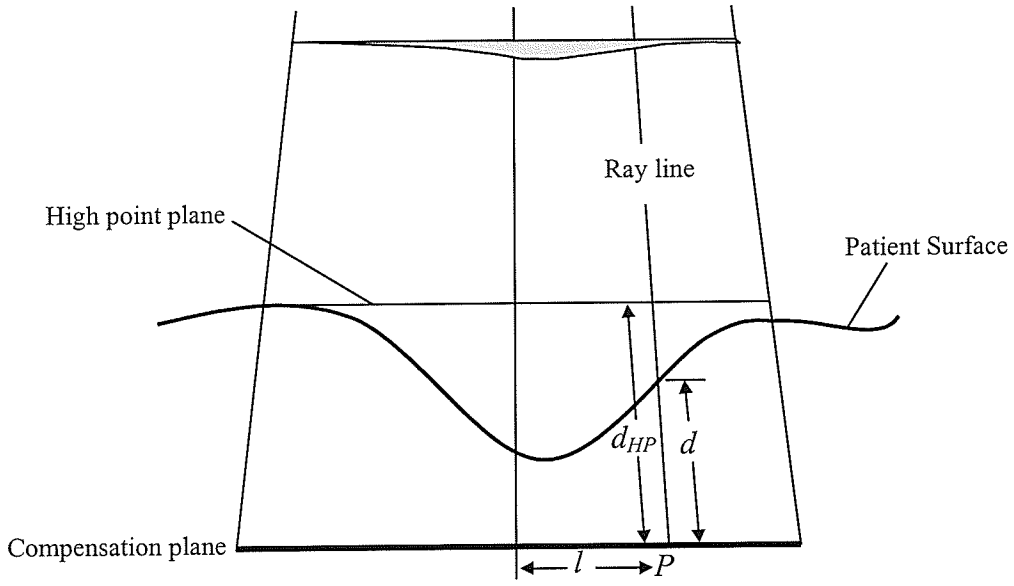

Figure 2-20: Geometry in the patient contour reconstruction from a missing tissue compensator.

An estimate of the dose at the point P in Figure 2-20 without the compensator, would be

(2-17) $D_{uncomp} = D(r_d, d_0) \times TPR(r_d, d) \times OAR(l, d)$

where $D(r_d, d_0)$ is the central axis dose at the reference depth d_0, and field size r_d, $TPR(r_d, d)$ is the tissue phantom ratio at depth d, and field size r_d, given by

$$(2\text{-}18)\quad TPR(r_d, d) = \frac{D(r_d, d)}{D(r_d, d_0)}$$

and $OAR(l,d)$ is the off-axis ratio at off axis position l, and depth d, given by

$$(2\text{-}19)\quad OAR(l, d) = \frac{D(l, d)}{D(l = 0, d)}$$

Since the compensator was designed to produce the dose incident on a flat phantom at the same SAD but at the high point depth, d_{HP}, we also have

$$(2\text{-}20)\quad D_{comp} = D(r_{d_{HP}}, d_0) \times TPR(r_{d_{HP}}, d_{HP}) \times OAR(l, d_{HP})$$

But since $r_d = r_{d_{HP}}$, combining equations (2-16), (2-17) and (2-20) yields

$$(2\text{-}21)\quad T = \frac{TPR(r_d, d_{HP}) \times OAR(l, d_{HP})}{TPR(r_d, d) \times OAR(l, d)}$$

Note that the patient depth, d, along the ray fan line is the only unknown variable in equation (2-21). For each point in the compensator, the transmission is calculated using equation (2-15), and tables of TPR's and OAR's are consulted to calculate

$TPR(r_d, d_{HP}) \times OAR(l, d_{HP})$. The program then searches the array of $TPR(r_d, d) \times OAR(l, d)$ to find the depth which satisfies equation (2-21). $TPR(r_d, d) \times OAR(l, d)$ monotonically decreases with depth beyond d_{max}, and therefore the searching is limited to depths greater than d_{max}. The reconstruction program repeats this procedure for each ray that passes through a compensator point in the thickness array.

Using a patient frame of reference in which the origin is coincident on the point where the central axis intersects the compensation plane, the distances, d, along the diverging fan lines from the compensation plane calculated above, are used to place points on the patient surface in 3 dimensions (as shown in Figure 2-20).

Since θ_x, θ_y and d vary as a function of position in the compensation plane, the placement of each patient contour point in 3-space will change significantly from ray to ray. The resulting array of patient contour points will be distributed irregularly in space. In order to then extract the patient contour at a specified transverse slice location, interpolation using "kriging" is applied. Kriging is a gridding technique applied frequently in geophysics. It is used to estimate the values of an irregularly gridded 3D data set to a regular Cartesian grid [La 86]. For an interpolation point (x,y), the interpolated value $f(x,y)$ is given by [IDL]

(2-22) $$f(x, y) = \sum w_i C(x_i, y_i, x, y)$$

where w_i is a weighting factor and $C(x_i,y_i,x,y)$ describes the covariance of the interpolation point with the data point at (x_i,y_i). An exponential covariance of the form,

(2-23) $$C(d) = \exp(-Ad)$$

where d is the distance between the interpolation point and data point, and A is a constant, was found to provide accurate interpolation (within ±1mm on the patient surface contour). This was determined by overlaying contour plots of the patient contour before and after the kriging routine.

The reconstructed contours are printed and overlaid with the original patient contours used by FOCUS on a light box. The overlay is made straightforward by including the diverging beam lines and compensation plane on the plot of the reconstructed profile (to be lined up with those on the contour printout from FOCUS) (Figure 2-21). Agreement between the contours is quantified by measuring the differences with a ruler, and expressing them as a percentage of the high point thickness.

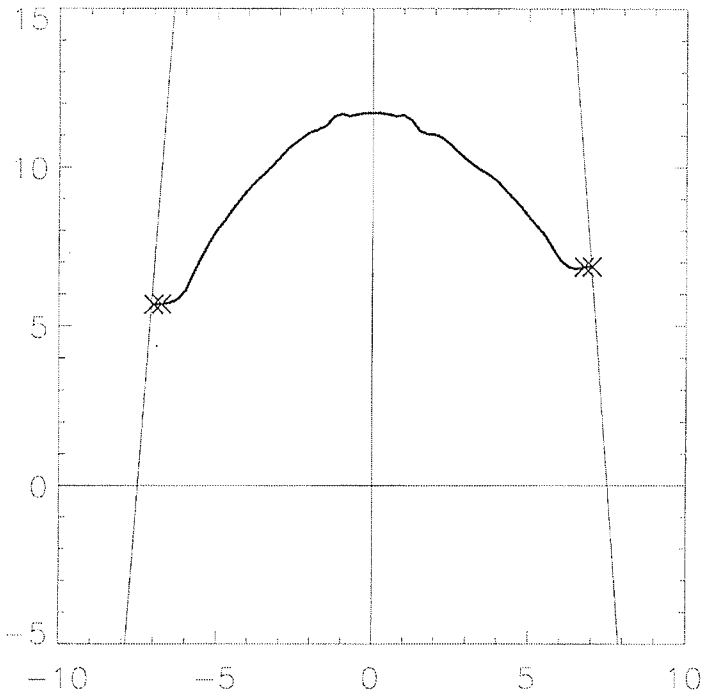

Figure 2-21: Typical output from the compensator design QA program. The patient contour at the specified transverse slice location (thick black line) is shown along with the diverging fan lines of the field edge and the compensation plane (at $y = 0$). This plot would be directly overlaid onto the original patient contour from the FOCUS computer. The meaning of the ×'s shown on the edges of the reconstruction will be discussed in Section 2.5.1.2.

2.5.1.2 Region of comparison

As mentioned previously, the compensator design QA process is a reverse of the method used by FOCUS to design the compensator. FOCUS calculates the transmission as a ratio of dose at the high point depth in a flat phantom to the dose at the same point in the uncompensated patient.

$$T = \frac{D(r_d, d_{HP})}{D(r_d, d)} \quad \textbf{(2-24)}$$

The patient contour reconstruction algorithm assumes that equation (2-24) can be approximated by equation (2-21). The off-axis ratios used in the patient contour reconstruction account for the non-uniformity in dose deposition in a plane perpendicular to the central axis due to the variation in beam hardening in the flattening filter. However, the physical penumbra also influences the transverse dose distribution near the field edges. These effects, which vary as a function of depth, are due to the finite source size (geometric penumbra), transmission through the secondary collimators (transmission penumbra) and scattering in the patient [Kh 94]. The patient contour reconstruction algorithm is limited by the fact that it does not explicitly model these penumbra effects when converting the transmission through the compensator to a patient thickness (penumbra effects are not included in equation (2-17) and therefore (2-21)). FOCUS, on the other hand, does include this phenomenon in determining T in equation (2-24). This effect is shown in Figure 2-22, for off-axis positions 5, 10 and 20mm from the edge of a 15 × 15cm 6MV beam incident a flat water phantom at an SSD of 98.5cm. The high point for this example was assumed to be 10cm. If we ignore the off-axis ratio correction in equation (2-21) then Figure 2-22 shows the manner in which the contour reconstruction algorithm determines the patient thickness, d, based on a transmission, T. Since the reconstruction algorithm ignores penumbra effects by simply using the TPRs measured along the central axis to determine d. For example, referring to Figure 2-22, the contour reconstruction program would interpret a transmission of 0.82 at distance of 10mm from the field edge as being due to a patient thickness of 2.5cm. To examine the magnitude of penumbra effects for this example, a flat water phantom was created in

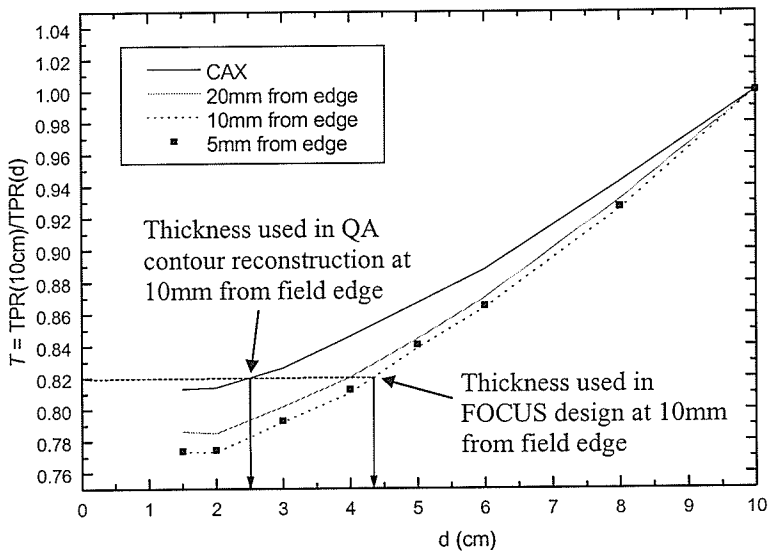

Figure 2-22: Transmission calculated in FOCUS as a function of depth, on the central axis and near the field edges of a 15×15cm^2 6MV photon beam. As shown, for a high point thickness of 10cm, if the patient depth is 4.4cm at a distance of 10mm from the field edge, then the transmission calculated in the FOCUS compensator design will be 0.82. However, the patient reconstruction contour reconstruction program would attribute this transmission as being due to a patient thickness of 2.5cm, since it uses TPRs measured on the central axis.

FOCUS and a 15×15cm 6MV beam at a SAD of 100cm was applied. Interest points were set up 5, 10 and 20mm from the field edge and the depth of the phantom surface was varied from 1.5 to 10cm. The FOCUS calculated transmission at these interest points as a function of depth, assuming a high point of 10cm, was determined by inserting the calculated doses into equation (2-24) for each of the three field edge distances. These curves are also shown in Figure 2-22. For the previously mentioned example, at 10mm from the field edge, a transmission of 0.82 actually corresponds to a patient thickness of 4.4cm, which is 1.9cm greater than that determined by the reconstruction program (a difference of 19% of the high point thickness). The figure also shows that as the patient thickness gets more comparable to the high point thickness this error diminishes, and the reconstruction becomes more accurate. This is because the

penumbra effects at the patient thickness, *d*, become approximately equal to those at the high point depth. By examining the behavior of the transmission as a function of depth and off-axis position, it was determined that reconstructed contours are not accurate within 2cm of the field edge if the patient thickness in that region drops below 5cm. This limit was established based on a high point depth of 10cm, which is typical of clinical head and neck compensators. Note however, that if the high point thickness was approximately 5cm, the agreement in the penumbra region would be expected to be much better, and this limitation would not strictly apply. For points where this limitation is encountered, ×'s are superimposed onto the contour reconstruction to indicate that the contours should not be compared in this region. Furthermore, regardless of patient thickness, points within 1cm of the field edge should not be compared due to the truncation of points in the compensator (recall Section 1.7.2.3), and consequently this region is also superimposed with ×'s.

2.5.2 Compensator fabrication QA

The method we have adopted for checking the accuracy of the compensator fabrication involves comparing the 2D array of compensator thicknesses generated by FOCUS with a film radiograph of the compensator taken in treatment position on the linear accelerator. The advantages of performing the check in this manner are that the verification of the position of the compensator in the treatment field is inherently included in the test (Figure 2-23).

The optical densities in the resulting radiographs are meaningless until they are converted to a corresponding thickness of compensator along each ray line. Accurate

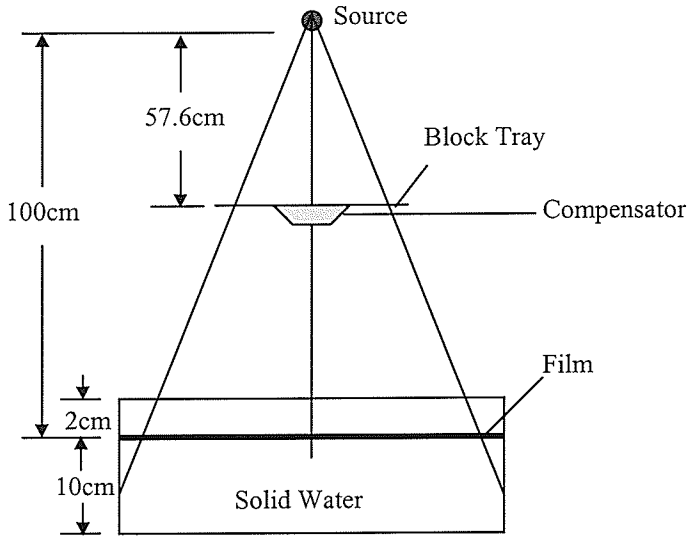

Figure 2-23: The film radiograph of the compensator is taken in treatment position, so that the position of the compensator in the treatment field is verified simultaneously with the thickness.

absolute dosimetry with film is difficult due primarily to variations in film processing. Pixel intensity is converted to Pb thickness using two calibrated step wedges, imaged simultaneously with the compensator (Figure 2-24). The wedges are placed on opposite sides of the compensator and the mean optical density for a given thickness of Pb on each wedge is averaged in order to account for any spatial non-uniformity remaining following the image processing (due primarily to the variability in film processing).

The film radiographs are digitized with a Lumiscan 50 (#000222) scanning laser densitometer. The Lumiscan 50 system sweeps a 2mW He-Ne laser beam across the film with a folding mirror. The light transmitted through the film is detected by a photomultiplier tube that converts the light energy to an analog signal, which is processed and amplified [Lu 50]. The scanner samples the optical density of the film at a rate of 20 points per centimeter over an image size of 612 × 500 pixels. The scanner acquisition is

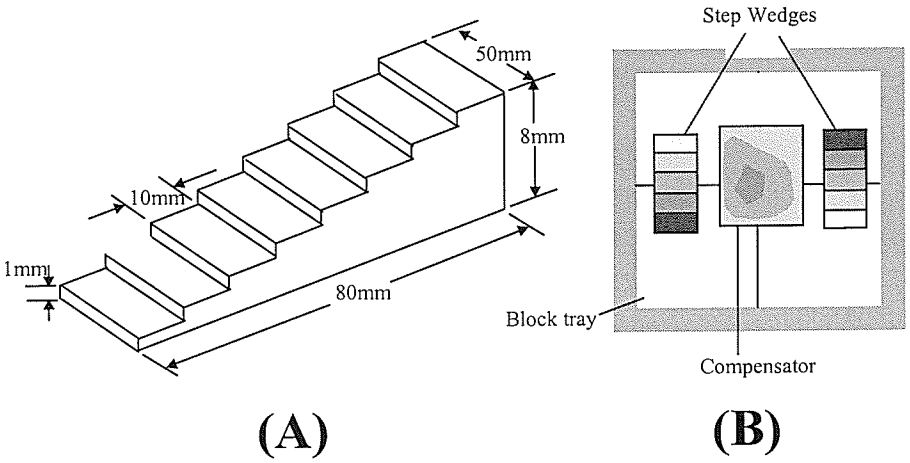

Figure 2-24: In the fabrication verification protocol, two step wedges are imaged with the compensator and used to calibrate pixel intensity into a known thickness of Pb. **(A)** Diagram of a single step wedge. **(B)** Arrangement of the pair of step wedges on the block tray during a typical exposure.

controlled through a software interface (FIPS Plus MEPHYSTO, PTW Frieburg) [MEPH], and the resulting 12 bit images are exported as TIFF files to be read directly into the compensator QA program. A number of corrections to the raw compensator/step wedge image are required prior to converting pixel intensity to Pb thickness.

2.5.2.1 Correction for film base and fog (background)

Each digitized raw film image, $F_{raw}(x,y)$, needs to be corrected for a constant offset due to the optical density of the film base plus fog. The film base is the physical layer which supports the emulsion layer(s) and fog refers to the development of unexposed silver halide grains, both of which contribute to a background density observed in every processed image [Cu 84]. The base plus fog density was determined by averaging the density across a developed film that had not been exposed to x-rays. The average pixel value, F_{BG}, from the digitized image of this film was subtracted from each subsequent image.

2.5.2.2 Correction for film scanner non-uniformity

The Lumiscan 50 was observed to possess a systematic spatial non-uniformity in the scanning *x*-direction. A maintenance cleaning of the scanner removed a great deal of silver deposit from the detector system, but did not alleviate the problem. The non-uniformity was also found to vary slightly as a function of optical density (Figure 2-25). This effect was corrected by using scans of films of an approximately uniform optical density. The uniform density, or *UD* films, were generated by positioning the entire film in the center of a 6MV open field with the largest possible collimator setting (40 × 40cm). The films were sandwiched between 9cm (build-up) and 7cm (backscatter) of acrylic and placed at a distance of approximately 223cm from the source. The resulting films showed a variation in optical density of less than 3% across the entire image, as measured using a manual densitometer, using a 1cm sampling resolution.

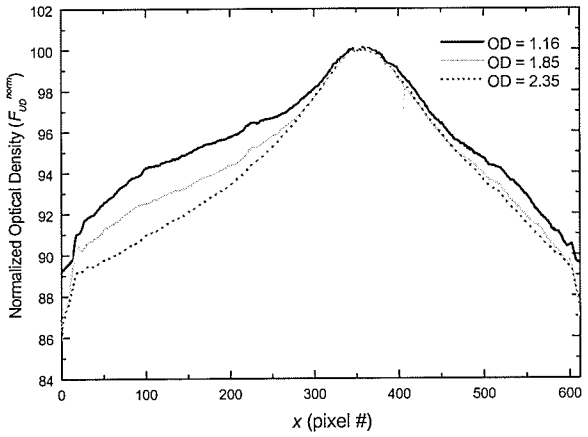

Figure 2-25: Variation along the x direction of the scanned images of the uniform density films. Note also the slight variation as a function of film density. The true variation in the film density (determined by sampling with the manual densitometer) was ± 3%.

To lessen the effects of this 3% density fluctuation, each film was fed through the film scanner in 4 different orientations and the results averaged. Three such films were

acquired at monitor unit settings of 200, 400, and 600, resulting in *UD* films with mean optical densities of 1.16, 1.85, and 2.35, respectively. These were sufficient to cover the range of optical densities encountered in a typical compensator QA radiograph. The x profiles in the digitized *UD* images were averaged to produce a single correction profile, $F_{UDi}(x)$, for each of the three images (i = 1,2,3). These profiles were then used to correct the intensity of the compensator image, $F_{comp}(x,y)$, along the x direction as follows. At each pixel location along the x direction, a three element array was generated containing the *UD* correction values at that pixel location for each of the three density levels ($F_{UD1}(x), F_{UD2}(x), F_{UD3}(x)$). Then a linear interpolation of this array was made, based on the actual pixel brightness in the compensator image, to determine the appropriate correction factor $F_{UD}'(x)$ for that particular x location and optical density. A raw compensator image was thus corrected for background and scanner non-uniformity using,

$$F'_{comp}(x,y) = \frac{F_{comp}(x,y) - F_{BG}}{F_{UD}'(x) - F_{BG}} \quad \textbf{(2-25)}$$

Note that any information on the absolute value of the pixel brightness is lost through this operation. To verify that this correction was appropriate, an x profile through the center of a 10 × 10cm open field image at 5cm depth was scanned, corrected using equation (2-25), and subsequently compared to manual density measurements with the calibrated Sargent–Welch densitometer described in section 2.4.2 (Figure 2-26). As shown, the raw

image profile showed large variation (±5% of the central axis density) due to the non-uniformity of the laser scanner. However, after the image was corrected for the non-uniformity, the agreement with measurements by the manual densitometer was excellent.

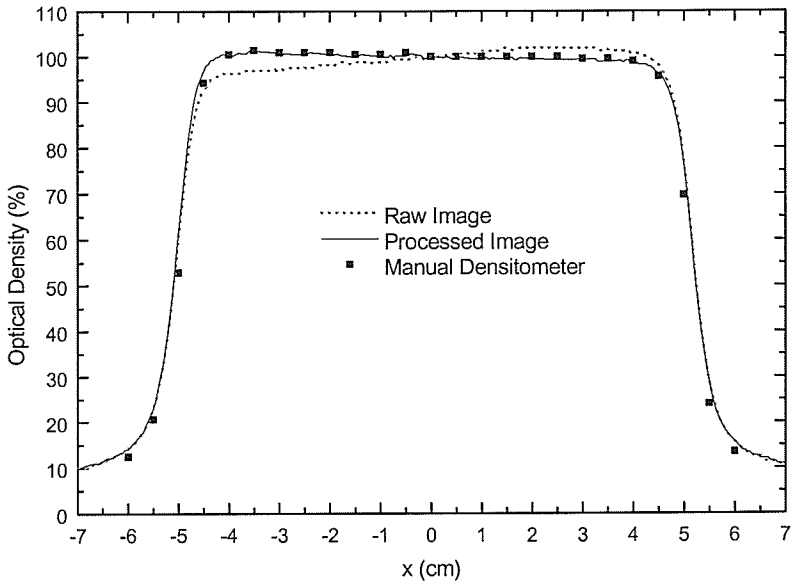

Figure 2-26: *x* profiles for a film acquired using a 10 × 10cm field at 5cm depth, normalized to the central axis value. The raw image, digitized with the Lumiscan 50, shows the non-uniform response of the detector system. After applying corrections for the scanner non-uniformity we obtain good agreement between the processed image and measurements with a calibrated manual densitometer.

2.5.2.3 Correction for the open field

The flattening filter in a radiotherapy x-ray beam is adjusted to provide a relatively flat dose profile in a plane perpendicular to the central axis at a single depth (usually 10cm). Due to scattering and absorption of the polyenergetic beam, transverse planes above and below this depth will not provide the same relative dose distribution. This effect must be removed, so that it doesn't influence the measurement of compensator thickness throughout the field at the depth of the film. This was accomplished using a radiograph of the open field with the same collimator opening and

experimental setup (minus the compensator), in what is often called a *flood field correction*. Note, that the digitized open field image, F_{open}, also needed to be corrected for background and scanner non-uniformity using equation (2-25).

The position of the beam central axis in the corrected open and compensator/step wedge images were referenced by prompting the user to sequentially click on the film pin pricks on the images (created at the time of film acquisition by making small holes in the film jacket at the corners of the field as indicated by the light field), while the program interactively retrieved the coordinates of each click. Then, with their central axes aligned, the compensator/step wedge image could be corrected for the open field non-uniformity by applying

$$(2\text{-}26)\quad F_{corr} = \frac{F'_{comp}}{F'_{open,norm}}$$

where $F'_{open,norm}$ is the corrected open field image, normalized to the pixel intensity along the central axis.

2.5.2.4 Pixel intensity to Pb thickness calibration

A typical compensator plus step wedge image, after undergoing all of the above corrections is shown in Figure 2-27. The final step in the processing is to convert the image from an array of 8 bit pixel intensities to an array of compensator thicknesses, using the step wedges. In the program, the user is prompted to click on the edge of both wedges, from which point the program can locate the center of each step. The number of

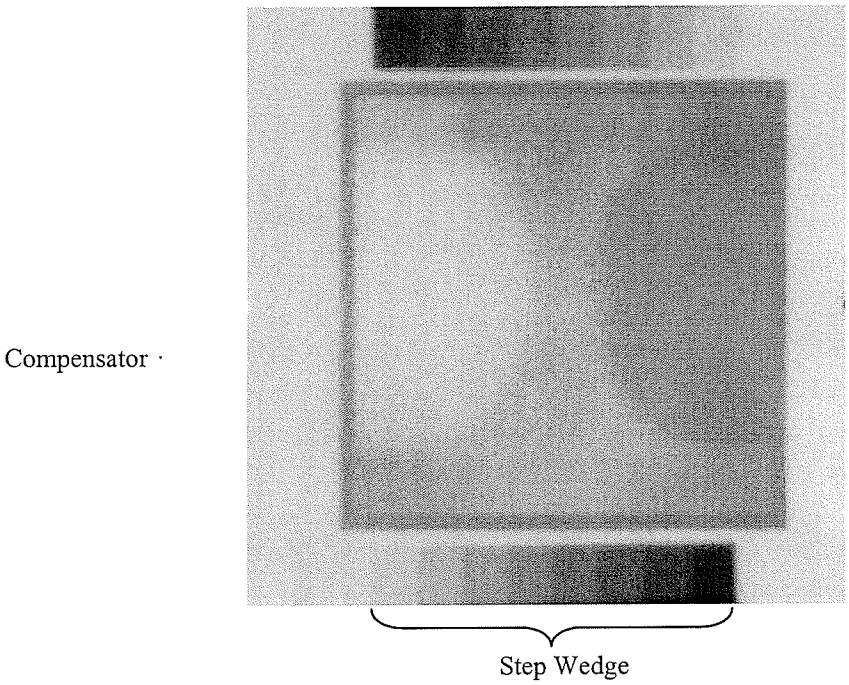

Figure 2-27: A fully processed compensator/step wedge image after application of all of the above mentioned corrections.

pixels averaged on a step in both the x and y directions could be easily adjusted in the program, but typically a rectangle of 9 × 25 pixels was used. Let us denote the mean pixel intensity for a step of thickness t on wedge i within the rectangle as $\bar{I}_i(t)$. The final mean pixel intensity, $I(t)$, for a known thickness of Pb was then found by averaging $\bar{I}_1(t)$ and $\bar{I}_2(t)$ (i.e. mean intensities for a given step thickness from each wedge) (Figure 2-28). The thicknesses as a function of pixel intensity were then least-square fitted to a 2nd order polynomial of the form

$$t(I) = a_0 + a_1 I + a_2 I^2 \quad \textbf{(2-27)}$$

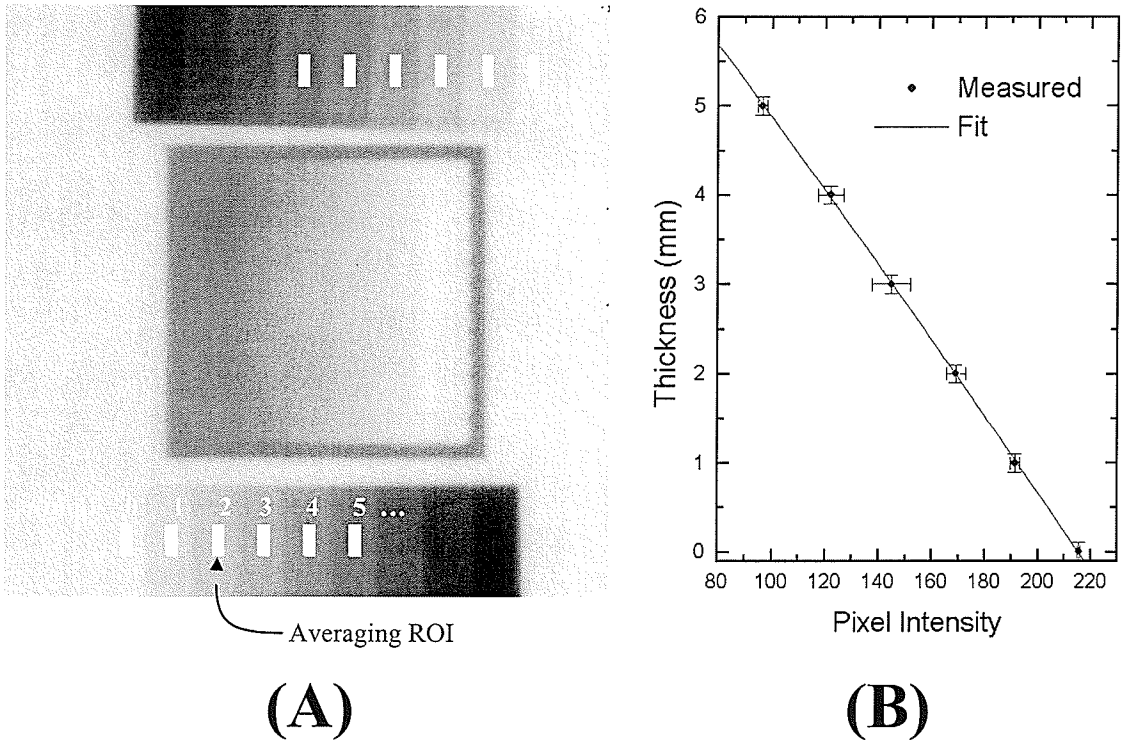

Figure 2-28:(A) Processed compensator image showing the 9 × 25 pixel regions of interest (ROI's) on the step wedge over which pixel intensities were averaged for a given thickness of Pb. **(B)** A plot of the known thicknesses of Pb as a function of the measured mean pixel intensities, and the corresponding 2nd order polynomial fit to the data. The maximum deviation in the thickness within each step was 0.1mm, from measurements with a digital caliper. The error bars in the intensity represent the deviation between the mean pixel intensity of the two wedges and the average intensity of each of the wedges.

When the resulting calibration curve from equation (2-27) was subsequently applied to F_{corr}, the corrected compensator/step wedge image was transformed into a thickness image. Before comparing directly with FOCUS, the transverse coordinates in the compensator image were scaled to the compensator tray distance, since the QA measurement was performed at an SAD of 100cm. The transverse positions (x_{film},y_{film}) in the film were converted to positions in the compensator (x_{comp},y_{comp}) using,

$$(2\text{-}28)\quad (x_{comp}, y_{comp}) = \left(\frac{s_{CT}}{100} x_{film}, \frac{s_{CT}}{100} y_{film} \right)$$

One significant source of error is the random error associated with film processing. By imaging the wedges on the same radiograph as the compensator, we remove the effects of any variability between films. However, the film processor may still develop the film in a spatially non-uniform manner. The motivation for using two step wedges on opposite sides of the field is to (roughly) account for this effect and get a handle on how its magnitude impacts the uncertainty in the QA results on a film by film basis. An uncertainty in the measured transmission was estimated by determining the maximum deviation between the final intensity, $I(t)$, and that from each of the wedges, $I_1(t)$ and $I_2(t)$, for a given step thickness. The corresponding effect on the transmission was calculated by propagating either $I_1(t)$ or $I_2(t)$ through the calibration equation (2-27) and examining the resulting difference in thickness (and hence transmission) from that calculated with $I(t)$.

2.5.2.5 Comparison with FOCUS CMS

Unlike point dose or manual thickness measurements where only a few points on the compensator are sampled, we can compare the thickness of the compensator at thousands of points over the entire compensator area. Although the thickness of the compensator is what we are ultimately checking, the more relevant parameter for comparison with FOCUS is the x-ray transmission through the compensator, as the magnitude of this difference is what will determine the corresponding effect on the dose distribution. The absolute difference in transmission, ΔT, at a given point, expressed as a percentage of full transmission through the compensator is given by,

(2-29) $$\Delta T = 100 \times (T_{meas} - T_{FOCUS}) = 100 \times (\exp(-\mu_f^{eff} t_{meas}) - \exp(-\mu_f^{eff} t_{FOCUS}))$$

The compensator QA program displays ΔT in a frequency histogram and calculates the percentage of sampled points that show greater than 5 and 10% transmission difference (excluding the approximately 1cm boundary at the edge of the field (corresponding to roughly 0.6cm in the compensator)) (Figure 2-29). The criterion for whether or not a compensator has passed or failed the fabrication check was determined by evaluating the performance of the compensators used in the experiments described in Section 2.3. To test the soundness of the passing criterion, two simulations were set up. Both tests were performed using the mantle phantom compensator. The first tested the ability of the QA procedure to recognize errors in the compensator thickness, which may arise from errors in the z referencing on the milling machine. The compensator thicknesses in the FOCUS export file were offset by 0.25, 0.5, and 1.0mm, and subsequently compared to the compensator thicknesses determined by the QA procedure. The second simulation examined the ability of the QA procedure to recognize transverse shifts in the compensator. Note that the effect of this error on the treatment will be highly dependent on the compensator geometry. For example, if the contour in the compensator has a very small gradient, then transverse shifts in the coordinates will have little effect on the dose distribution in the patient (provided the compensator has been fabricated past the geometrical boundaries of the field, otherwise the patient would be irradiated by an open beam). On the other hand, transverse shifts in compensators which possess steep contour gradients will result in more serious error in dose delivery. As a representative example, the compensator designed for the mantle phantom above was used for this simulation

because it presented the largest amount of thickness variation across its surface, for the experiments performed in this work. Transverse shifts of 2.5, 5.0, 7.5, and 10.0mm were applied to the thicknesses in the FOCUS export file, and these shifted compensators were subsequently compared to the compensator thicknesses determined by the QA procedure.

The uncertainty in the fabrication QA was estimated by comparing the thickness measurements with the CNC probe at the 9 interest points described in Section 2.2.4, with the corresponding thicknesses measured by the QA procedure for the 6 compensators used in the dosimetric verification experiments (described in Section 2.3).

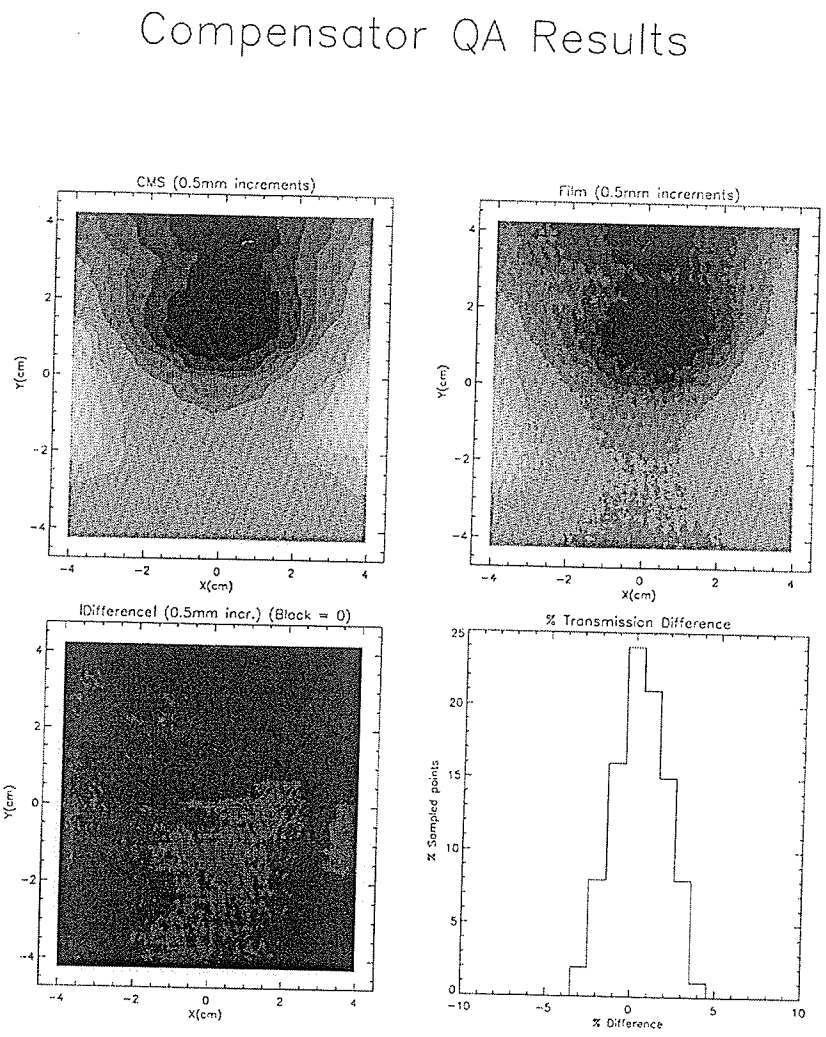

Figure 2-29: Typical output from the compensator fabrication check program.

3 Results & Discussion

In this chapter, measured and FOCUS calculated dose profiles along the compensation plane are compared for the 5 experiments outlined in Section 2.3. The QA procedure that was performed on each experimental compensator also will be discussed. Note that the design verification using patient contour reconstructions is, at present, meaningless for compensators designed to account for internal inhomogeneities. Therefore, the compensator design QA is not presented for experiments 2 and 3. Conclusions on the criteria for acceptability of a clinical compensator are drawn after examining the QA results.

3.1 Experiment 1: Ramp phantom

3.1.1 Results

Dose profiles in the open and compensated fields are shown in Figure 3-1, and the mean and RMS deviation across the profiles are summarized in Table 3-1. The RMS deviations were both within the TG 53 recommended limits set out in

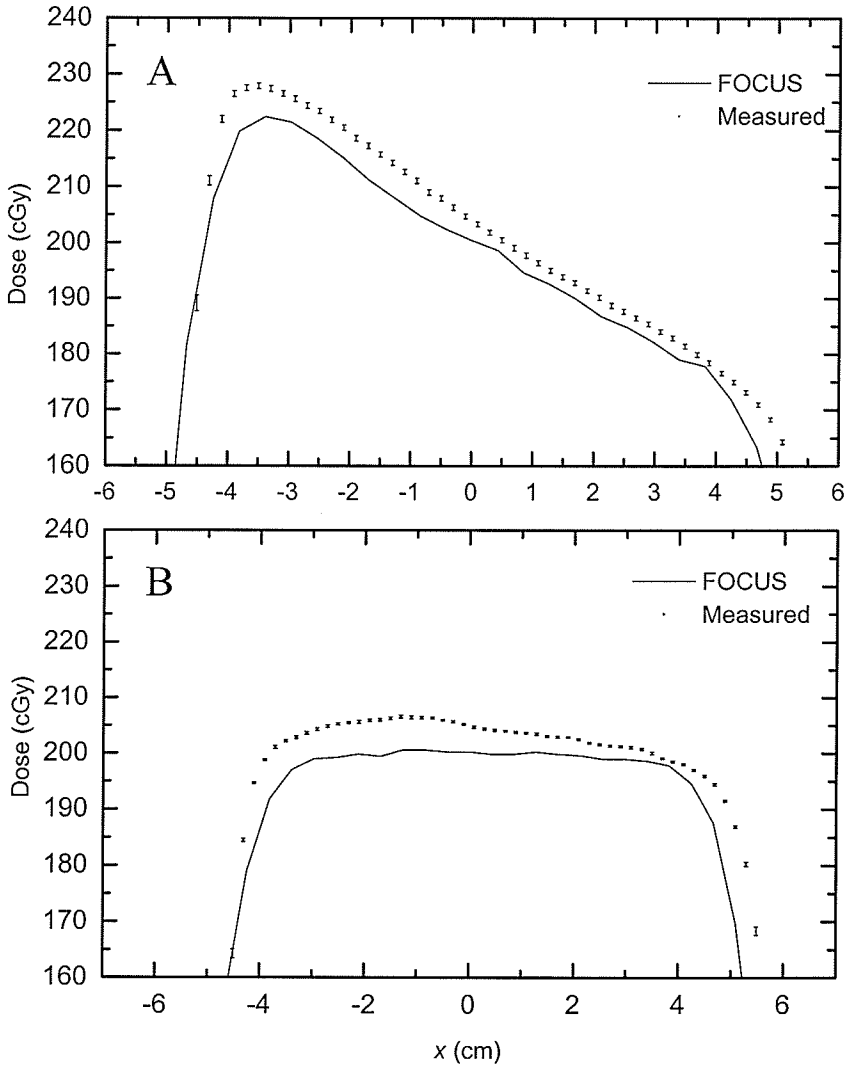

Figure 3-1: Profiles at the compensation plane for both (A) the open field and (B) the compensated field for the ramp phantom. The error bars represent the standard error of each measured point from a series of 5 measurements.

Table 3-1: Agreement between FOCUS and measured data along the dose profile.

	RMS deviation (%)	Maximum deviation (%)
Open Field	1.8	-3.8
Compensated Field	1.8	-4.4

As indicated in Figure 3-1, the measured profile in the compensated field was not as flat as that predicted by FOCUS. This is expected considering the manner in which

FOCUS designs its compensators. Recall that the FOCUS design is based on transmission, defined as the ratio of dose, assuming the patient is flat with thickness equal to the high point thickness, to that with the actual patient geometry at the compensation plane. On the other hand, the in-phantom measurements are performed with and without the compensator in the path of the beam. FOCUS does not account for the changes in the scattering between the Pb compensator in the head of the treatment unit, and the missing tissue that it is designed to simulate. The scatter reaching the compensation plane is different depending on whether it originates in the retracted compensator, or a tissue-equivalent bolus lying on the patient contour. In addition, the dose calculation that FOCUS performs for a compensated beam is only an approximation since it uses a single constant value for the effective linear attenuation coefficient of the beam modifier, even though this parameter is actually a complex function of the compensator material and thickness, the beam energy spectrum, and the compensator to patient surface distance [Ba 90].

The deviations between FOCUS calculations and measurements in phantom were relatively consistent between the open and compensated fields. One should expect the FOCUS calculations in the compensated field to be no better than the open field, especially in light of the fact that the compensated field calculations utilize the effective attenuation coefficient approximation. The consistency of the FOCUS calculation accuracy between the open and compensated fields is best observed by examining the ratio of measured dose to FOCUS predicted dose (Figure 3-2).

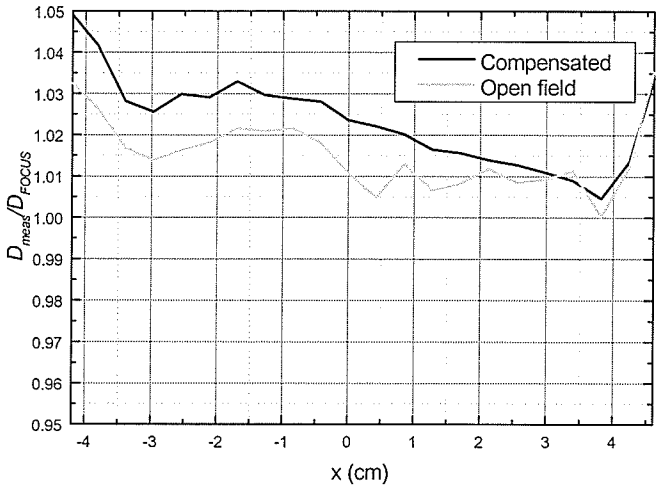

Figure 3-2: Ratio of measured to FOCUS dose along the dose profile for both the open and compensated fields within the high dose-low dose gradient region.

This graph suggests that some of the variation between calculated and measured compensated fields could be due to FOCUS inaccuracy in calculating open field doses and not just shortcomings in the compensator design alone.

The positive offset in the measured profiles, with respect to the FOCUS calculated profiles in Figure 3-1, was unlikely to be an error in the measurement technique. The five experiments used in the average were done on separate days and the results varied by less than 1%. Also, measurements in the cork inhomogeneity phantom were performed on the same days as the ramp phantom, and an offset was not observed in the open field in those open field measurements (see section 3.2), further substantiating that the technique was valid.

3.1.2 QA

The compensator design was verified using three transverse patient contour reconstructions: through the central axis and at slice positions +2 and –3 cm from the central axis. As shown in Figure 3-3, the agreement between the reconstructed and original patient contours was excellent throughout the region of comparison.

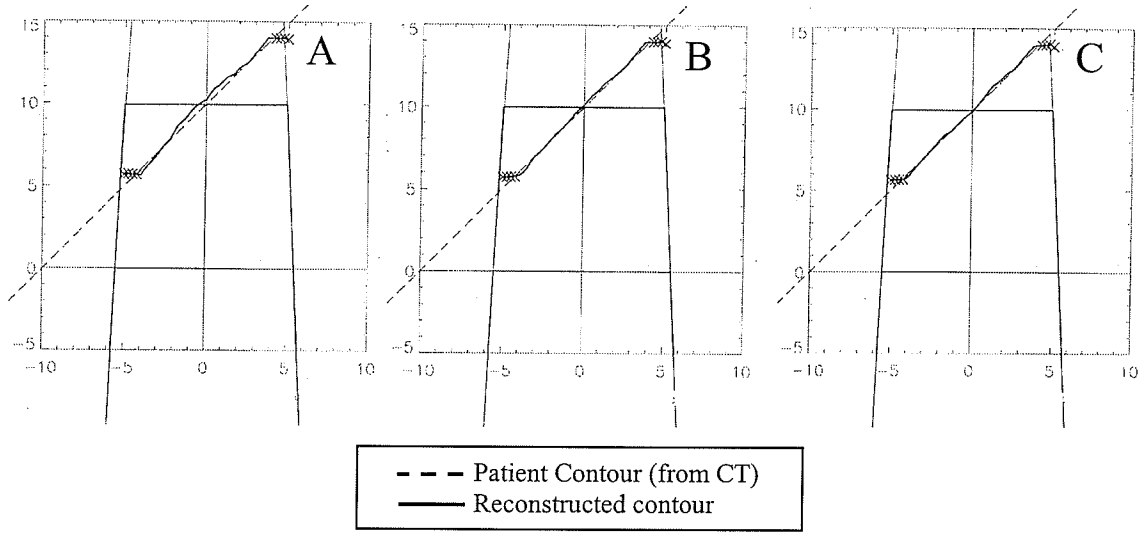

Figure 3-3: Comparison of the original patient contour from the CT simulation (dashed line) and the reconstructed patient contour. Three slices were compared at (A) 0.0cm (B) 2.0cm and (C) –3.0cm, relative to the central axis. The scaled coordinate system present on each reconstructed contour indicates distances in centimeters.

The discrepancy between the reconstructed and original patient contours in this case, expressed as a percentage of the high point thickness, was less than 3% (0.5cm) in all three contours. Such excellent agreement was observed mainly because the patient thickness was never less than 5cm, so that the changes in the shape of the penumbra between the high point depth and the patient thickness were relatively small (recall the penumbra discussion in Section 2.5.1.2).

Compensator fabrication was checked first by physical measurements with the CNC as described in Section 2.2.4 (Table 3-2). All but one of the 9 measured points were within measurement error of the FOCUS design thickness. However, this outlying point showed a deviation of only 0.2mm.

Table 3-2: Thickness measurements in the ramp phantom compensator.

Point	FOCUS (mm)	Measured (CNC) (mm)	Measured (QA) (mm)
1	2.3	2.2 ± 0.1	2.0 ± 0.3
2	4.9	4.7 ± 0.1	4.3 ± 0.4
3	0.0	0.0 ± 0.1	0.0 ± 0.3
4	2.4	2.4 ± 0.1	2.5 ± 0.3
5	2.4	2.4 ± 0.1	2.4 ± 0.3
6	3.9	3.8 ± 0.1	3.2 ± 0.3
7	3.9	3.8 ± 0.1	3.6 ± 0.3
8	0.9	0.8 ± 0.1	0.6 ± 0.3
9	0.9	0.8 ± 0.1	0.5 ± 0.3

Furthermore, the maximum deviation between the thickness measured by the compensator fabrication QA procedure and that in the FOCUS export file at these 9 points was 0.7mm, a difference of 3.3% in transmission. The average difference in transmission between the two was only 1.4%.

Differences in thickness measured via the QA procedure and the FOCUS design will be expected, due to some of the inherent approximations involved with the QA procedure. One approximation in the fabrication QA procedure is that it does not account for beam divergence, when relating the film density demarcating the step wedges to that in the compensator. Since the step wedges are generally placed near the edges of the field, the x-ray path length through a step in the wedge will be larger than its thickness due to the divergent nature of the x-ray beam.

(3-1) $$pathlength = t/\cos\theta$$

where t is the step thickness and θ is the divergence angle of the ray passing through the step. The change in transmission resulting from this effect is given by,

(3-2) $$F = \frac{\exp(-\mu_f^{eff}\ t/\cos\theta)}{\exp(-\mu_f^{eff} t)}$$

However, since θ is at most 9°, the divergence correction factor , F, ranges from 0.999 to 0.996, for step thicknesses of 1 to 5mm, respectively, and therefore would have a negligible effect on the thickness determination throughout the entirety of the compensator.

A second assumption made by the fabrication QA procedure is that the scatter contribution directly under the compensator is the same as that directly under the step wedges. Although the thickness at a point in the compensator may be equal to the thickness of one of the steps in the wedges, the thicknesses in the neighboring regions of the compensator and step wedge may be vastly different. Thus, locations in the film that receive the same exposure from the primary beam (as a result of passing through the same thickness of compensator material along their respective diverging ray line) will receive different exposures from scattered photons. The impact of this "equal scatter approximation" will vary both within a compensator and between compensators.

A third phenomenon that is not accounted for in the QA procedure, is the change in transmission through a given thickness of Pb depending on its position in the field due to differences in beam hardening throughout the flattening filter. For instance, one might expect that the transmission through a 1mm Pb plate on the central axis would be greater than that 5cm off-axis. This is because a beam of photons along the central axis has passed though a greater amount of flattening filter, and therefore has a higher average energy as it enters the compensator.

The uncertainty in the fabrication QA procedure as a result of the above approximations was assessed by comparing the thicknesses determined by the QA procedure at 9 points in each compensator used in experiments 1 through 5 to that determined using the CNC probe (see Section 3.6.3 for the results).

The output from the fabrication QA procedure for the ramp phantom is shown in Figure 3-4 along with the summarizing results in Table 3-3. We observed good agreement between the thicknesses measured in the QA procedure, and that of the original FOCUS design, as over 99% of the points were within ±5% of full transmission. The difference plot (lower left corner in Figure 3-4) is a useful means of visualizing the regions in the compensator where deviations between the QA measured thickness and FOCUS design occurred. In this case, the small differences observed were not localized to any single region in the compensator. In the reporting of subsequent results of the fabrication QA, only the transmission histogram and percentage of points exceeding 5 and 10% differences in transmission will be presented.

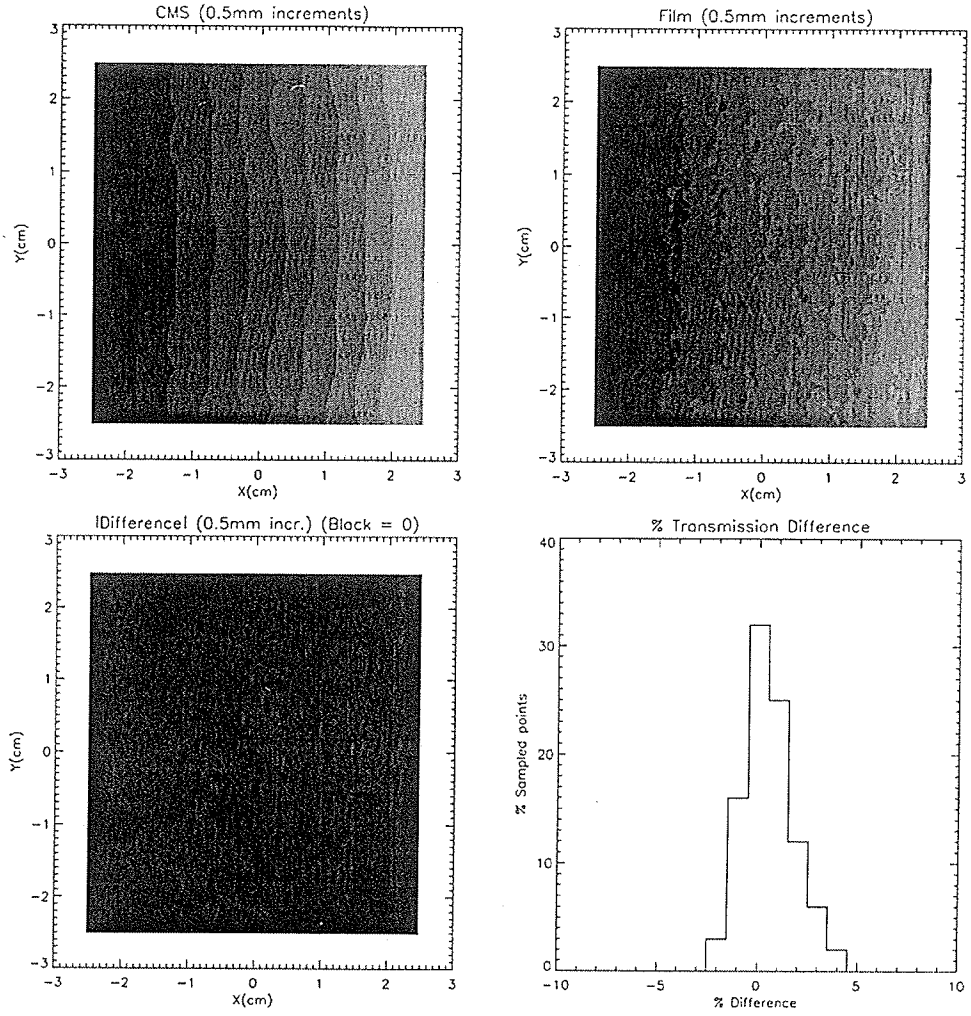

Figure 3-4: Fabrication QA results for the ramp phantom compensator.

Table 3-3: Fabrication QA results: Ramp Phantom

# points sampled	Average ΔT (%)	% of points with ΔT>5%	% of point with ΔT > 10%
30276	1.0 ± 1.7	0.3	0.0

3.2 Experiment 2: Cork phantom

3.2.1 Results

Agreement between the measured and FOCUS calculated doses in the high dose-low dose gradient region were all within the 5% limit. Examination of the ratio of measured to FOCUS predicted dose in this case showed a relatively constant offset of the compensated ratio by 1-2%, indicating that the compensator transmission was slightly larger than that calculated by FOCUS.

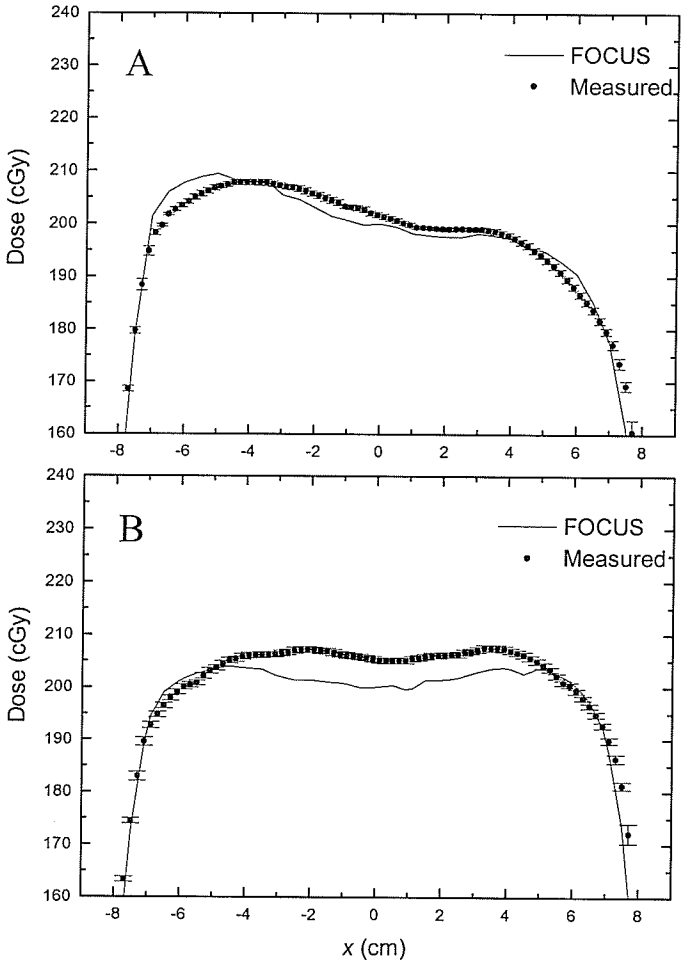

Figure 3-5: Profiles at the compensation plane for both (A) the open field and (B) the compensated field for the cork inhomogeneity phantom. The error bars represent the standard error in the measured points from a series of 5 measurements.

Table 3-4: Agreement between FOCUS and measured data along the dose profile.

	RMS deviation (%)	Maximum deviation (%)
Open Field	1.1	2.2
Compensated Field	1.8	-2.8

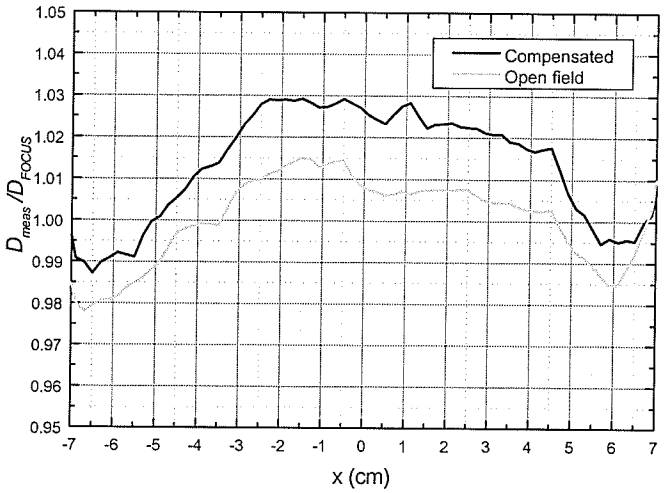

Figure 3-6: Ratio of measured to FOCUS dose along the dose profile for both the open and compensated fields within the high dose, low dose gradient region.

3.2.2 QA

Since the compensator was designed for an internal inhomogeneity, we can only examine the fabrication QA results. Firstly, the thickness measurements are presented at the 9 interest points in the compensator (Table 3-5). Here, the maximum deviation between the CNC measured and FOCUS thicknesses was 0.2mm.

The agreement between the thicknesses measured via the QA routine and the FOCUS design was also quite good for this compensator as all but point 8, which showed a transmission difference of 2.3% of full transmission, were in agreement within the limits of uncertainty. The results of the QA procedure are shown in Figure 3-7 and Table 3-6.

Table 3-5: Thickness measurements in the cork inhomogeneity phantom compensator.

Point	FOCUS (mm)	Measured (CNC) (mm)	Measured (QA) (mm)
1	1.3	1.1 ± 0.1	0.9 ± 0.3
2	1.8	1.6 ± 0.1	1.7 ± 0.3
3	0.2	0.0 ± 0.1	0.0 ± 0.3
4	1.3	1.2 ± 0.1	1.1 ± 0.3
5	1.3	1.3 ± 0.1	1.2 ± 0.3
6	1.7	1.6 ± 0.1	1.3 ± 0.3
7	1.7	1.6 ± 0.1	1.8 ± 0.3
8	0.7	0.7 ± 0.1	0.3 ± 0.3
9	0.7	0.6 ± 0.1	0.5 ± 0.3

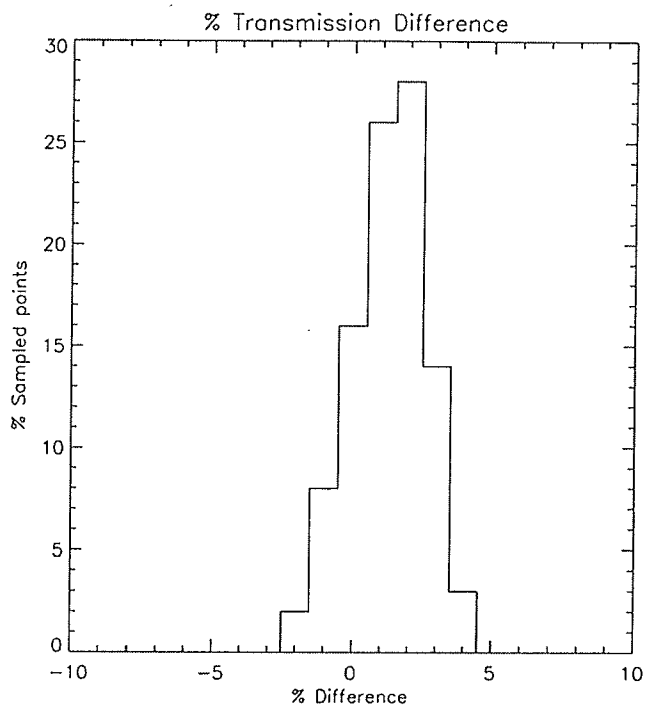

Figure 3-7: Transmission difference histogram for the cork inhomogeneity phantom compensator.

Table 3-6: Fabrication QA results: Cork Inhomogeneity Phantom

# points sampled	Average ΔT (%)	% of points with ΔT>5%	% of point with ΔT > 10%
77284	1.8 ± 1.1	0.5	0.0

The fabrication QA results were good, as in experiment 1. Any discrepancies between the QA measured thicknesses and the FOCUS design were distributed fairly uniformly throughout the compensator, as indicated on the thickness difference plot (not shown).

3.3 Experiment 3: Anthropomorphic phantom

3.3.1 Results

The agreement between FOCUS and the measured data is quite good for this complex geometry, considering the relative simplicity of the correction-based Clarkson algorithm [Wo 90]. The RMS deviations along the profiles were about 2% for both the open and compensated situations. The maximum deviation in both the open and compensated field profiles was within the TG 53 recommended limit of 7%. The dose ratio within the high dose, low dose gradient regions of the profile (Figure 3-9), was again greater in the compensated field than in the open field. The difference between the dose ratios was at worst 5%, but most often in the range of 1-2%.

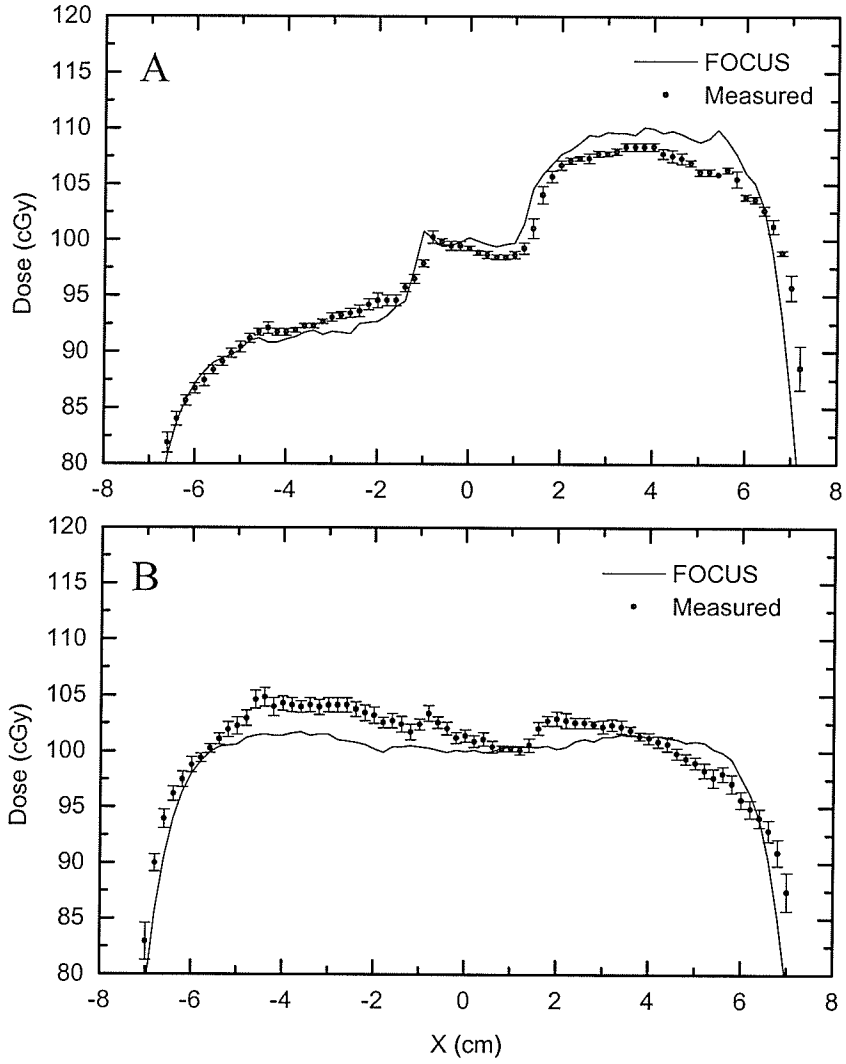

Figure 3-8: Profiles at the compensation plane for both (A) the open field and (B) the compensated field for the anthropomorphic phantom. The error bars represent the standard error in the measured points from a series of 5 measurements.

Table 3-7: Agreement between FOCUS and measured data along the dose profile.

	RMS deviation (%)	Maximum deviation(%)
Open Field	1.7	-5.7
Compensated Field	2.2	-6.4

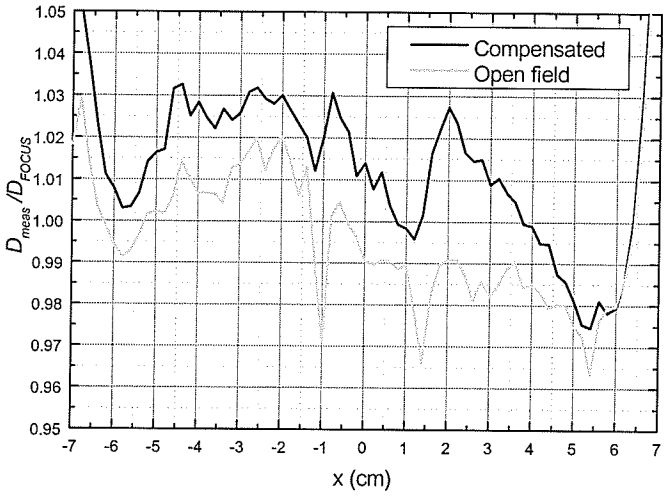

Figure 3-9: Ratio of measured to FOCUS dose along the dose profile for both the open and compensated fields within the high dose-low dose gradient region.

3.3.2 QA

Again we are restricted to the QA of the compensator fabrication only in this case. As shown in Table 3-8, all CNC thickness measurements were in agreement with the FOCUS design, within the limit of the uncertainties on the measured values.

Table 3-8: Thickness measurements for the anthropomorphic phantom compensator.

Point	FOCUS (mm)	Measured (CNC) (mm)	Measured (QA) (mm)
1	2.1	2.0 ± 0.1	1.4 ± 0.1
2	0.1	0.0 ± 0.1	0.2 ± 0.1
3	3.5	3.5 ± 0.1	2.6 ± 0.2
4	2.1	2.0 ± 0.1	1.8 ± 0.2
5	3.0	2.9 ± 0.1	2.4 ± 0.2
6	0.9	0.8 ± 0.1	0.9 ± 0.1
7	0.3	0.2 ± 0.1	0.3 ± 0.1
8	3.7	3.7 ± 0.1	3.0 ± 0.2
9	3.6	3.5 ± 0.1	3.3 ± 0.2

In this instance, the maximum deviation between the thickness measured by the QA procedure and the CNC probe was 0.9mm (point 3), corresponding to a transmission difference of 4.4%.

The results of the fabrication QA procedure are shown in Figure 3-10 and Table 3-9.

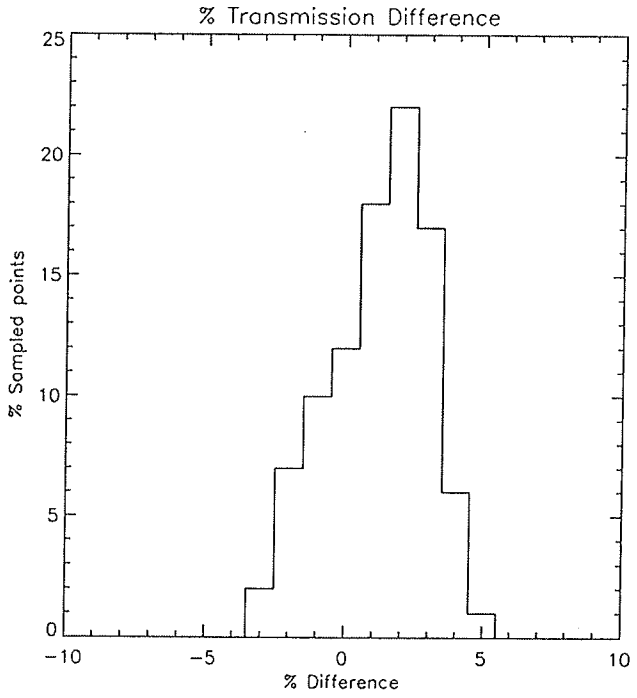

Figure 3-10: Transmission difference histogram for the anthropomorphic phantom compensator.

Table 3-9: Fabrication QA results: Anthropomorphic Phantom

# points sampled	Average ΔT (%)	% of points with ΔT>5%	% of point with ΔT > 10%
77284	1.7 ± 0.8	2.1	0.0

We observed a broader transmission difference histogram in this case compared to the compensators of experiments 1 and 2, with 2.1% of the sampled points differing from the FOCUS design by more than 5% of full transmission.

3.4 Experiment 4: Clinical trial A; Head & neck phantom

3.4.1 Results

Although the RMS deviations along the open and compensated profiles were at acceptable levels, the maximum deviation exceeded the recommended limit of 3% in both cases. It should be pointed out however, that in the open field only the outermost point at $x = 9$cm exceeded 3%. This was not the case for the compensated field where several points in the region $-3.8 < x < -2.6$cm surpassed the acceptability criterion.

Isolating the effect of the compensators on the in-phantom measurements and calculations, using the dose ratios, we observed that they provided approximately 1-2% more attenuation than FOCUS predicted (Figure 3-12).

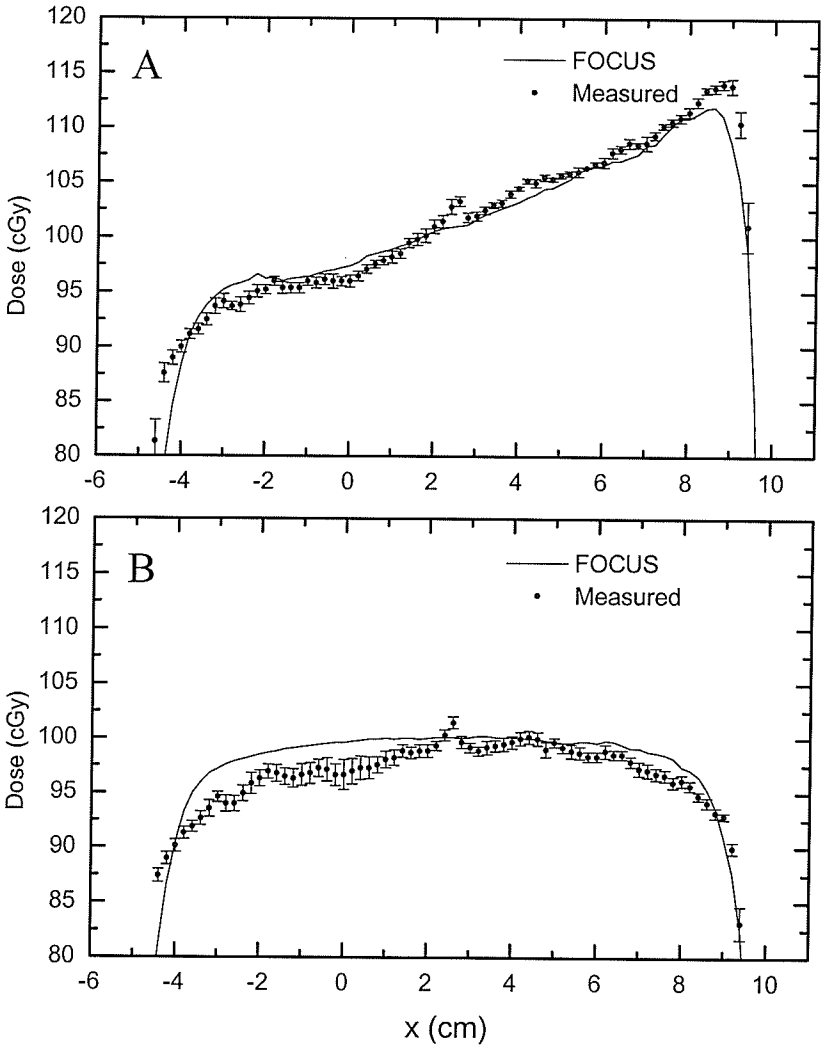

Figure 3-11: Profiles at the compensation plane for both (A) the open field and (B) the compensated field for the head and neck phantom. The error bars represent the standard error in the measured points for a series of 5 measurements.

Table 3-10: Agreement between FOCUS and measured data along the dose profile.

	RMS deviation (%)	Maximum deviation(%)
Open Field	1.2	-4.5
Compensated Field	2.0	4.2

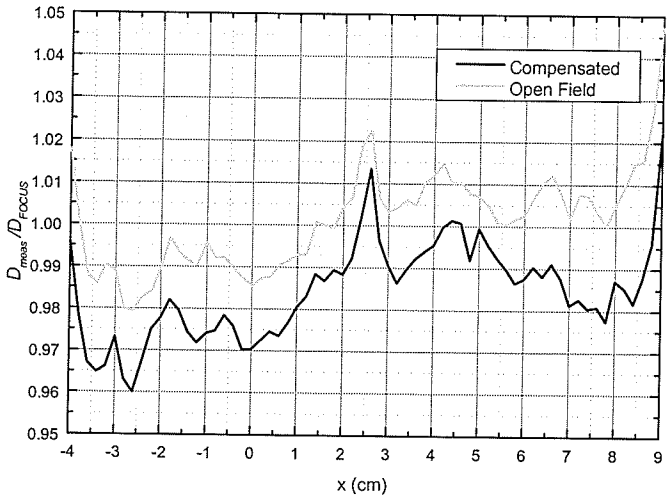

Figure 3-12: Ratio of measured to FOCUS dose along the dose profile for both the open and compensated fields within the high dose, low dose gradient region.

3.4.2 QA

The agreement between the reconstructed and original patient contours in the region of comparison was not as good as with the ramp phantom, with a maximum deviation of 8% of the high point thickness (or 0.8cm) for all three slices. However, the deviations throughout the majority of the comparison regions on the three slices were well within 5%. The results of the thickness measurements for the 9 interest points are shown in Table 3-11.

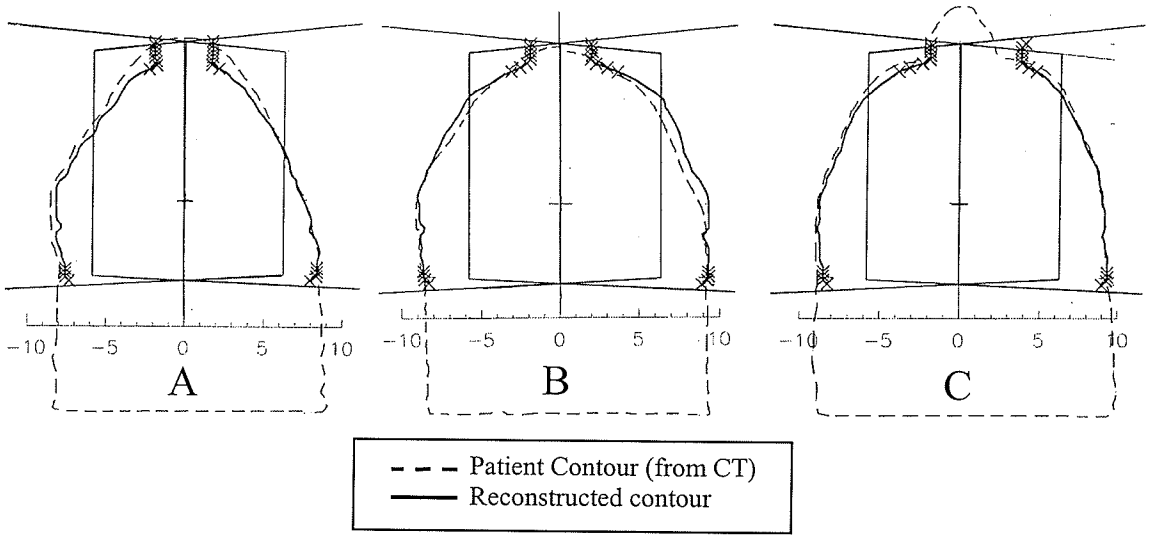

Figure 3-13: Comparison of the original patient contour from the CT simulation (dashed line) and the reconstructed patient contour. Three slices were compared (A) 3.5cm (B) 7.4cm (approximate center of field in super-inferior direction) and (C) 9.5cm, relative to the central axis. Note that the scaled coordinate system on each reconstructed contour indicates thicknesses in centimeters.

Table 3-11: Thickness measurements in the two-beam head and neck phantom compensator.

Point	Left Lateral (mm)			Right Lateral (mm)		
	FOCUS	Meas.(CNC)	Meas.(QA)	FOCUS	Meas.(CNC)	Meas.(QA)
1	0.8	0.9 ± 0.1	1.1 ± 0.3	0.4	0.6 ± 0.1	1.1 ± 0.3
2	2.6	2.7 ± 0.1	2.8 ± 0.4	0.2	0.3 ± 0.1	0.4 ± 0.3
3	0.1	0.3 ± 0.1	0.2 ± 0.3	2.8	3.1 ± 0.1	3.2 ± 0.3
4	0.9	1.1 ± 0.1	1.3 ± 0.3	1.3	1.5 ± 0.1	1.6 ± 0.3
5	2.2	2.4 ± 0.1	2.2 ± 0.4	1.9	2.1 ± 0.1	2.2 ± 0.3
6	1.5	1.7 ± 0.1	1.7 ± 0.4	0.4	0.6 ± 0.1	0.1 ± 0.3
7	2.6	2.8 ± 0.1	3.0 ± 0.4	0.8	1.0 ± 0.1	0.4 ± 0.3
8	0.9	1.1 ± 0.1	0.7 ± 0.3	2.5	2.7 ± 0.1	2.1 ± 0.3
9	0.2	0.4 ± 0.1	0.1 ± 0.3	1.7	2.0 ± 0.1	2.3 ± 0.3

For the left lateral compensator, only 2 of the 9 points measured via the CNC were in agreement with the FOCUS design. However, the other 7 points showed a deviation of only 0.2mm, or approximately 1.2% transmission. The measured thicknesses via the QA procedure showed a maximum deviation from FOCUS of 0.4mm for the left lateral compensator (point 4), corresponding to a transmission difference of 2.2% of full

transmission. The results are similar for the right lateral compensator, where 6 of the CNC measured thicknesses were 0.2mm thicker than the FOCUS design, 1 was in agreement and 2 points deviated from FOCUS by 0.3mm. Here, the maximum deviation between the QA thickness and FOCUS thickness was 0.7mm, or 4.0% in terms of x-ray transmission.

It is interesting to note that in this case the compensated field dose profile was offset below that of the open field (Figure 3-12) whereas in the previous 3 experiments the opposite shift was observed. This is a good indication that the single value of μ_f^{eff} used in the FOCUS compensator design was a reasonable approximation for the variety of situations that will be encountered in clinical practice (this topic will be discussed further in Section 3.6.1). The results of the fabrication QA on the entire compensator are shown in Figure 3-14 and Table 3-12.

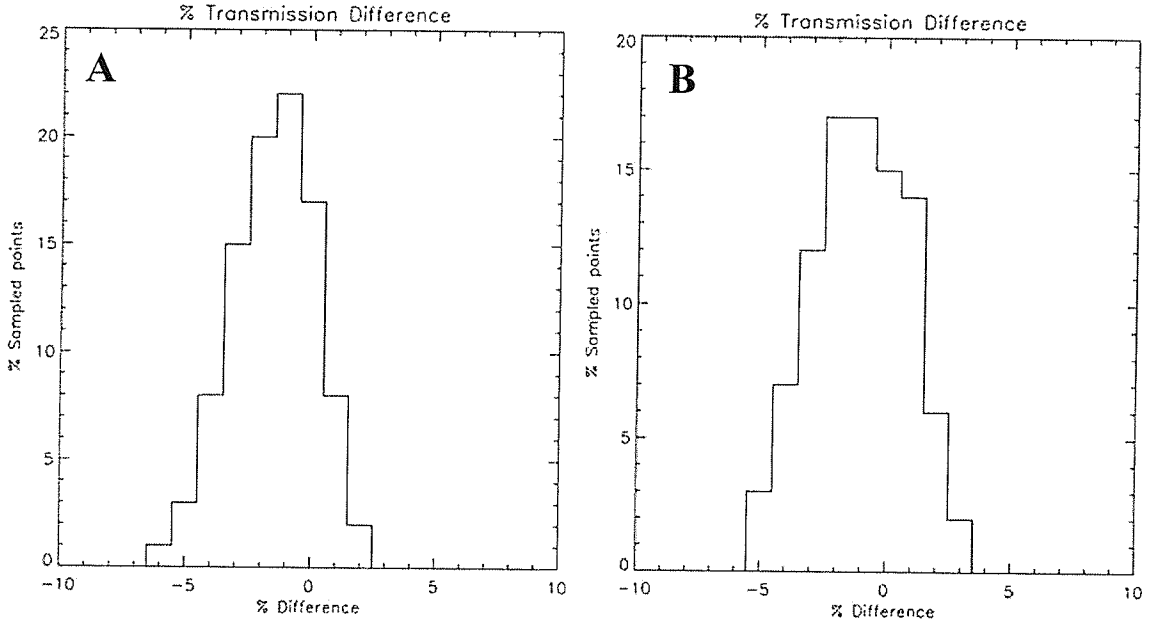

Figure 3-14: Transmission difference histograms for **(A)** the left lateral and **(B)** the right lateral compensators used in the two beam treatment of the head and neck phantom.

Table 3-12: Fabrication QA results: Head and Neck Phantom

Compensator	# points sampled	Average ΔT (%)	% of points with ΔT>5%	% of point with ΔT > 10%
Left lateral	76729	-1.0 ± 1.9	1.7	0.0
Right lateral	76729	-0.6 ± 1.6	1.2	0.0

The fact that the average transmission differences were negative in this case is consistent with the measured thicknesses using the CNC being steadily about 0.2mm greater than the FOCUS design for both compensators. Note, however, that no firm conclusions can be drawn about this consistency, since in both compensators the deviation of the ΔT from 0 was within measurement error. Less than 2% of the points exceeded a 5% transmission difference in these cases, and the thickness difference plot indicated that the discrepancies between FOCUS and the QA measured thicknesses were not localized to any particular region in the compensators.

3.5 Experiment 5: Clinical trial B; Mantle phantom

3.5.1 Results

For this highly non-uniform profile, FOCUS had difficulty predicting the dose accurately, especially in the high dose region around x = -4cm, where the maximum deviation of -4.5% was encountered in the open field. This error is likely due to the approximations in the scatter contribution to the dose at this point in the phantom, since the Scatter Phantom Ratio (SPR) calculation in the FOCUS Clarkson algorithm assumes that the surface is flat at the depth of the given fanline projected to the central axis (Figure 3-16). Scatter originating in layers above this plane will not be accounted for. The differences exceeded the recommended limit of 3% for both the open and compensated fields. The dose ratios are shown in Figure 3-17. It is evident that the discrepancies between FOCUS

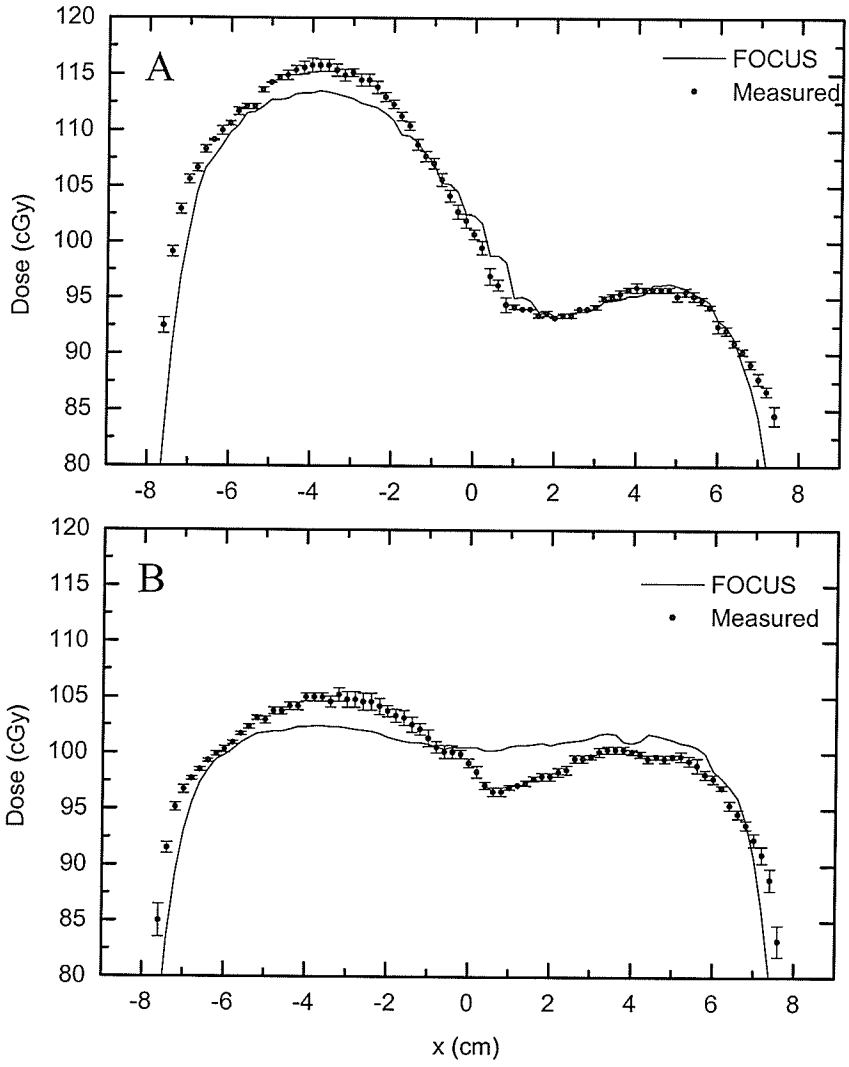

Figure 3-15: Profiles at the compensation plane for both (A) the open field and (B) the compensated field for the mantle phantom. The error bars represent the standard error in the measured points from a series of 5 measurements.

Table 3-13: Agreement between FOCUS and measured data along the dose profile.

	RMS deviation (%)	Maximum deviation(%)
Open Field	1.5	-4.5
Compensated Field	2.1	3.9

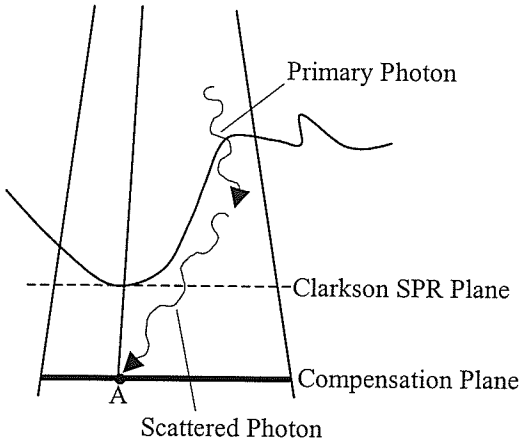

Figure 3-16: The SPR calculation in the Clarkson algorithm only accounts for scatter originating in below the Clarkson SPR plane shown. This plane is placed where the current fanline intersects the phantom surface. In this case, contribution to the dose at point A from scattered photons originating above the SPR plane (as shown) would not be accounted for. Therefore, the measured dose at point A would be higher than that calculated by FOCUS.

and measurements in the compensated field for $x < 0$cm were very similar to that of the open field. Thus, greater accuracy in the compensated dose calculations than was observed should not be expected. Furthermore, the fluctuation of the compensated dose ratio above and below that of the open field along this profile, indicated that an appropriate value for μ_f^{eff} was used in the design of this compensator.

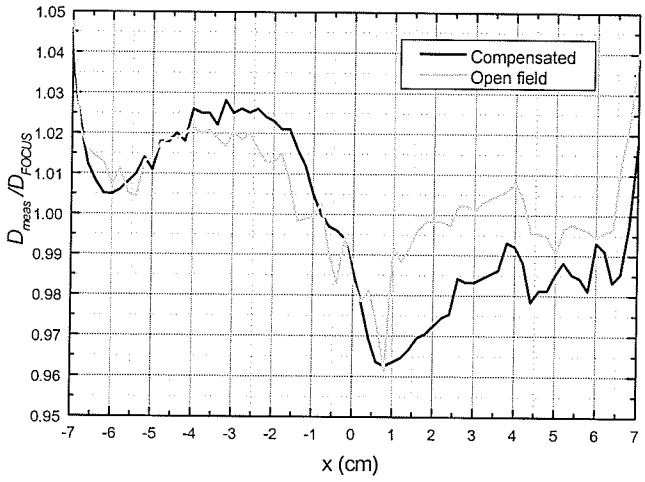

Figure 3-17: Ratio of measured to FOCUS dose along the dose profile for both the open and compensated fields within the high dose, low dose gradient region.

3.5.2 QA

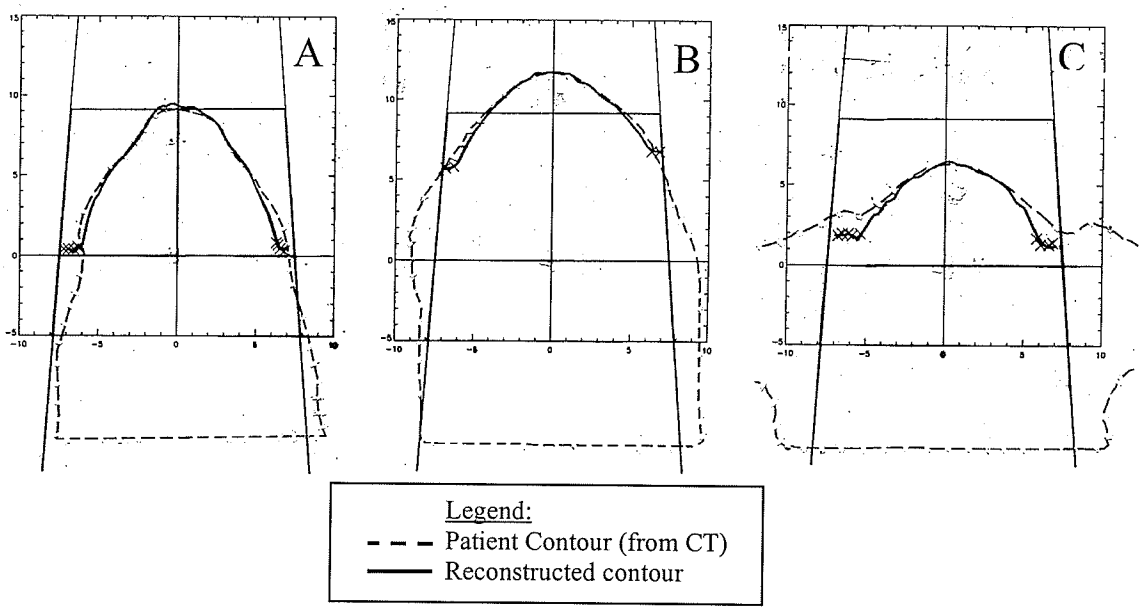

Figure 3-18: Comparison of the original patient contour from the CT simulation (dashed line) and the reconstructed patient contour. Three slices were compared (A) 0.0cm (B) +4cm and (C) -3cm, relative to the central axis.

The reconstructed patient contour overlays are shown in Figure 3-18. Here the agreement with the original patient contour from the CT simulations was excellent in the region of comparison. The maximum deviation between the contours, again expressed as a percentage of the high point thickness, was 5% (or 0.6cm).

As for the compensator fabrication, all but 1 of the 9 points sampled with the CNC were in agreement with the FOCUS design. This single point however, showed a deviation of only 0.2mm.

Table 3-14: Thickness measurements in the mantle phantom compensator.

Point	FOCUS (mm)	Measured (CNC) (mm)	Measured (QA) (mm)
1	1.5	1.6 ± 0.1	0.9 ± 0.3
2	4.5	4.6 ± 0.1	4.3 ± 0.3
3	4.4	4.5 ± 0.1	3.7 ± 0.3
4	0.1	0.1 ± 0.1	0.4 ± 0.3
5	2.9	3.0 ± 0.1	2.5 ± 0.3
6	1.2	1.2 ± 0.1	1.0 ± 0.3
7	4.0	4.0 ± 0.1	3.6 ± 0.3
8	3.7	3.9 ± 0.1	3.5 ± 0.3
9	1.2	1.3 ± 0.1	1.8 ± 0.3

The thickness as calculated by the QA procedure showed a maximum deviation of 0.7mm from FOCUS, corresponding to a transmission difference of 3.2% (point 3). The fabrication QA results are shown in Figure 3-19 and Table 3-15.

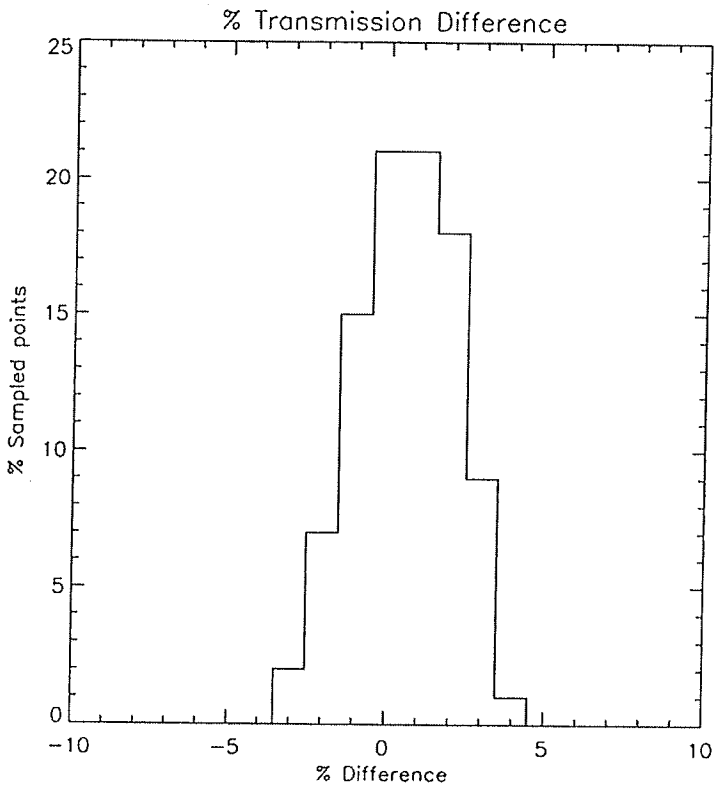

Figure 3-19: Transmission difference histogram for the mantle phantom compensator.

Table 3-15: Fabrication QA results: Mantle Phantom

# points sampled	Average ΔT (%)	% of points with ΔT>5%	% of point with ΔT > 10%
82288	1.1 ± 1.5 %	0.2	0.0

The agreement between the QA and FOCUS design transmission was excellent in this case, with only 0.2% of the points falling outside a 5% difference. Moreover, the thickness difference plot indicated that the small differences that remained were distributed relatively uniformly throughout the compensator.

3.6 Summary of the results

3.6.1 Phantom Measurements

Within the 5 experiments, we observed fluctuations in the level of agreement between the FOCUS calculations and the in phantom measurements along the dose profiles. These fluctuations were to be expected, due to the limited accuracy of the correction-based Clarkson algorithm. With reference to the TG 53 criteria for the acceptability of a TPS, only the cork inhomogeneity (experiment 2) and the anthropomorphic (experiment 3) showed agreement within the tolerance levels. Note, however, that in that ramp phantom (experiment 1) and head and neck phantom (experiment 4) only the last measurement point at the outer edge of the high dose, low dose gradient region was out of tolerance. In the 5th experiment, involving the mantle phantom, deviations beyond the limitations of these acceptability criteria were observed.

Although the ability of FOCUS to accurately calculate the dose in various phantom geometries directly impacts the results of this study, recall that the main objective was to examine the ability of FOCUS to provide accurate compensation under various situations. In this respect, a comparison between FOCUS and measurements was made in both the open and compensated fields. Since in general the errors present in the compensated field calculations were consistent with those of the open field, we can conclude that the FOCUS compensator design was satisfactorily accurate, *within the limitations of the Clarkson calculation algorithm.* A more sophisticated calculation algorithm would be required at the compensator design stage to produce a measurable improvement of the uniformity of the dose distribution at the compensation plane.

The ratio of measured dose to FOCUS calculated dose was also used to assess the performance of the compensators. The fact that the compensated field dose ratio fluctuated above and below the open field dose ratio for the five experimental configurations studied here, indicated that the value of μ_f^{eff} was a good choice for generalization to clinical beams. In general, the percent deviation between the dose ratios was approximately less than or equal to the percent deviation between the open field FOCUS calculations and in-phantom measurements for each experiment. Therefore, adjusting μ_f^{eff} depending on the relevant compensated beam parameters (i.e. field size, depth of compensation plane) is not justified.

We observed variations in the ability of FOCUS to design accurate compensators for the five listed experiments. These differences were not surprising, due primarily to the limitations of using a single effective linear attenuation coefficient to describe the compensator transmission properties, which does not account for beam hardening, as well as the simplifying assumptions used by FOCUS to calculate dose from photon scatter. However, the discrepancies between FOCUS predicted dose and dose measurements were less than 2% in terms of mean transmission, for the compensators produced. Furthermore, these variations tended to distribute themselves about zero.

3.6.2 Design QA

In all three examples presented, the agreement between the reconstructed and original patient contours was quite good in the region of comparison (with deviations generally less than 5% but reaching as high as 8% of the high point thickness). It should be noted that in its present form, this procedure is simply meant to be a quick check that

the compensator design was reasonable. Since, at present, contours cannot be exported from FOCUS for an automated comparison with the reconstructed contour, it is unlikely that the detailed quantitative comparisons performed in this report would be done in everyday clinical practice. More realistically, the treatment planners would generate a few transverse patient contour printouts for each beam and have the QA program reconstruct these contours. The planner would then manually overlay the images on a light box and visually examine the shape and general agreement in the comparison region for gross errors. This accomplishes an important verification with minimal additional time and effort.

3.6.3 Fabrication QA

A strength of the fabrication check presented here, is that both the compensator thickness and its position in the treatment field are verified. This eliminates the possibility of improperly mounting an accurately milled compensator.

The accuracy of the fabrication QA procedure (that is, its ability to measure a known thickness of compensator) was determined by calculating the standard deviation between the nine points measured with the CNC probe and the corresponding thickness measurements via the QA procedure. Gathering the data for all six experimental compensators described above, this provided a collection of 45 random points to be sampled. These points showed a standard deviation between the QA measured thickness and the CNC measured thickness of 0.37mm, corresponding to a transmission difference of 1.9% of full transmission at 6MV.

The main sources of error in the fabrication QA procedure are the non-reproducibility of the film processor, the equal scatter approximation, and the neglecting of the dependence on position in the field due to variable beam hardening. These errors gave rise to measured transmission uncertainties of approximately 2% (obtained from the comparison of pixel intensity on each of the two step wedges for a given wedge thickness).

Finally, a criterion was defined for the automated compensator fabrication QA procedure to quantify the accuracy of the milling process. The general practice of radiation therapy planning is to deliver a uniform dose to the target volume, restricting the dose variation to within +7% and –5% of the prescription dose [IC 50]. Therefore it seems reasonable to aim for an accuracy of approximately ±5% in the compensator transmission. After all, the QA procedure must show a statistically significant error beyond its own inherent 1.9% accuracy (for a 68% confidence level). Furthermore, since the phantom measurements showed that the dose distributions calculated by FOCUS in the compensated fields were within approximately 5% of measurements, there is no justification for aiming for a higher accuracy in the compensator QA procedure. In practice, requiring all of the sampled compensator points to be within 5% of those in the FOCUS thickness array may be difficult to achieve (especially in light of the approximately 2% uncertainty in the fabrication QA procedure due to the approximations stated above). Deciding on how many points one should let stray beyond 5% is difficult.

As an initial acceptability criterion, it was established that it would be permissible to allow up to 5% of the points to exceed the 5% transmission difference limit, provided that none of the points surpass a 10% difference, which would present much more serious

repercussions clinically. All of the compensators constructed for the experiments above would pass this criterion. Note that this is simply a first approximation to a more rigorous acceptability criterion. In future work, more sophisticated image analysis techniques will be used to analyze and quantify the magnitude of the differences between the measured and FOCUS thickness arrays. A more complete acceptability criterion will be established at that time.

The results of the thickness offset tests on the current passing criterion (described in Section 2.5.2.5) are summarized in Table 3-16.

Table 3-16: Results of thickness offset simulation.

Thickness offset (z-axis) (mm)	% of points with ΔT>5%	% of points with ΔT>10%	QA result
0.0	0.2	0.0	PASS
0.25	3.3	0.0	PASS
0.5	15.7	0.0	FAIL
1.0	65.3	0.2	FAIL

As shown in the Table, an offset of 0.5mm was required before the QA procedure could recognize that an error had occurred. Considering that a 0.5mm change in thickness corresponds to only an approximately 3% change in transmission, this criterion can identify errors in thickness before they pose clinical significant problems.

The results of the transverse shift tests on the current passing criterion are shown in Table 3-17. Although a result of FAIL was indicated for a shift of 5.0mm, it should be noted that the uncertainty in the transmission in this case was 1.5%, and so the result was not a statistically significant fail. However, shifts of 7.5mm in this case did result in a statistically significant failing of this compensator. Naturally, a smaller shift would be

Table 3-17: Results of transverse shift effect simulation.

Transverse shift (x-axis) (mm)	% of points with ΔT>5%	% of points with ΔT>10%	QA result
0.0	0.2	0.0	PASS
2.5	1.4	0.0	PASS
5.0	5.6	0.0	FAIL
7.5	18.1	0.3	FAIL
10.0	26.6	1.8	FAIL

expected to result in the compensator failing the fabrication QA procedure had its contour been more strongly varying.

4 Conclusions

Compensators are an effective means of providing a uniform dose distribution in a specified plane perpendicular to the central axis. Both external patient contour and internal tissue inhomogeneities can be accounted for in the compensator design.

We found Pb doped with a small fraction of antimony to be a suitable compensator material due primarily to its recycleable nature, and its high density, which resulted in small filter thicknesses that allowed for convenient mounting. Using a special fixture setup on the mill, which mimicked the block tray with an additional set of 4 tapped holes, we were able to position compensators in the treatment field with high precision. The position of the compensator in the field was determined by the milling procedure itself.

The compensator resolution of 2.5mm was shown to provide sufficient accuracy by examining the performance of FOCUS designed compensators for five experiments ranging from simple surface contours to an anthropomorphic phantom. Typically the deviations in the compensated field were consistent with those in the open field, indicating that the discrepancies between FOCUS and the measured data in the compensated field were more a limitation of the FOCUS Clarkson algorithm rather than the fabrication process. This was confirmed by comparing the ratio of measured dose to FOCUS calculated dose for both the open and compensated fields, in order to isolate the effect of the compensator.

A comprehensive QA protocol was presented, which independently verified both the compensator design and fabrication prior to its application in a patient treatment. The design verification involved comparing a reconstruction of specified transverse slices in

the patient with the original patient contours from the CT simulation. Due to the truncation of the compensator points in the FOCUS design and the lack of penumbra modeling in the reconstruction program, it was only valid to compare contours within roughly the inner 80% of the field. For a total of 9 transverse slices both on and off the central axis, the maximum deviation between the original and reconstructed patient contours was 8% of the high point thickness (0.9cm of missing tissue), however, the average deviations were generally much smaller than that (<5%). The fabrication QA involved taking a film radiograph of the compensator in treatment position simultaneously with a set of calibrated step wedges, which were used to convert pixel intensity in the digitized film images to compensator thickness. The mean transmission difference between FOCUS and the measured compensators was less than 3% for all of the compensators used in experiments one to five. The fabrication QA procedure was determined to have an accuracy of 0.37mm (1s.d.) reflecting a difference in transmission of only 1.9%. A passing criterion was established which stated that in a satisfactory compensator, no more than 5% of the sampled points should show a transmission difference from FOCUS greater than 5% of full transmission.

Establishing an automated compensator process provides a significant benefit to a radiation therapy clinic. Compensators designed by 3D treatment planning computers generally are more accurate than their manually designed counterparts, which are based simply on missing tissue. More sophisticated dose calculation algorithms have recently been developed, which account for the effects of compensator scatter and beam hardening in the design as well [CMS 01]. In this report we observed that the FOCUS Clarkson algorithm, generally thought to be obsolete by today's standards, provided

acceptable performance in terms of its compensator design, and dose calculation in the high dose, low dose gradient region of the beam. We also observed that our compensator fabrication process was able to accurately reproduce the FOCUS design in the manufactured compensators (to within approximately 0.2mm), and that we were able to quantitatively judge their performance in the patient treatment prior to their actual application using the automated QA procedure.

5 References

[Kh 94] (1994) Khan FM, *The physics of radiation therapy, 2nd ed.*, Lippincott Williams & Wilkins, Baltimore, USA.

[IC 46] (1992) International Commission on Radiation Units and Measurements, *Photon, Electron, Proton and Neutron Interaction Data for Body Tissues*, ICRU Report 46, (International Commission on Radiation Units and Measurements, Washington).

[El 59] (1959), Ellis F, Hall EJ, Oliver R, *A compensator for variations in tissue thickness for high energy beams*, Brit. J. Radiol., **32**, 412.

[Bo 82] (1982) Boyer AL, *Compensating filters for high energy x-rays*, Med.Phys. **9**(3) 429-433.

[Ju 94] (1994) Jursinic PA, Podgorsak MB, Paliwal BR, *Implementation of a three-dimensional compensation system based on computed tomography generated surface contours and tissue inhomogeneities*, Med. Phys. **21** (3) 357-365.

[Ch 00] (2000), Chang SX, Cullip TJ, Deschesne KM, *Intensity modulation delivery techniques: "Step & shoot" MLC auto-sequence versus the use of a modulator*, Med. Phys. **27** (5), 948-959.

[Fi 01] (2001) , Field C. *et al*, *Inverse planned IMRT developments at the Cross*, WESCAN 2001 Conference Proceedings, http://www.cancercentre.com/wescan/program.cfm.

[Be 71] (1971), Beck GG, McGonnagle WJ, Sullivan CA, *Use of Styrofoam block cutter to make tissue-equivalent compensators*, Radiology **100** 694.

[Kh 68] (1968), Khan FM, Moore VC, Burns DJ, *An apparatus for the construction of irregular surface compensators for use in radiotherapy*, Radiology **90** 593.

[Kh 98] (1998) Khan FM, Potish RA, *Treatment Planning in Radiation Oncology*, Williams & Wilkins, Baltimore, Maryland, USA.

[Pa 70] (1970) Page V, Gardner A, Karzmark CJ, *Physical and Dosimetric Aspects of the Radiotherapy of Malignant Lymphomas: I. The Mantle Technique*, Radiology **96** 609-618.

[Ch 99] (1999) Chang, SX, Deschesne KM, Cullip TJ, Parker SA, Earnhart J, *A comparison of different intensity modulation treatment techniques for tangential breast irradiation*, Int. J. Radiation Oncology Biol. Phys. **45** (5) 1305-1314.

[Ha 61] (1961) Hall EJ, Oliver R, *The use of standard isodose distributions with high energy radiation beams – the accuracy of a compensator technique in correcting for body contour*, Brit. J. Radiol. **35** 41-52.

[El 87] (1987) El-Khatib EE, Podgorsak EB, Pla C, *Broad beam and narrow beam attenuation in Lipowitz's metal*, Med. Phys. **14** (1) 135-139.

[CMS] (1998) CMS, *Calculation physics and clinical application manual, Vol.1*, Computerized Medical Systems.

[CMS 01] (2001) FOCUS CMS Newsletter, Winter 2001, Vol. 4 Issue 3.

[Ch 93] (1993), Chu T, Lee K, *A technique for the evaluation of a missing tissue compensator system*, Med.Phys. **20** (3) 713-716.

[Lo 96] (1996), Low DA, Li Z, Klein EE, *Verification of milled two-dimensional photon compensating filters using an electronic portal imaging device*, Med. Phys. **23** (6), 929-938.

[Pa 99] (1999), Pasma KL, Kroonwijk M, van Dieren EB, Visser AG, *Verification of compensator thicknesses using a fluoroscopic electronic portal imaging device*, Med. Phys. **26** (8), 1524-1529.

[An 01] (2001) Andres HJ, Unpublished Internal Document.

[ORIG] (1995) ORIGIN™ User's Manual Version 4.0, MICROCAL™ Software, Inc.

[An 92] (1992) Ansbacher W, Robinson DM, Scrimger JW, *Missing tissue compensators: Evaluation amd optimization of a commercial system*, Med.Phys. **19** (5) 1267-1272.

[VS 95] (1995) Van Santvoort JPC, Binnekamp D, Heijmen BJM, Levendag PC, *Granulate of stainless steel as a compensator material*, Rad. Onc. **34** 78-80.

[OSU] (2001) Ohio State University, Department of Physics, *Melting points of various metals*, http://www.physics.ohio-state.edu/~kelch/melting.html.

[NIST] (1998) National Institute of Standards and Technology, *XCOM: Photon cross sections database*, http://physics.nist.gov/PhysRefData/Xcom/html/xcom1-t.html.

[Ba 99] (1999) Basran PS, Ansbacher W, Field GC, Murray BR, *Evaluation of optimized compensators on a 3D planning system*, Med. Phys. **25** (10) 1837-1844.

[TG 21] (1983) Task Group 21, Radiation Therapy Committee, AAPM, *A protocol for the determination of absorbed dose from high-energy photon and electron beams*, Med. Phys. **10** (6) 741-771.

[SA 78] (1978) Sarget-Welch Densichron Instruction Manual, Sargent-Welch scientific Company.

[TG 53] (1998) Fraass B, Doppke K, Hunt M, Kutcher G, Starkschall G, Stern R, Van Dyke J, *American Association of Physicist in Medicine Radiation Therapy Committee Task Group 53: Quality assurance for clinical radiotherapy planning*, Med. Phys. **25** (10) 1773-1829.

[La 86] (1986) Lancaster P, Salkauskas K, *Curve and Surface Fitting, An Introduction*, Academic Press, London, UK.

[IDL] (1997) *IDL v. 5.0 Reference Guide Volume 1 Routines A-M*, Research Systems Inc.

[Lu 50] (1996) *Lumiscan 50/75/85 Operator's Reference Guide*, Lumisys, Inc.

[MEPH] (1995) *Mephysto MP3/MP3-S Therapy Beam Analyser, Description of the Components and Installation Maual*, PTW Freiburg.

[Cu 84] (1984) Curry TS, Dowdey JE, Murry RC, *Christensen's Introduction to the Physics of Diagnostic Radiology, 3rd ed.*, Lea & Febiger, Philadelphia.

[Ba 90] (1990) Bagne FR, Samsami N, Hoke SW, Bronn DG, *A study of effective attenuation coefficient for calculating tissue compensator thickness*, Med Phys. **17**(1) 117-21.

[Wo 90] (1990) Wong JW, Purdy JA, *On methods of inhomogeneity corrections for photon transport*, Med.Phys. **17** (5) 807-814.

[IC 50] (1993) International Commission on Radiation Units and Measurements, *Prescribing, recording, and reporting photon beam therapy*, ICRU Report 50 (International Commission on Radiation Units and Measurements, Washington).